NTNU

Norwegian University of
Science and Technology

Design of Large PM-Generators for Wind Power Applications

Anders Lagerström

Master of Energy Use and Energy Planning
Submission date: August 2011
Supervisor: Robert Nilssen, ELKRAFT

Norwegian University of Science and Technology
Department of Electric Power Engineering

Anders Lagerström:

Design of Large Permanent Magnet Generators for Wind Power Applications

Master Thesis
June 2011

Supervisors:
Prof. Robert Nilssen
Dr.ing Alexey Matveev

Norwegian University of Science and Technology
Department of Electric Power Engineering

SmartMotor AS

Abstract

This report describes generator design for wind power applications. It explains a modern design procedure which uses both analytical and numerical analysis. The numerical analysis uses finite element analysis and in this report it is performed in Comsol. The report is done in cooperation with the industrial company, SmartMotor AS.

A new Matlab-based script is developed in order to handle the winding layout of distributed windings which will be used in the finite element analysis. The script saves the designer valuable time.

A new method that uses Fourier analysis for calculating iron losses for the analyzed geometry is suggested. It is concluded that the Fourier analysis is an incorrect approach as it returns not plausible losses. The new method could however be used without a Fourier analysis. It is concluded that this method is more accurate and less time consuming compared to the method that was used before.

In recent papers concentrated windings have been suggested to be more suitable for wind power applications than the conventional distributed windings. In this report distributed winded and concentrated winded generators have been designed and simulated. The results from these simulations are the basis of the comparison. The comparison uses key performance indicators for each machine, which will give an overview of how well the machines perform.

In this report it is concluded that both generators offer equal performance regarding voltage waveform and vibrations. The concentrated winded generator does however allow easier manufacturing, better efficiency and shorter length. It is superior in terms of torque per weight. It is therefore concluded that the concentrated winded generator is more suitable for wind power applications.

List of abbreviations

DD – Direct drive

DW – Distributed winding

Cp – Turbine characteristics

CW – Concentrated winding

EP – Electromagnetic pole

FEA – Finite element analysis

GHG – Green-house gas

GTO – Gate-turnoff thyristor

IGBT – Insulated-gate bipolar transistor

KPI – Key performance indicators

MPPT – Tracking algorithm

PM – Permanent magnet

PMSG – Permanent magnet synchronous generator

PWM – Pulse width modulation

SCR – Silicon-controlled rectifiers

Acknowledgments

The author would like to thank Astrid Røkke, Njål Rotevatn, Eirik Husum, Espen Schüller and Børge Noddeland at SmartMotor for their help with this paper. He would also like to thank Lars-Ottar Kvåle at SmartMotor for help with script updates and implementations.

He would like to thank his supervisors Dr.ing Alexey Matveev at SmartMotor AS and Professor Robert Nilssen at NTNU, for valuable discussions regarding electric machines.

The author gives his special regards to Elisabeth Slevolden for great support and good advices concerning language and writing.

About the author

Anders Lagerström is a Master student at the Department of Electric Power Engineering, Norwegian University of Technology and Science (NTNU), Trondheim, Norway. He started his education in 2006 at University of Uppsala at Energy System Engineering program. During his third year he studied at the University of British Columbia in Vancouver, Canada. He returned to Uppsala for his fourth year and for his fifth year he applied for an exchange with NTNU, where he wrote his Master's thesis in cooperation with SmartMotor AS.

Table of Contents

1 Introduction

1.1 Wind power today

During the last couple of decades renewable energy has grown into a large scale industry in order to satisfy the demand to reduce green-house-gas (GHG) emissions. Wind power is one of the fastest growing technologies both in numbers of installations and in size of each installment.

In Table 1-1 the ten largest wind power manufactures are listed with their market percentage and their type of drive-train. [1] There are three main drive-trains:

- Direct drive (DD) with permanent magnets (PMs)
- DD with electromagnetic pole (EP)
- Geared (also called asynchronous, could also use PMs)

Table 1-1 List of the top ten wind power manufactures. [1]

Company	Market share [%]	Drive-train
Vestas	12.5	Geared
GE Energy	12.4	Geared and DD PM
Sinovel	9.2	Geared
Enercon	8.5	DD EP
Goldwind	7.2	DD PM
Gamesa	6.7	Geared
Dongfang Electric	6.5	DD PM
Suzlon	6.4	Geared
Siemens	5.9	Geared and DD PM
REPower	3.4	Geared
Others: Acciona, Nordex, XEMC Darwind, Leitwind, Americas Wind Energy Inc., Lagerwey, Northern Power, among others	21.3	Several solutions

The standard size of wind turbines today is about 2MW, although several companies have turbines up to 5 MW. The largest wind turbine today is Enercon's E-126, which has a rated power of 7.5 MW. The size and rated power of wind turbines keep on growing and today there are four companies, listed in Table 1-2, that are working on 10 MW wind turbines, all based off-shore. Each concept is illustrated in Fig. 1-1.

Table 1-2 List of the four companies that have announced 10 MW wind turbine projects.

Company	Country	Special Feature
Sway AS [2]	Norway	Floating turbine
AMSC[1] Windtec [3]	United States	High temperature superconductors
Clipper Windpower [4]	Great Britain	4 PM Generator Gear
Wind power Ltd. [5]	Great Britain	Vertical axis

[1] American Superconductor Corporation

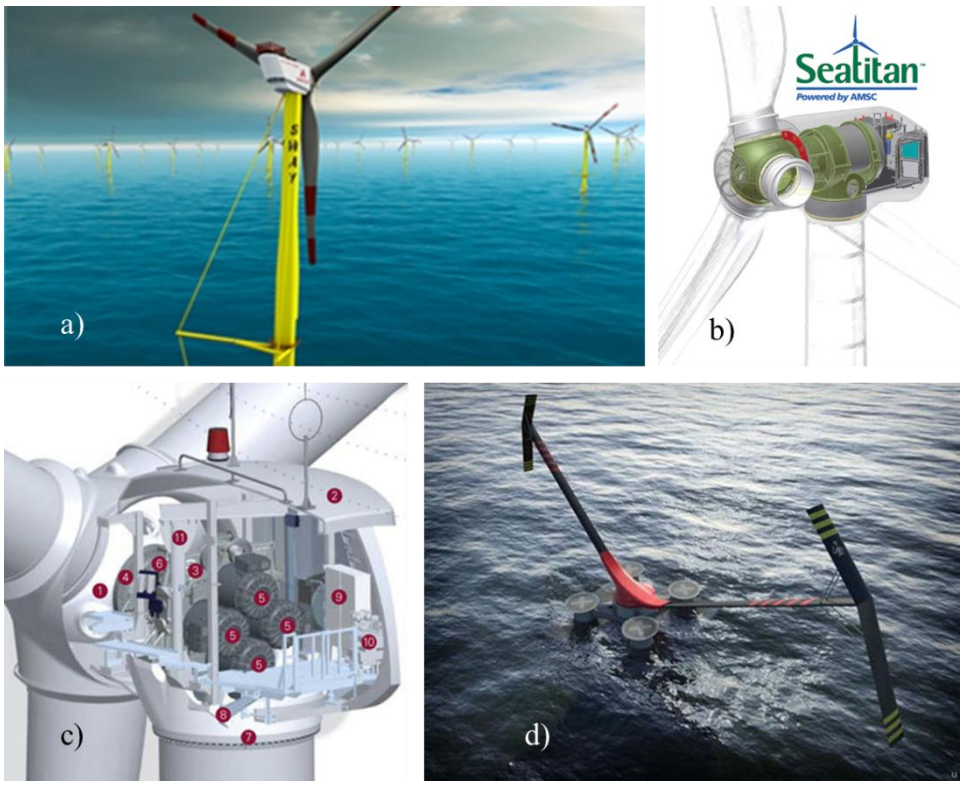

Fig. 1-1 Illustration of the four 10 MW projects: a) Sway AS [2] b) AMSC Windtec [3] c) Clipper Windpower [4] d) Wind power Ltd. [5]

In later years there has been a change from geared squirrel cage generators to DD synchronous permanent magnet generators (PMSG). These generators can operate gearless and thus have less maintenance and higher efficiency compared to the geared solutions. [6]

As the new generation of DD wind turbines has higher rated power compared to older wind turbines, generators need to be larger. This has caused several problems, one being weight as the wind turbine's tower can only withstand a certain load. Other problems are logistics due to the large diameter of the machines and electrical disadvantages caused by low rotational speed. The companies that have DD solutions are listed in Table 1-3.

Table 1-3 List of companies with DD wind generators.

Company	Model	Rated power [MW]
Americas Wind Energy Inc. (AWE) [7]	AWE 52-750 AWE 52-900 AWE 54-900	0.75 0.9 0.9
Enercon [8]	E-33 E-48 E-53 E-44 E-70 E-82 E-82 E-82 E-101 E-126	0.33 0.8 0.8 0.9 2.3 2 2.3 3 3 7.5
Dongfang Electric [9]		1 1.5 2 2.5
GE Energy [10]	4.0-110	4
Goldwind [11]	1.5 MW PMDD 2.5 MW PMDD	1.5 2.5
Lagerwey Wind [12]	L82 L90 Under development	2 2.5 3.5
Leitwind AG [13]	LTW70 LTW77 LTW77 LTW80 LTW80 LTW101	2 (1.7) 1 1.5 1.5 1.8 3
Northern Power [14]	Northwind 100 Northwind 100 Artic NPS 2.2	0.1 0.1 2.2
Siemens AG [15]	SWT-3.0-101	3
XEMC Darwind [16]	Under development	5

To achieve lower weight, easier sectioning and better electrical properties, concentrated windings (CW) have been suggested as an alternative to the conventional distributed windings (DW).

1.2 Objective

In this study the student is going to design a state-of-the-art 4 MW generator with permanent magnets. In cooperation with an industrial company, SmartMotor AS, a generator for wind power application is to be designed to fulfill a given set of general specifications.

The student is going to investigate a specification given by a customer. New design tools must then be developed by the student in order to take account the company-specific features and

new ideas that are introduced in this case. The student is supposed to find an optimal winding layout by investigating both distributed and concentrated windings in a quantitative comparison. A thermal analysis must be a part of the comparison.

The student must demonstrate methods and tools to be used in such a modern design and in general illustrate how classical challenges such as losses, vibrations and cogging torques are taken into account.

In addition the student shall focus the investigation on modern cooling concepts and integration of the generator for wind power applications.

1.3 Key performance indicators and state-of-the-art

It is generally hard to compare generators since comparisons highly depend on the chosen parameters. It is however possible to compare them to the available state-of-the-art and key performance indicators (KPIs), which are parameters that give an indication of the machine performance. KPIs are important for a good comparison since one parameter alone does not necessarily tell how well the generator performs.

Important KPIs when comparing CW and DW wind generators are:

- Torque per weight: The parameter is independent of rotational speed up to a certain rpm. More importantly the parameter defines the developed torque of the generator per weight of active material, giving an indication of how weight efficient the machine is. The active material is the stator and rotor cores, magnets and copper windings. [17] Torque per weight can be combined with power per weight, as in Fig. 1-2.
- Efficiency: It is important to keep a high production of electricity and low losses resulting in heat.
- Length: Is the active axial length with end-windings of the generator. It gives an indication of how much space the machine needs in axial direction, which is important for integration of the generator.
- Power factor: Describes how much reactive power the generator uses, which in turn could affect the choice of converter.
- Tangential tension: The parameter indicates how much force the machine produces per surface area at the air gap. Tangential tension is given below in Equation (1).

$$\sigma_{AG} = \frac{T}{\frac{d_{AG}}{2} * d_{AG} * \pi * L} \qquad (1)$$

  Where T is torque, d_{AG} is the air gap diameter and L is the active length of the machine. [18]
- Torque ripple: It is important to keep the torque ripple low not to create vibrations which could harm the structure. In this report the parameter will be presented in ripple per unit (p.u.). This means that the torque's maximum value subtracted by its minimum value is divided by the mean torque.
- THD: Is the total harmonic distortion of the induced voltage or current. THD describes the content of higher harmonics in a voltage or current waveform. If the waveform has a low THD, it means that the first harmonic is dominating and the content of higher harmonics is low. Usually a low THD is desired since only the first harmonic is

contributing to power production, while higher harmonics causes both copper and iron losses. [19]

Because of high confidentiality in the industry, it is difficult to get a good overview of the state-of-the-art of each KPI. In Table 1-4 is the available state-of-the-art that is considered relevant for this report:

Table 1-4 A summary of current state-of-the-art for the relevant KPIs.

KPI	Current state-of-the-art value
Torque per weight [Nm/kg]	See Fig. 1-2
Efficiency [%]	96 [20]
Length with end-windings [m]	-
Power factor	~0.9
Tangential tension [kN/m^2]	40-50 [18]
Torque ripple [%]	< 1
THD [%]	< 2

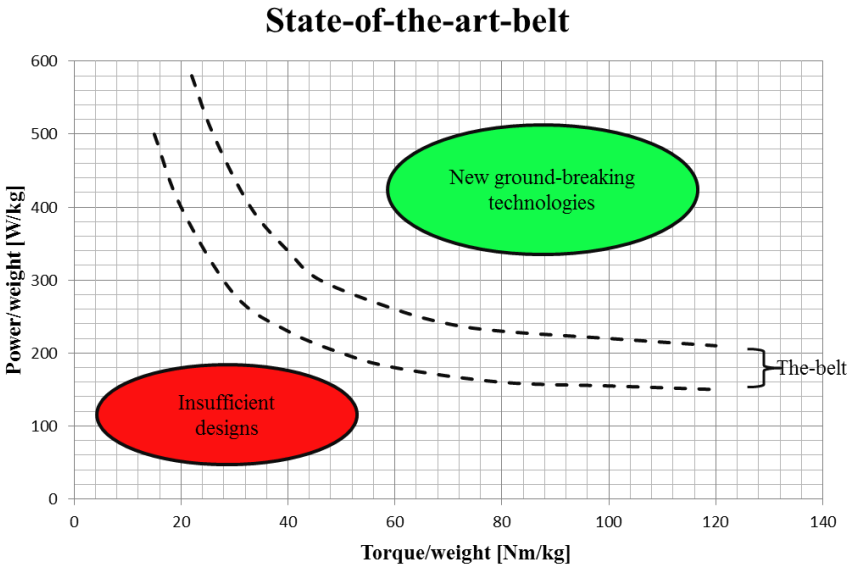

Fig. 1-2 Illustration of the state-of-the-art relation between Torque/weight and Power/weight. [21]

2 Theory

2.1 Machine theory

2.1.1 Direct drive generators

If a generator has a sufficient number of poles, it can be attached directly on the main shaft, removing the need of a gearbox. This is referred to as a DD generator. [22] The main reasons for using a DD generator are a reduction of the cost of the produced electricity and the noise of the wind turbine. The noise is an important factor when applying for building permission close to populated areas or animal habitats. Concerning cost reduction, the DD generator can reduce cost of drive-train, losses in energy conversion and improve the availability of the wind turbine. [23] The availability increases because below rated wind speed, the rotor can operate at different rpms, thus keep a constant tip speed ratio which results in higher energy extraction. Another positive feature is that the drive-train in a variable-speed turbine is subjected to lower fluctuating stresses which reduce fatigue of materials. [22]

An important difference between DD and geared generators is that the DD generators require a high rated torque due to the low rotational speed. As a result of this DD generators are usually designed with a large diameter. Having multiple poles they can also reduce the weight of rotor and stator yokes and keep end-winding losses small compared to geared solutions. [23]

2.1.2 Permanent magnet synchronous generator

Wind turbines that are meant for wide ranch variable-speed operation normally use PMSG together with power electronic converters.

The term synchronous generator results from that the rotor rotates at same speed as the magnetic field changes in the stator. The PMSG is in principle exactly the same as a normal synchronous generator, except that the magnetic field is supplied by PMs instead of rotor windings with applied field current. The power in a PMSG is taken from the stationary armature, hence no need for commutator, slip-rings or brushes. Without previously mentioned axillaries and no loss in field windings, the PMSG has a high efficiency and low maintenance cost. [22]

2.1.2.1 Permanent magnet materials

PMs normally consist of either sintered or bonded materials. They can be shaped in any desired shape and magnetized in any desired direction. The most common shape is rectangular but it is not unusual with disc- and wedge shapes. [6] Demagnetization has previously been a problem with PMs. Today the quality is higher and PMs are quite insensitive to external fields. Only short-circuits in hot machines can cause a risk of demagnetization.

The most common PM materials in commercial production today are:

- AlNiCo magnets: The most important alloying metals are aluminum, nickel and cobalt.
- Ferrite magnets: Made of sintered oxides, barium and strontium hexa-ferrite.
- RECo magnets: Rare-earth cobalt magnets are produced by a powder metallurgy technique, and comprise rare-earth metals, mainly samarium, and cobalt in the ratios of 1:5 and 2:17. The latter also includes iron, zirconium and copper.
- Neodymium magnets: Consist of neodymium–iron–boron, produced by a powder metallurgy technique.

Neodymium PMs are one of the most common magnets in PMSG due to their high energy product and magnetic remanence. Neodymium magnets were invented in 1983 and typically consist of 65 % iron, 33 % neodymium and 1.2 % boron, with small amounts of aluminum and niobium. They are sensitive to changes in temperature and become weaker as the temperature rises. The Curie temperature, the demagnetization temperature, is about 320 °C. To avoid lowering the performance, they should not be exposed to temperatures above 120 °C. [24]

2.1.3 Machine topologies

There are several different machines which can be suited as wind power generators. In wind power PMSGs there are two main categories called radial- and axial-flux machines. The names explain the magnetic flux direction in the air gap relative to the shaft.

The radial-flux machines either have inner- or outer-rotor. The conventional type is the inner–rotor radial-flux machine. The rotor is cylindrical and has PMs attached on the surface facing the stator. The rotor of the outer radial-flux machine encircles the stator. Both types are illustrated in Fig. 2-1. [17]

In Table 2-1 the main advantages are presented for inner- respectively outer-rotor radial flux generators for wind power applications.

Table 2-1 Comparison of inner- and outer rotor radial flux machines. [17]

Inner-rotor	Outer-rotor
• A more stable structure since the whole cylinder is attached directly on the shaft. • For a passive cooling system the inner-rotor will allow the stator to be easier cooled by ambient air, as the main losses will be located in the stator for a wind turbine generator.	• The blades can be bolted directly on the front face of the drum which allows a simple drive-train coupling for DD. • For a given nacelle diameter it will have larger rotor diameter. This leads to easier fitting of multi-pole structure which in turn leads to higher frequency and a slimmer yokes. • For a closed cooling system of the stator, the outer rotor will be exposed to ambient air which allows better cooling of rotor yoke and magnets. • Has a higher torque per weight compared to the inner-rotor. • The outer-rotor use less magnets compared to the inner-rotor which leads to lower cost of active material. • It will use less copper due shorter end-windings which in turn is due to the stator's shorter diameter.

The outer-rotor is better suited for wind power application. [17]

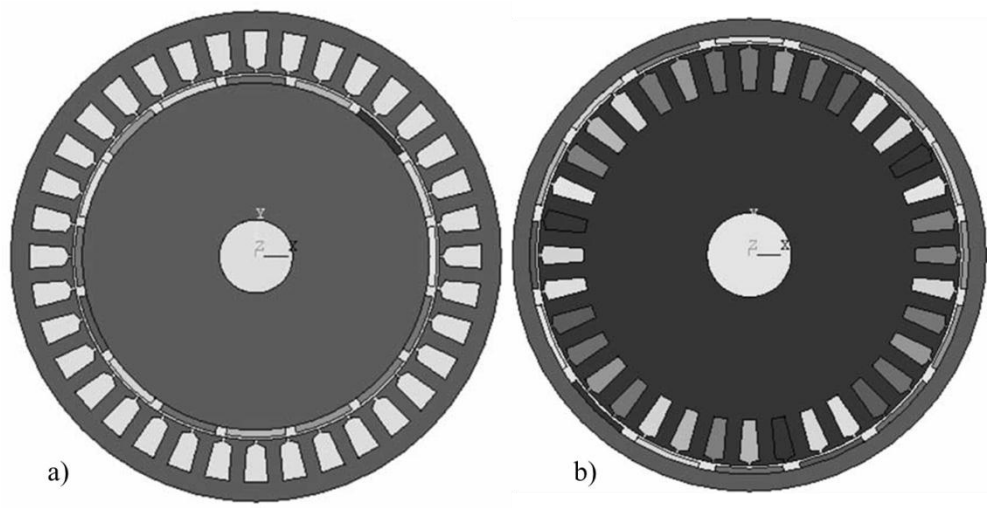

Fig. 2-1 Illustration of a) inner rotor b) outer rotor. [17]

The axial-flux machines have a flat and pancake like rotor, hence the nickname pancake machines. The PMs are attached on the rotors axial direction. The axial-flux machines can have a single stator, double stator or double rotor. Single and double stator axial-flux machines are illustrated in Fig. 2-2. [17]

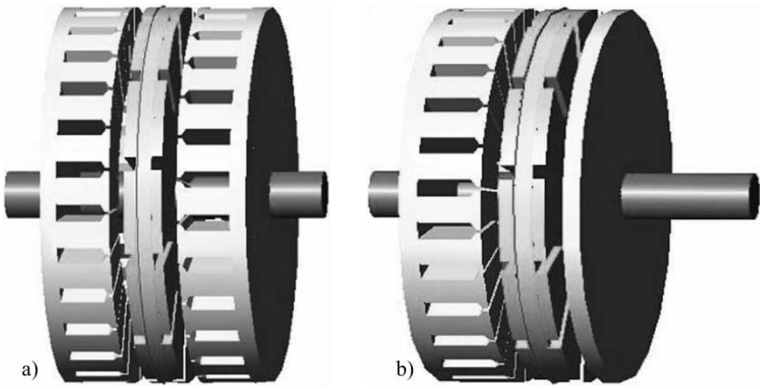

Fig. 2-2 Illustration of a) double stator b) single stator axial-flux machines. [17]

2.1.4 Windings

2.1.4.1 Winding layout

When each slot contains one coil-side it is called a *single-layer* winding and when each slot contains two coils-sides, it is called a *double-layer* winding. When the winding contains three or more coil-sides in each slot it is called *multiple-layer* winding. [25]

The main advantages of single- and double-layer windings are presented in Table 2-2.

.

Table 2-2 Comparison of single- and double-layer windings. [26]

Single-layer	Double-layer
• Have a higher utilization of the slots due to elimination of interlayer insulation. • Easier segmentation of the stator since the windings can have a broken chain.	• Allows easy implementation of fractional slotting and use of short-pitching to reduce cogging and certain harmonics. • Have coils with the same shape which leads to easier manufacturing and lower cost compared to single-layer. Single-layer needs different coil shapes to be able to fit the end-windings.

Terminology regarding winding layout is given in Table 2-3.

Table 2-3 The common terminology regarding winding layout.

Feature	Symbol
Number of slots	N_s
Number of poles	N_p
Number of phases	N_{ph}
Number of slots per pole per phase	q
Number of coils	N_c
Number of turns in each coil	N
Angular slot pitch	γ_s
Phase spread	σ_e

The parameter q is given in Equation (2).

$$\boldsymbol{q = \frac{N_s}{N_p \times N_{ph}}} \qquad (2)$$

Windings are separated into two categories depending if q is an integer or a fractional number. The windings are consequently called *integer*- and *fractional-slot windings*; the latter is further explained in chapter 2.1.5.1.

The winding layout is based on the slots relative electrical position. Each slot will be separated by the angular slot pitch, γ_s, which is given in electrical radians in Equation (3).

$$\boldsymbol{\gamma_s = \frac{\pi \times N_p}{N_s} = \frac{\pi}{q \times N_{ph}}} \qquad (3)$$

Each slot can then be assigned to a phase depending of the phase spread, σ_e, which is normally $\pi/3$ radians. For almost all larger electric generators N_{ph} is 3. [6]

Each slot will have an induced voltage, also called electromotive force (emf), from the magnetic field from the rotor. To achieve a high emf it is therefore important that the windings are laid out in such manner that the sum in each phase is as large as possible and

that the phases are evenly distributed. For a three-phase winding this means that the phases should be separated by 2π/3 electrical radians. To achieve this, N_s/N_{ph} or $N_s/(2*N_{ph})$ must be an even numbers for double-layer respectively single-layer windings.

The standard procedure for the winding layout for a double-layer winding is given in Table 2-4. [26]

Table 2-4 The standard procedure for winding layout of a double-layer winding. [26]

Relative electrical position range	Phase and polarity
[0 π/3[	A+
[π/3 2π/3[	C-
[2π/3 π[	B+
[π 4π/3[	A-
[4π/3 5π/3[	C+
[5π/3 2π[	B-

An example of this is visualized in a vector diagram in Fig. 2-3, where N_p is 2, N_s is 18 and N_{ph} is 3.

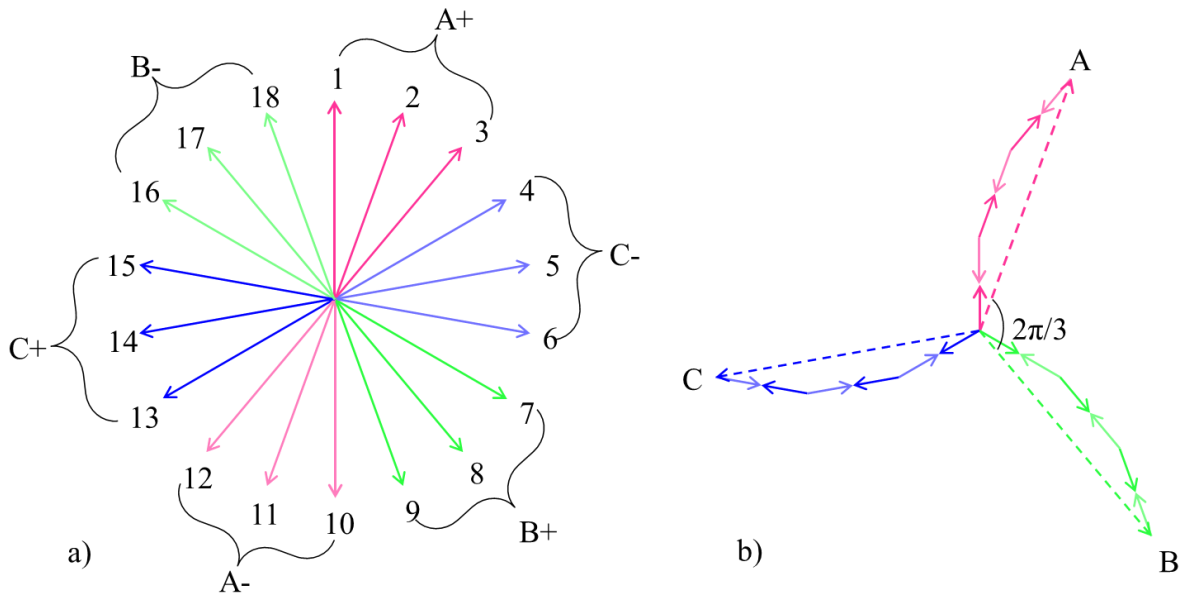

Fig. 2-3 Illustration of emf vector diagrams, where colors indicate each phase with polarity. In a) the vector for each slot where $\gamma_s = \pi/9$ b) the dashed line indicates the vector sum of each phase and direction.

2.1.4.2 Distribution factor

The back-emf is a sum of several coils in each phase as illustrated in Fig. 2-3 b). The slots emf vector sum for each phase is often less than the arithmetic sum of each phase. The ratio between the vector sum and the arithmetic sum is called the distribution factor. The distribution factor, K_d, is derived in Equation (4):

$$K_{dn} = \frac{\sin\left(\frac{1}{2}n\sigma_e\right)}{q \times sin\left(\frac{1}{2}\left(\frac{n\sigma_e}{q}\right)\right)} \qquad (4)$$

Where n is the n:th harmonic.

However, for fractional slot windings the formula becomes slightly different:

$$K_{dn} = \frac{\sin\left(\frac{1}{2}n\sigma_e\right)}{u \times sin\left(\frac{1}{2}\left(\frac{n\sigma_e}{u}\right)\right)} \quad (5)$$

Where u is the numerator of q, once q has been reduced to its smallest fraction. [26]

2.1.4.3 Pitch factor

The pitch factor accounts for when the coil span is not a full pole-pitch, hence it is also called the coil-span factor. Whenever the coil span is not a full pole-pitch, it will reduce the vector sum of the coils emf. The conductors are not directly additive but will be a sum of the vectors that have the displacement angle ε, which is the angle that departs from the full-pitch value π. The pitch factor, K_p, is derived in Equation (6):

$$K_{pn} = \cos\frac{1}{2}n\varepsilon \quad (6)$$

Where n is the n:th harmonic, n = 1 is the fundamental harmonic. [26]

2.1.4.4 Winding factor

The product of the distribution factor and the pitch factor is called the winding factor. In an optimal case the winding factor will be 1. The winding factor, K_w, is derived in Equation (7).

$$K_w = K_d K_p \quad (7)$$

2.1.4.5 Distributed and concentrated windings

The conventional *distributed windings* (DW) have end-windings that are overlapping. The name is derived from DW having several coils distributed over one pole. To achieve this, DWs have a q > 1/2. [6] A section of a single-layer DW is illustrated in Fig. 2-4 b).

Coils which have non-overlapping end-windings are called *concentrated windings* (CW) and have a q < 1/2. [6] A section of a single-layer CW is illustrated in Fig. 2-4 a).

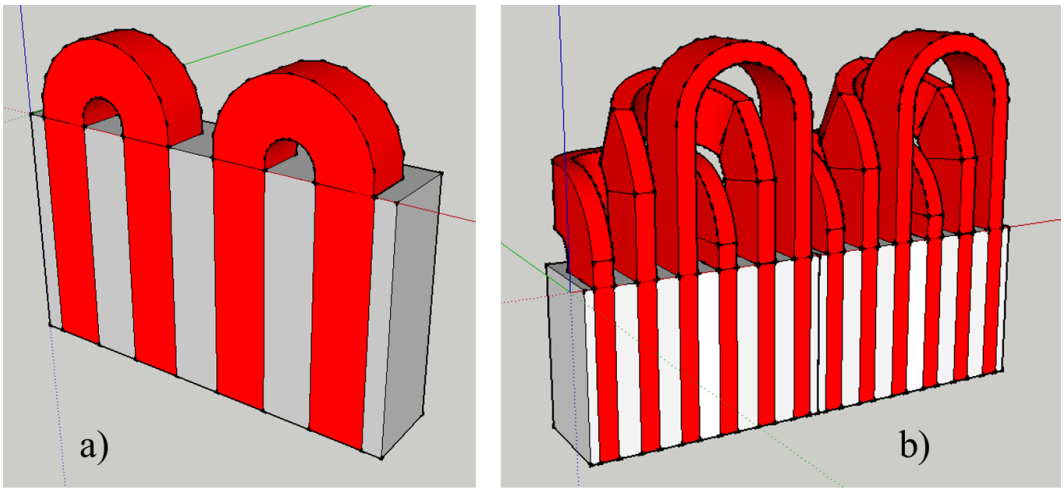

Fig. 2-4 Illustration of single-layer a) CW b) DW end-windings.

For low-speed high-torque electric machines, such as a DD wind turbine generator, the stator winding could be the limiting factor due to low rotational speed. This requires the rotor to have a large number of poles to get a suitable electrical frequency. For conventional DW-machines with a high q-value, the pole arch cannot be reduced to increase the number of poles because it is limited by the slot width. [6] This should not be reduced since it will reduce the slot fill factor. The slot fill factor could however be kept constant with a reduced slot width if the depth is increased. An increased slot depth would however increase the reactance, which in turn would increase the size of the converter, thus making the machine more costly. There are also thermal limitations on how much heat that can be removed through the long teeth to the stator yoke. [27]

To optimize the generator with a high q-value, trade-offs has to be made between the frequency and the diameter of the machine. By introducing CW-coils, where the number of slots is close to the number of poles, the slot width could be increased while still maintaining a high slot fill factor and a high level frequency. [6]

There are several strong incentives to introduce CW. One is the simple procedure of assembly and repair since they do not have overlapping windings such as the DW-machine. It will also be simple to section the machine, which would ease manufacturing and transportation. The end-windings would be shorter compared to DWs, which reduce copper losses and copper material. [6]

2.1.5 Cogging torque

Cogging torque is an undesirable element in electric motor design. It arises due to the interaction between the rotor's poles and the stator's teeth. Cogging torque can cause vibrations in the structure which may lead to mechanical failure. The cogging torque, T_{cog}, is given in Equation (8):

$$\boldsymbol{T_{cog} = -\frac{1}{2}\varphi_g^2 \frac{dR}{d\theta}} \qquad (8)$$

Where φ_g is the air gap flux, R the air gap reluctance and θ is the rotational angle.

Since cogging torque is a problem in machine design, several methods have been developed to reduce the unwanted output. These are presented in the following sections.

2.1.5.1 Fractional slot windings

The same rules that apply for integer-slot windings also apply for fractional-slot windings. A requirement that needs to be met is that once q has been reduced to its smallest fraction, the denominator is not allowed to be a multiple of number of phases; otherwise the phases will be unbalanced. In the normal case, phases will be unbalanced over one pole pitch or more, but will be balanced over a complete unit of poles. [26]

Fractional-slot windings reduce cogging by utilizing the contribution of dR/dθ for each pole over the whole machine. In an ideal case this sum will be zero. [25]

Further advantages of fractional-slot windings are that they reduce high frequency slot harmonics. They can also be used when the geometry sets a limit for q, for instance when q = 2 is too low and q = 3 is not possible, then q = 2.5 could be used in this case to achieve a better emf output. [26]

A disadvantage of fractional-slot winding is that a sub-harmonic of the magnetic flux density distribution (B-field) can occur during a unit of poles. The sub-harmonic could create radial forces between the rotor and stator which in turn could result in vibrations leading to mechanical failure.

2.1.5.2 Skewing

Another method of reducing cogging is skewing. Skewing, on the contrary to fractional slot windings, is trying to zero dR/dθ over each pole pitch either by skewing the magnets or the slots. Both skewing techniques have disadvantages. Skewing the slots increase the copper losses due to longer slots, while skewing the magnets increase the magnet cost. Another disadvantage with skewing is the formation of a normal force. For a radial flux machine this phenomenon can be described as when the rotor rotates, it tries to screw itself through the stator. Skewing can be used instead of having a winding layout, which lowers the winding factor. Similarly to the winding factor, skewing has a skewing factor. The skew factor, K_s, for a sinusoidal B-field is given in Equation (9). [25]

$$K_s = \frac{\sin\left(\gamma_s/2\right)}{\left(\gamma_s/2\right)} \quad (9)$$

For a square wave B-field, K_s is given in Equation (10).

$$K_s = 1 - \frac{\gamma_s}{2\pi} \quad (10)$$

The square wave skew factor will give a greater reduction of emf. Also notice that a low γ_s will give a high skew factor. This means that skewing a machine with a high number of slots will have less effect on the performance compared to skewing one with a low number of slots. [25]

After a simulation it is possible to calculate the skewing factor by shifting the back emf for each magnet with its relative angle to the first magnet. If all emf-curves are summed up, the skew factor will be given by the ratio between the first harmonic of the new emf and the old emf. Calculating from the simulation will be the most accurate procedure. [18]

2.1.5.3 Magnet shaping

Cogging torque is often a result of a rapid change of air gap flux density, B_g. To achieve a smoother B_g-change, the magnets can be shaped in different manners to have a lower B_g as the magnet moves over the stator tooth. [25] One way to reduce cogging torque and get a sinusoidal flux distribution, and thus sinusoidal back emf, is to have sinusoidal shaped magnets. [20]

2.1.6 Inductance, power factor and converter

2.1.6.1 Inductance

The inductance in a machine appears in the machine's coil since the current flowing through the coil produces a magnetic field. The inductance that appears in the coil due to its own current is called *self-inductance*, and the inductance that appears in the coil due to the surrounding coils is called *mutual inductance*. The inductance is used when calculating the power factor. [25]

When the inductance is calculated analytically it is often divided in three major components. The three contributing components are: the air gap, the slot and the end-windings.

The self-inductance in the air gap, L_g, is due to magnetic flux crossing the gap. For one coil L_g is given by Equation (11). [25]

$$L_g = \frac{N^2 \mu_R \mu_0 L \tau_p}{2(l_m + \mu_R g_e)} \quad (11)$$

Where μ_R is the magnetic relative permeability, μ_0 the permeability of free space, τ_p the pole pitch, L the active length of the machine, l_m is the magnet thickness and g_e the effective air gap given by the Carter coefficient.
The slot self-inductance, L_s, is due to the magnetic field crossing over the slot. It is highly dependent on the slot shape and the distribution of the winding in the slot. For a rectangular slot with assumed uniformly distributed coil turns, L_s is given by Equation (12). [25]

$$L_s = \frac{N^2 d_s \mu_0 L}{3^2 w_s} \quad (12)$$

Where d_s is the slot width and w_s is the slot depth.

The last inductance component is the end-windings. It hard to determine the value since the layout of the end turns are subject to few restrictions, and a set magnetic field distribution is impossible to define. The end-winding inductance, L_e, is therefore only roughly approximated. For a single-layer coil L_e is given by Equation (13). [25]

$$L_e = \frac{N^2 \mu_0 \tau_p}{8} ln\left(\frac{{\tau_p}^2 \pi}{4 d_s w_s}\right) \quad (13)$$

The mutual inductance has the same three components as the self-inductance. It is normally lower in a PM machine compared to the self-inductance. The mutual slot inductance is negligible due to the high permeability of the stator teeth and yoke. The end-windings mutual inductance is extremely difficult to calculate because the end turn placement is not well defined and the field distribution around the winding is difficult to define. Hence it is common only to calculate the mutual inductance for the air gap. For a three phase case it is derived that the air gap mutual inductance, M_g, is a third of the air gap self-inductance given in Equation (14). [25]

$$M_g = \frac{L_g}{3} \quad (14)$$

When simulating a machine numerically such as in software like Comsol, one could calculate the self-inductance by applying a current on one phase. The resulting field from the current will induce a voltage in the phase. As the simulation assumes no resistance in coil and the current and voltage is known, the inductance ($L_{numerical}$) can be calculated using the basic Equation (15).

$$L_{numerical} = \frac{V}{I\omega} \quad (15)$$

Where ω is angular frequency $2\pi f$, I the peak to peak current and V peak to peak the induced voltage.

In a 2-D simulation the end-winding inductance will not be accounted for.

2.1.6.2 Power factor

The ratio of real power to the apparent power is called the power factor. It is a dimensionless number between zero and one. Real power is the capacity of the circuit to perform work in a particular time. Apparent power is the product of the current and voltage of the circuit. Due to energy stored in the load the apparent power will be greater than the real power.

For same active power a load with low power factor will draw more current compared to a load with high power factor. High currents increase the losses in the distribution system, and require larger wires and other equipment. Because of the costs of larger equipment and wasted energy, electrical utilities will usually charge a higher cost to industrial or commercial customers where there is a low power factor.

For a DD PMSG the power factor affects the choice of converter. A low power factor implies that the converter must be able to handle more reactive power.

The power factor for a generator is calculated assuming the current directly in the q-axis hence in phase with the back emf. To calculate the output voltage and the power factor, cosφ, one uses the resistance and the reactance of the generator. A vector diagram visualizes the procedure in Fig. 2-5. [21]

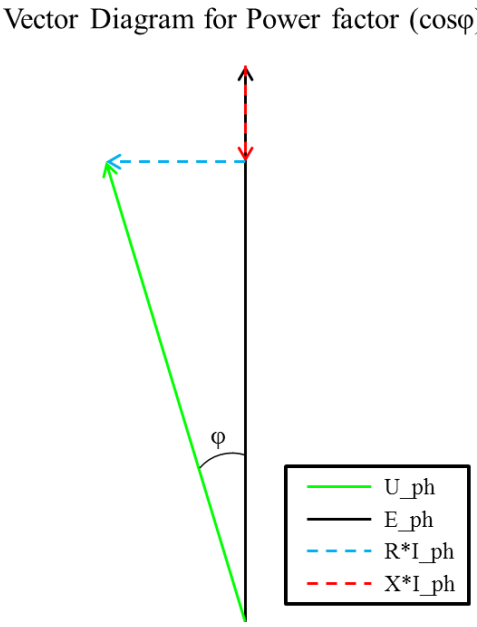

Fig. 2-5 Illustration of vector diagram for power factor.

2.1.6.3 Converter

This section will handle converters, how they control and interact with the PMSG. A larger chapter on wind turbine control and brakes can be found in Appendix 0.

A brief introduction to different power electronic elements that are used in converters for wind turbines is given below. There are diodes, silicon-controlled rectifiers (SCRs also known as thyristors) and gate-turn-off thyristors (GTOs) and power transistors such as the insulated-gate bipolar transistors (IGBTs). Diodes have one-way valves, SCRs are diodes which can be turned on by an external pulse but only turned off when the voltage across them reverses and GTOs are basically SCRs which can be turn on and off. Transistors as the IGBTs require the gate signal to be continuously applied to stay on. The present trend in the wind power industry is to use IGBTs. [22]

In a PMSG the frequency is directly dependent on the number of poles and the rotational speed and the voltage can no longer be controlled because of the constant magnetic field. Therefore frequency and voltage have to be controlled elsewhere. They are controlled in the

converter consisting of a rectifier and an inverter, the drive-train including the converter is illustrated in Fig. 2-6. [22]

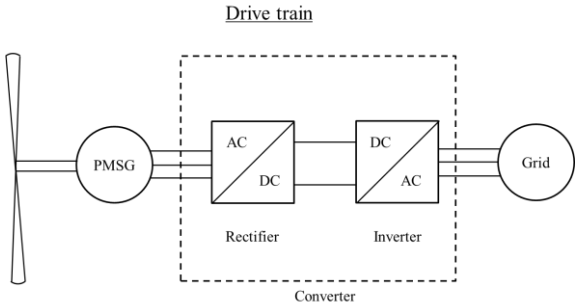

Fig. 2-6 Illustration of the drive-train of a wind turbine with a PMSG, converter an connection to grid.

As in Fig. 2-6 the AC output is first rectified to DC, using either SCR, which can control voltage output, or diode-bridges, which cannot control voltage output. The DC-link is connected to an inverter which inverts the DC back to AC. The inverter controls the output frequency, which is set to the grid frequency, and depending on which rectifier used, it may or may not control the voltage output. [22]

The inverter typically consists of circuit elements that switch high currents and control circuitry, coordinating the switching of the elements. There are two main inverter categories; voltage source inverters and current source inverters. In current source converters the DC current is held constant. This feature is typically used in high power factor loads. Voltage source inverters operate from a constant DC voltage power source. These are normally used in wind turbines. [22]

Two main types of voltage source inverters are used in the wind power industry; six-pulse inverters and pulse width modulation (PWM) inverters. The six-pulse inverter switches on and off of a DC power source in certain intervals, much like the rectifier, except the output is AC instead of DC. The six-pulse inverter normally uses GTOs or SCR as switching elements. The PWM inverter synthesizes an AC signal through high-frequency switching on and off the supply voltage to create pulses of fixed height. The rate of switching is limited to losses that occur in switching process. The efficiency is usually 94 % and they normally use IGBTs or GTOs as switching elements.

Converters are normally sized for ranges of voltages and currents, and they are often rated in the unit of apparent power, volt-amperes (VA). This accounts for the power factor of machines. Hence it is often the case that the same converter can be used for several different machines with different power ratings. An example of a converter for mid-voltage (~3.3 kV) large wind turbines is ABB's PCS 6000 Wind, which is rated for 3-8 MVA, illustrated in Fig. 2-7. [28]

Fig. 2-7 Picture of ABB's converter PCS 6000 Wind. [28]

2.2 Thermal properties

2.2.1 Losses

The main heat source in a PMSG is the resistive loss in stator windings and iron losses due to hysteresis and eddy-currents in teeth, stator and rotor yoke. Other causes of heat are magnets, bearings and eddy-currents in winding losses. If the heat is not removed it can cause the machine to overheat. This reduces the magnets performance and harms the stator windings.

The windings losses depends on the resistance of the winding, R, which is given in Equation (16).

$$R = \frac{L_w}{\sigma_w A_{cu}} \quad \textbf{(16)}$$

Where L_w is the length, σ_w the conductivity and A_{cu} is the area of the conductor. The conductivity decreases with the temperature. The reference conductivity for copper used in electric machines is normally calculated at 20°C. For a given operational temperature, T_{op}, the conductivity, σ_{op}, is given by Equation (17).

$$\sigma_{op} = \frac{\sigma_{20}(234.5 + 20)}{(234.5 + T_{op})} \quad \textbf{(17)}$$

Where 234.5 implies the point of zero conductivity for copper on the Celsius scale. [24]

In an alternating current machine the conductors will, according to Lenz's law, have so called eddy current losses due the alternating magnetic field. The eddy currents are dependent on the conductor geometry. The power losses due to these eddy currents appear as an increased resistance in the winding. The eddy current losses are often given as a ratio of the normal losses described above. The ratio, Δ_{ed}, has been derived in Equation (18). [25]

$$\Delta_{ed} \equiv \frac{1}{9}\left(\frac{d_s}{\delta}\right)^2 \left(\frac{h}{\delta}\right)^2 \quad \textbf{(18)}$$

Where δ is the skin depth, d_s the slot depth and h is the conductor height.

Because of this relation, conductors are often dived in several strands to minimize Δ_{ed}. It is also possible to twist the windings in a certain way to allow the winding to obtain all electrical positions; this will then optimally cancel all eddy currents. This type of winding is called a Roebel bar. Another version which differs somewhat from the Roebel bar but works on the same principle is called Litz wire.

Iron losses have its hysteresis and eddy current losses due to the alternating magnetic field. These are difficult to isolate experimentally; therefore their combined losses are usually measured. The measured losses are simply called core losses and are usually presented in a table by the manufacturer of the laminations. The core loss tables are based on letting the lamination be exposed to a sinusoidal magnetic field with different amplitudes and frequencies. This then gives a measured loss per unit weight. The core loss, P_{core}, is given by Equation (19). [25]

$$P_{core} = k_h f B_m^n + k_e f B_m^2 \quad \textbf{(19)}$$

Where k_h, k_e are constants for the hysteresis and eddy currents properties depending on the material and dimension. n is a material-dependent exponent between 1.5-2.5, f the frequency and B the magnetic fields amplitude.

2.2.2 Thermal equivalent circuit

Proper heat transfer design is as important as the electromagnetic design in electric machines. It can be a limiting factor when designing machines since the temperature increase during operation decides the maximum output power at a constant load.

There are two important aspects of heat transfer in electric machines; heat removal and heat distribution. Heat removal is done by conduction, convection and/or radiation. Regarding heat distribution, the normal scenario is that the temperature is higher in the stator winding compared to the stator yoke, since the windings often have higher heat dissipation.

Heat transfer is however a complex problem. The problem is three-dimensional which implies that numerous elements and parameters have to be accounted for.

Simplification is however possible. One way is to use a thermal equivalent circuit. This method uses the same approach as an electric circuit where the heat flows are equal to currents, temperature differences equal to voltages and conduction and convection resistances to electric resistances. For transient analysis, energy stored in a material corresponds to a capacitance in an electric circuit. [24]

2.2.3 Cooling techniques

Insulation material and magnets are affected by the temperature in the machine. Insulating materials are classified after their ability to resist high temperatures without failures. It is most common to use thermal classes with letter codes. The most common thermal class in electrical machines is F, which withstands temperatures up to 155°C. The use of class B (130°C) and H (180°C) also occur. Machines are often run a class below of the design temperature, for instance a machine with thermal class F often runs at 130 °C (class B), this increases the life-time of the insulation. [24]

2.2.3.1 Indirect cooling

Motors and generators below 100 MVA normally apply indirect cooling. The reason for the term “indirect” is related to the medium never being in direct contact with the conductors. There are two types of indirect cooling systems, with and without recirculation. The one without recirculation, also known as *open ventilated*, draws air from the surrounding environment. The system is equipped with filters to prevent moisture, dust and particles entering the machine. Recirculation systems are often used if the machine needs further protection from the elements. These systems are equipped with heat exchangers. In air-systems an air-to-water heat exchanger is often used to cool the heated air. [29]

The recirculation air-cooled machines can have cooling in axial direction when the air flows over inner rotor, air gap and outside of the stator. The cooling could however be applied in both axial and radial direction. The machine is then segmented so that air can flow in to the rotor and then out in radial direction into the stator. A radial ventilated machine is illustrated in Fig. 2-8. [30]

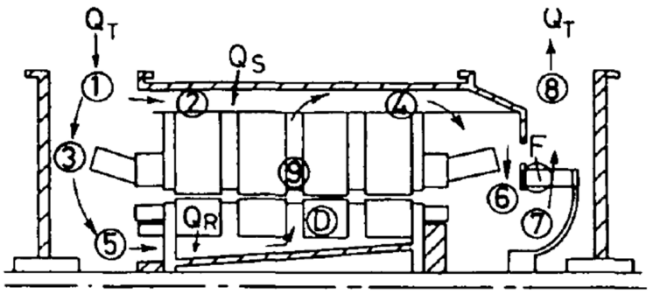

Fig. 2-8 Illustration of a radial ventilated machine. The air enters (1), flows behind stator (2) or over end-winding (3) into the rotor (5) through the slits (9), then leaves over end-windings (6) and flows out (8). [30]

For larger turbo generators, hydrogen gas is often used as a cooling medium since the molecules are smaller and lighter than oxygen, thus giving a lower windage loss. Hydrogen gas can also transfer more heat compared to oxygen gas. These advantages make it profitable to use hydrogen cooling although the system is more expensive. The generator needs to be of a certain size to benefit from hydrogen cooling. This size has been disputed, but in general machines rated with more than 300 MVA uses indirect hydrogen cooling.

Indirect cooling can also use water as cooling medium. This system has ducts, often in or at the surface of the stator yoke, where the water is lead through. [29] One example of these ducts is illustrated in Fig. 2-9.

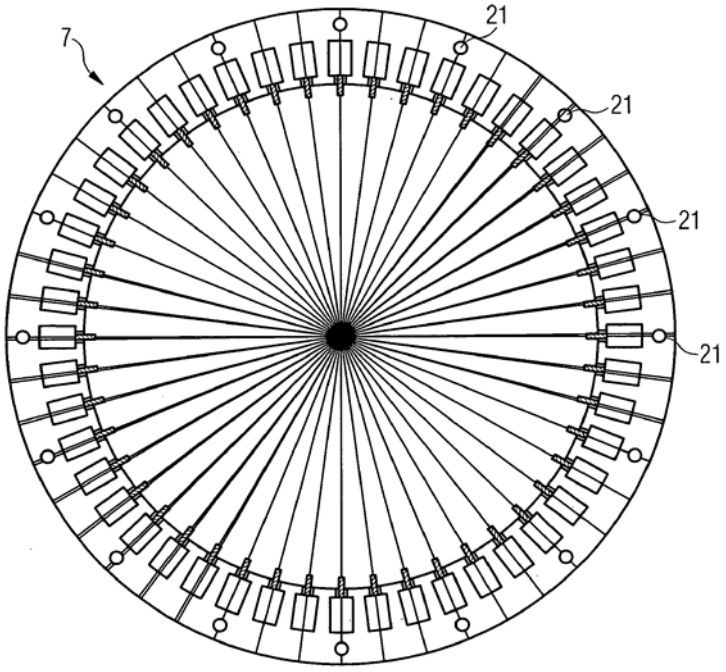

Fig. 2-9 Illustration of machine with ducts (21) in stator yoke (7). [31]

2.2.3.2 Direct cooling

When machines have intense heating, so called direct cooling is applied, either with water or hydrogen gas as medium. The machine could then use hollow copper conductor bars where pure water or hydrogen gas can pass through as in Fig. 2-10. [32] This system is more efficient compared to indirect cooling since the heat is directly removed from the main heat source. [29]

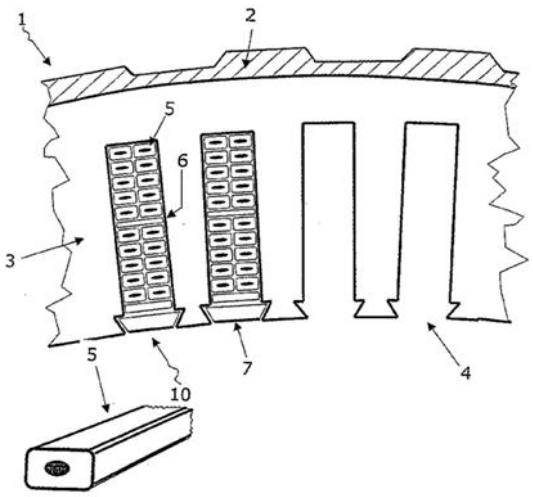

Fig. 2-10 Illustration of direct liquid cooling with hollow copper bars (5). [32]

2.2.3.3 Empirical relations

Convection related heat transfer problems can often be difficult to solve by analytical calculations. Formulas which are useful for certain forced-convection problems have been developed from experimental data. These formulas are based on empirical correlations between the flow processes, based on significant parameters such as Reynolds (Re) or Prandtl (Pr) number, and geometry features. [33]

The Nusselt number (Nu_d) for heat transfer in fully developed turbulent flow in smooth tubes is given by the Dittus-Boelter correlation, which is shown in Equation (20).

$$Nu_d = 0.023 Re_d^{0.8} Pr^n \qquad (20)$$

Where Re and Pr are calculated at average fluid bulk temperature. The exponent *n* equals 0.4 when heating and 0.3 for cooling the fluid. Equation (5) is valid for fluids with Pr number ranging from 0.6 to 100 and Re numbers ranging from 2500 to 125 000. [33]

2.3 Classification of drive-train and cooling technologies

There are many challenges regarding generator design which need to be met, such as integration into the nacelle (“generator house”), cooling system and segmentation and logistics of the generator. When designing a new wind turbine generator it is therefore important to investigate solutions that are used in the industry and the possible upcoming ones. This is not always obvious due to the high secrecy and the importance of protecting ideas from being stolen. It is also important to make sure that the chosen concept is not patented by another company.

2.3.1 DD generator integration into nacelle

Integration of the generator into the nacelle or to the wind turbine is important for installation, maintenance and cooling. There are several ways the DD generator can be integrated to the nacelle. Table 2-5 it is presented different company concepts and solutions for integrating the DD generator.

Table 2-5 A summary of different integration techniques for DD generator.[2]

Company	Solution
Back of nacelle	
GE • Generator placed in the back of nacelle, similar to geared solutions.	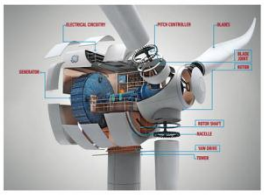
Between hub and tower	
Enercon • Attaching the generator on the shaft between hub and tower. • Use EM instead of PM.	
AWE • Picture display mounting of generator.	
GE	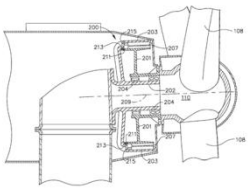
Large diameter bearing instead of shaft	
Leitwind • Placing rotor directly on bearing, hence no shaft.	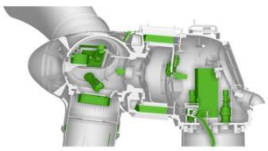
XEMC Darwind • Same as above.	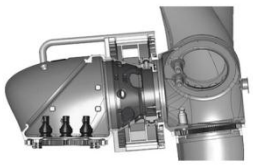
Inside hub	
Non-commersial solution • Not announced to be used by any large company.	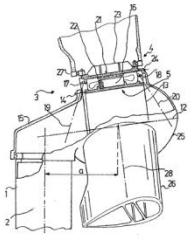

[2] References: GE [10], Enercon [8], GE [41], AWE [7], GE [42], Leitwind [13], XEMC [16], Non-commerical [43].

2.3.2 Companies cooling solutions

Table 2-6 present different company cooling solutions for a wind turbine generator.

Table 2-6 Summary of different companies cooling solutions.[3]

Company	Solution
Passive cooling	
a) Lagerwey b) Northern power c) Leitwind d) XEMC Darwind • Attached fins on generator for better heat transfer to ambient air.	
Forced air-to-air cooling	
Siemens SWT-3.0-101 • Closed cooling system. • Use on-top cooler heat exchanger to cool primary system with ambient air.	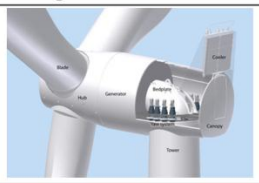
a) Wobben Aloys b) XEMC Darwind • Use tower as heat sink to cool primary system with ambient air. • Example on Enercon's E-66.	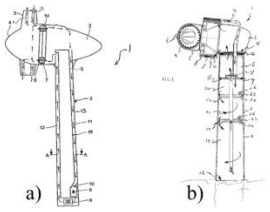
Rolic Invest Sarl • Fan inside hub. • Deflector body inside generator which forces air close to the rotor.	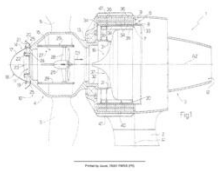
Forced air-to-liquid cooling	
The Switch • Supplier of generators to Goldwind, Dongfang and GE. • Closed air radial ventilated cooling system. • Use liquid heat exchanger to cool primary system. Liquid is cooled with ambient air. • More effective compared to air heat exchanger.	
Liquid cooling	
Vestas V112-3.0 • Liquid primary system cooled by air heat exchanger. • Use CoolerTop to cool primary liquid system.	
NEG Micon AS • Use liquid-to-liquid heat exchanger. • For off-shore wind turbines.	

[3] References: Lagerwey [12], Northern Power [14], Leitwind [13], XEMC [45], Siemens [15], Wobben Aloys [44], Rolic Invest Sarl [46], The Switch [41], Vestas [43], NEG Micon AS [48].

For a better overview of both integration and cooling techniques, chosen companies are summed up in Table 2-7.

Table 2-7 Summation of different integration and cooling techniques for chosen companies.

Generator DD Integration and Cooling Techniques					
Integration Technique					
Placement	Behind Tower	Before tower		Shaftless	
	Inner rotor		Outer rotor	Outer rotor	Inner rotor
	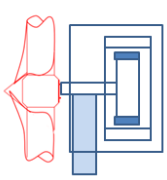	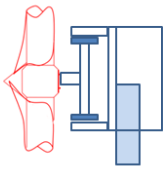	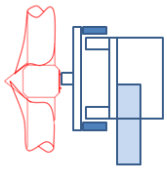	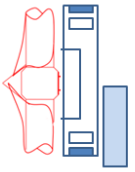	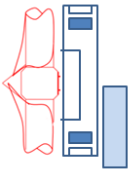
Cooling Technique – Primary to secondary system (secondary to ambient air)					
Liquid to liquid		Enercon			
Air to Liquid	GE, The Switch	Goldwind, The Switch	Dongfang, The Switch		
Air to Air		Enercon	Siemens		
Passive Air		Lagerwey, Northern Power		XEMC Darwind	Leitwind

2.4 Segmentation and logistics of DD generator

For a large radial flux machine, the stator core normally consists of stator lamination segments that are placed sequentially to form a round stator. The laminations are placed so that the segment ends are overlapped in order to create a magnetically continuous stator core. Assembling a stator in such manner requires an extremely firm and rugged support structure.

Low-speed DD wind turbine generators rated 2MW and above are large diameter machines, usually in the range of 5-6 m, and have a high weight, typically in the range of 80-100 metric tons, assuming a steel construction. Due to the large diameter there are only a few factories in the world that are capable of manufacturing such large machines in one piece. With an intensive expanding market the manufacturing capacity cannot supply the wind turbine market. [20] Hence there is an incentive for segmenting the machine to smaller pieces allowing a simpler manufacturing.

Another problem with the size is the transportation of the generator. A trailer or a train might not be able to transport the generator due to the limiting number of routes to choose from.

A double-layer DW can be sectioned by leaving half empty slots in start and end of each sectioned, as in Fig. 2-11. This will however lower the machine performance since the overall slot fill factor will drop. [20].

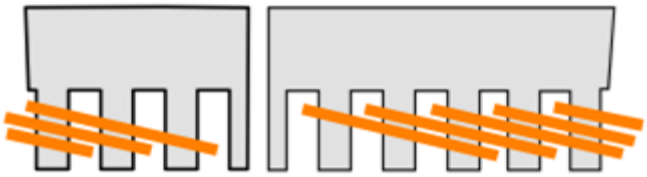

Fig. 2-11 Illustration of how the last slots are half-filled. [20]

A single-layer machine, either DW or CW, has so called broken chain and could theoretically be sectioned where the chain is broken. This was explained in chapter 2.1.4.1 and illustrated in Fig. 2-4.

2.5 Design tools

2.5.1 SmartTool

SmartTool is an analytical Matlab-based software developed by SmartMotor AS. It can calculate a CW-machine based on different geometrical and electrical parameter inputs, such as outer diameter, rated power, rotational speed, voltage level, number of poles and slots, etc. The tool can optimize different machines by varying parameters to achieve high efficiency, low weight, etc.

SmartTool has direct link to Comsol Multiphysics where more accurate calculations can be executed once a machine has been chosen. It makes design and evaluation of machines a rapid process, which allows the designer to optimize different ideas and designs. [21]

2.5.2 Comsol Multiphysics

When estimating the performance of a machine, analytical calculations are not accurate enough. Design calculations for coil inductance, air gap flux and magnet leakage, iron losses, back-emf and cogging torque are difficult to evaluate. They should be complimented with finite element analysis (FEA) for better accuracy.

FEA is a numerical technique for solving partial differential equations (PDE) as well as integral equations. The solutions either solve a steady state problem by eliminating the differential equation completely, or reproducing the PDE as an approximating system of ordinary differential equations (ODE). The ODE's are evaluated by numerical techniques such as Euler's method, Simpson, Runge-Kutta, etc.

Comsol Multiphysics is a FEA-simulation software which facilitates all steps in a modeling process. In Comsol, custom definitions of geometry and meshing are possible. Physics can also be specified to fit the purpose. The results can be visualized, with illustrations, graphics and numbers after the multiphysical problem is solved. [34]

3 Methodology

In part one a control model will be designed. This will allow validation and testing of new updates and improvements, explained in chapter 3.1.1 and 3.1.2.

In part two a comparison of the CW- and DW-generator will be carried out. In the comparison results from part one will be used. The basis of the comparison is explained in chapter 3.2.

All scripts will be Matlab-based and all simulations are time-dependent, performed in 2-D in Comsol Multiphysics 3.5, based on fundamental electromagnetic equations and relations that can be found in electric machine theory.

3.1 Part I

3.1.1 Geometry script update

An important aspect in machine design is optimization. In order to achieve a good optimization the simulation must be trustworthy.

One objective of SmartTool is to draw the machine geometry for Comsol through a Matlab-link. It is vital that the parts of the machine are defined correctly so that physical FEA calculations can be set up automatically for each part.

In SmartTool the geometry and FEA are adapted for SmartMotor's own patented solutions for CW-machines. It is however desirable to draw the geometry for DW-machines to be able to design more machines, hence finding the most optimized solutions for the application in question.

For the CW geometry all the slots were designated as one single object, this is possible since the winding layout always follows a known pattern. For DW-machines the winding layout does not always follow the same pattern. A new geometry script that could handle both CWs and DWs was developed. It was suggested to have following features:

- Designate each phase with its polarity as its own object based on the given winding layout. For a 3-phased machine this means 6 objects.
- Handle 3-phased machines, which is the most common machine for wind power applications.
- A secondary script finds shortest possible sequence for the winding layout, which is based on both the base winding layout and Comsol's limitation of number of sections. The small section allows faster FEA simulations.

The idea of the geometry update is presented in the block-diagram in Fig. 3-1.

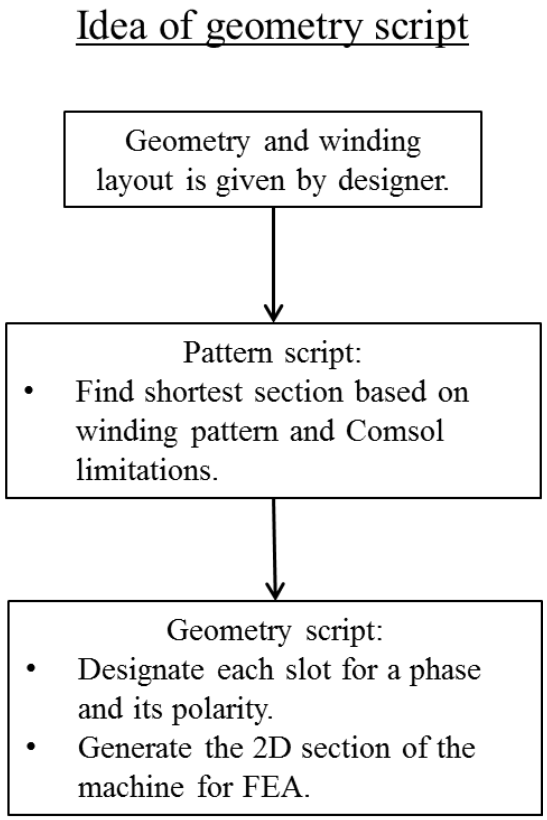

Fig. 3-1 Illustration of block-diagram for the geometry script in update of SmartTool.

3.1.2 New iron loss calculations

Iron losses are according to Equation (19), dependent on the B-field, the frequency and the material properties. Based on the material properties given by the lamination manufacturer, a loss function can be created, which extrapolates values for certain amplitude of the B-field and its frequency.

In a CW-machine the B-field is assumed to be close to maximum around a tooth since there is about one tooth per pole. Therefore stator losses can be evaluated in the area surrounding the tooth and rotor losses between two poles. This method will be referred to as "old method". The idea of the used areas for a DW-geometry is illustrated in Fig. 3-2.

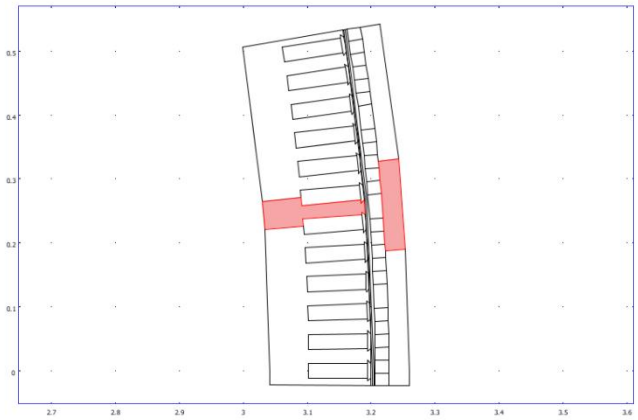

Fig. 3-2 Illustration of areas which is used in the old method for iron loss calculations.

As a DW-machine has several teeth per pole, the B-field in the tooth and the yoke could have maximum at different times. The B-field could also contain higher harmonics.

One method to get more accurate results is to mark an area in the yoke and one tooth which have similar phase for their B-field. This is however a time consuming process and still only a fair approximation. Hence, it is suggested that a new iron loss calculation approach is needed. The new method needed following features:

- Evaluates the B-field in each element, instead of specified area.
- Converts the B-field into a signal, meaning that the values vary around zero, to be able to perform the Fourier analysis. This is a result of that Comsol normally return the absolute value for the B-field. The script will need to use the B-field's x- and y-component. The B-field will need a reference direction into where its values can be aligned to in order to create the signal for each time step.
- Performs a Fourier analysis on the signal to account for the harmonic content. The evaluation will be sent to the same loss function, based on the manufacturer's loss table, which then calculates the total loss based on the lamination properties. This is illustrated in Fig. 3-4. [35]

With the new method it is not necessary to go through the tedious process of choosing suitable areas. The results will be more precise and the accuracy increases for loss calculations. It is applicable in both DWs and CWs. The idea of the new method is illustrated in Fig. 3-3.

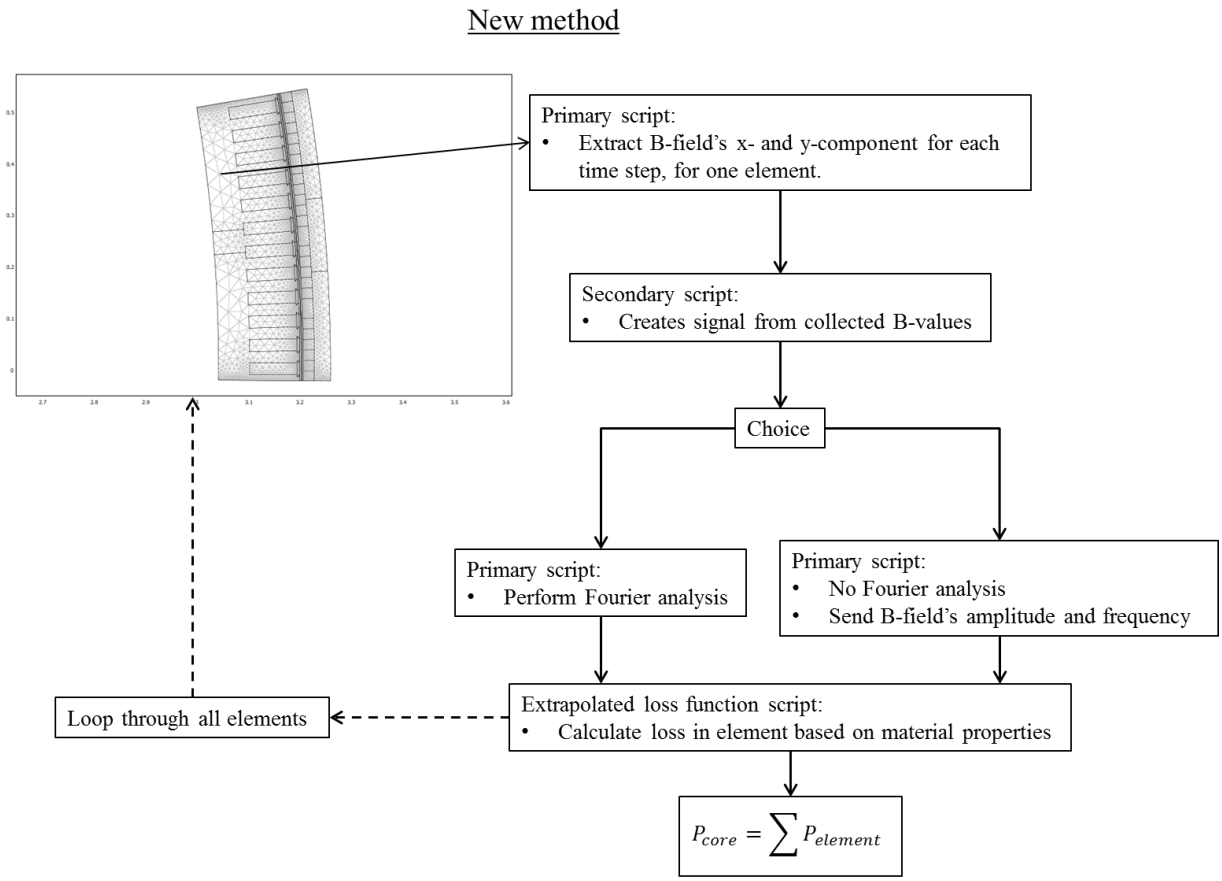

Fig. 3-3 Illustration of the new method for iron loss calculation.

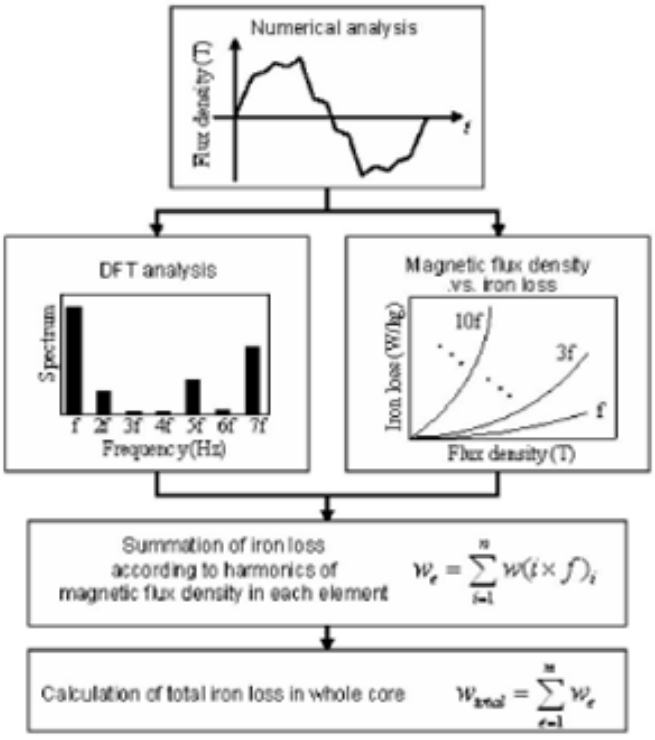

Fig. 3-4 Illustration of how the primary script will account for higher harmonics. [35]

3.2 Part II

3.2.1 The comparison

The report compares a DW-generator to CW-generator based on the simulation results.

The DW's geometry is supplied by SmartMotor. [21] As the geometry is known and the torque is proportional to the current, the current will be chosen to meet the required torque.

A CW-machine will be designed with SmartTool to achieve an optimal design.

3.2.1.1 Assumptions

A literature study was carried out on papers that have compared CW- and DW-machines. The result from this study, found in Appendix A.2, will be used to make a fair comparison. Certain parameters will be kept constant for both machine types, while others are allowed to be different as the machines have different advantages. The general assumption is that the CW-generator must fit in the same nacelle as the DW one.

The parameters which will be used on both generators are:

- Outer diameter: Will be kept constant as both must fit into the same nacelle.
- Active length with end-windings: Will be limited to the DW-generator as both must fit into the same nacelle. The active length with end-windings gives a good indication of the real length of the generator compared to only the active length.
- Air-gap length: Will be kept constant to have same tolerance in the manufacturing process.
- Magnet thickness: Will kept constant to have the same magnetically air-gap length.
- Rated mechanical power: Will be kept constant as both are designed for the same turbine.
- Magnetic remanence: Is assumed to be 1.27 T, which is a state-of-the-art Neodymium magnet. [21]
- Lamination iron: Is assumed to be lamination called M800-50A. Based on previous designs. [21]
- Litz wire: Is assumed to remove eddy-currents in conductors which were explained in chapter 2.2.1.

Assumptions regarding the DW-generator:

- Skewing: It is assumed that the DW-generator is skewed, otherwise the winding layout would most likely give high cogging. A significant part of the losses will be in the conductors. Longer slots due to skewing will increase copper losses and reduce the efficiency further. It is therefore suggested that the skewing will be done on the magnets.
- Slot fill factor: The slot fill factor is unknown for the DW-machine. It is however stated to vary from 0.5-0.65 for low voltage machines and 0.35-0.45 for high voltage machines [24]. Based on this, the slot fill factor of the DW-machine is assumed to be 0.5 below the slot wedge, being a medium voltage machine.
- Number of layers: The DW-generator is assumed to have single-layer windings, based on theory from chapters 2.1.4.1 and 2.4. This will allow easier segmentation because of the windings has a broken chain, as in Fig. 2-4 b). The cost of different shaped coils is assumed to be lower compared to lower the performance with half-empty slots. The

winding-layout is not suitable for fractional-slots or slot-pitching which is a common advantage of double-layer.

Assumptions regarding the CW-generator:

- Slot fill factor: The CWs fill factor is based on earlier experience in SmartMotor for similar machines and is assumed to be 0.65 below the slot wedge.
- Current density: The current density will be updated so the CWs winding temperatures are similar to the DWs.

3.2.1.1.1 Thermal analysis

The DW-generator is air radial ventilated, as in Fig. 2-8, and the CW-generator is normally water-cooled. In order to make a proper comparison of the generators thermal properties, the thermal analysis will assume a water cooling circuit for both generators.

The cooling system will place one duct per tooth on the stator yoke surface. A worst case scenario is assumed, where no heat is transferred from either end-windings or stator surface towards air gap to ambient air. The heat from the end-windings is thus transferred through the windings to the stator core and then to the cooling liquid. The calculated temperatures will thus be higher compared to the true values. These simplifications are necessary to limit the scope of this report. The thermal analysis will however provide important comparable information on the DW- and CW-generators.

The thermal analysis will use a thermal equivalent circuit, explained in chapter 2.2.2. With this approach, it is possible to assume a constant temperature of the cooling medium in the calculations. Since a constant temperature is assumed, it is common to assume a low temperature rise (ΔT) of the fluid. [24] The cooling water is assumed have a ΔT of 10°C.

The inlet temperature for the water is assumed to be 45 °C to account for a high outside temperature. The necessary data about the fluid is collected at the middle temperature, 50 °C.

The cooling system is assumed to have a flow of 500 l/min and the same pressure head in both generators.

The thermal analysis will be performed on the stator since the main part of the losses will be located there. The copper is assumed to be a solid piece surrounded by mica insulation, dependent on the fill factor. This does not reflect the actual design as copper is divided in several turns and strands; it will however give an acceptable approximation for the thermal analysis.

Material and liquid properties which are used in the thermal analysis are given in Table 3-1.

Table 3-1 Thermal properties of materials at 300 K if not other is stated. [24]

Material	Thermal conductivity [W/(m*K)]	Density [kg/m^3]	Specific heat capacity [J/(kg*K]	Dynamic Viscosity [Pa/s] 10^{-3}
Iron (1% silicon)	40	7700	460	-
Copper	394	8960	385	-
Mica (insulation)	0.5	2800	-	
Water (50°C)	0.6	988	4182	0.547

3.2.1.2 Generator specifications

The geometry, mechanical and electrical specifications for the compared generators are given in Table 3-2.

Table 3-2 Specification of the DW- and CW-generators. [21]

Feature	DW	CW
Geometry		
Rotor outer radius, R_{rio} [mm]	3260	3260
Stator inner radius, R_{si} [mm]	3042	3091
Air gap, g [mm]	6.5	6.5
Wedge depth, d_{sw} [mm]	5	5
Active length, L [mm]	969	1033
Number of poles, N_p	144	176
Number of slots, N_s	432	192
Mechanical		
Mechanical power, P_{mech} [MW]	4	4
Rotational speed, n [rpm]	12.6	12.6
Rotor type	Outer	Outer
Slot shape	Rectangular	Rectangular
Electrical		
Rated RMS voltage, U_n [kV]	3.9	3.9
Frequency, f [Hz]	15.12	18.48
Slot fill factor, k_{cu}	0.5	0.65
Number of layers, N_{lay}	1	1
Number of turns, N	6	10

Table 3-3 presents the base winding layouts of the two generators.

Table 3-3 Base winding layouts for DW- and CW generators.

	Base winding layout
DW	A+, C-, B+, A-, C+, B-
CW	A+, B-, B-, C+, C+, A-, A-, B+, B+, C-, C-, A+

The sections for the DW- and CW-generator that are simulated in Comsol are presented in Fig. 3-5.

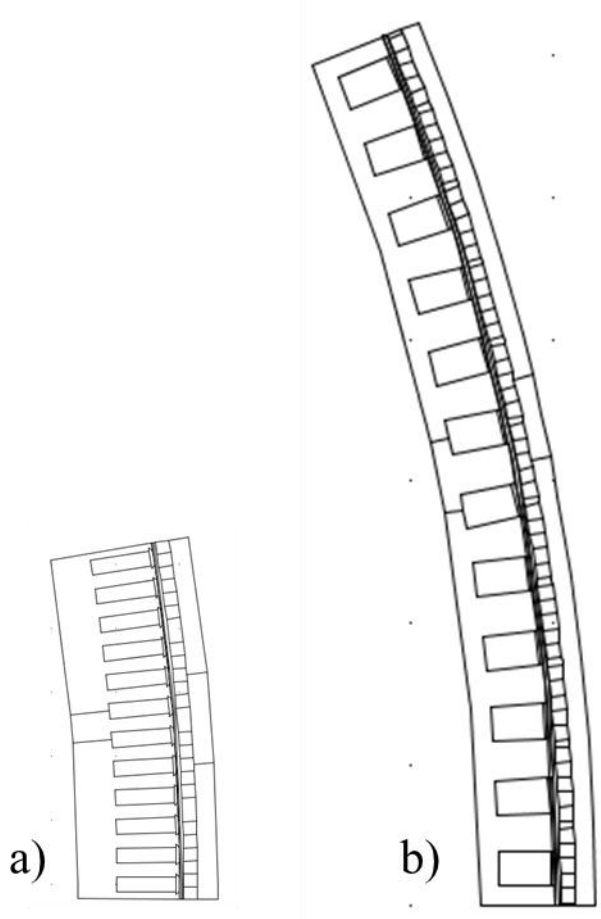

Fig. 3-5 Illustration of a) DW-section b) CW-section that are used in the Comsol simulation.

4 Results and discussion

4.1 Results

4.1.1 Part I

4.1.1.1 Geometry script update

A primary script that creates a DW FEA structure was written. This script was complimented with a secondary script that finds the shortest possible sequence. These two scripts can be found in Appendix B.1 and B.2. The result from the scripts is illustrated in Fig. 4-1.

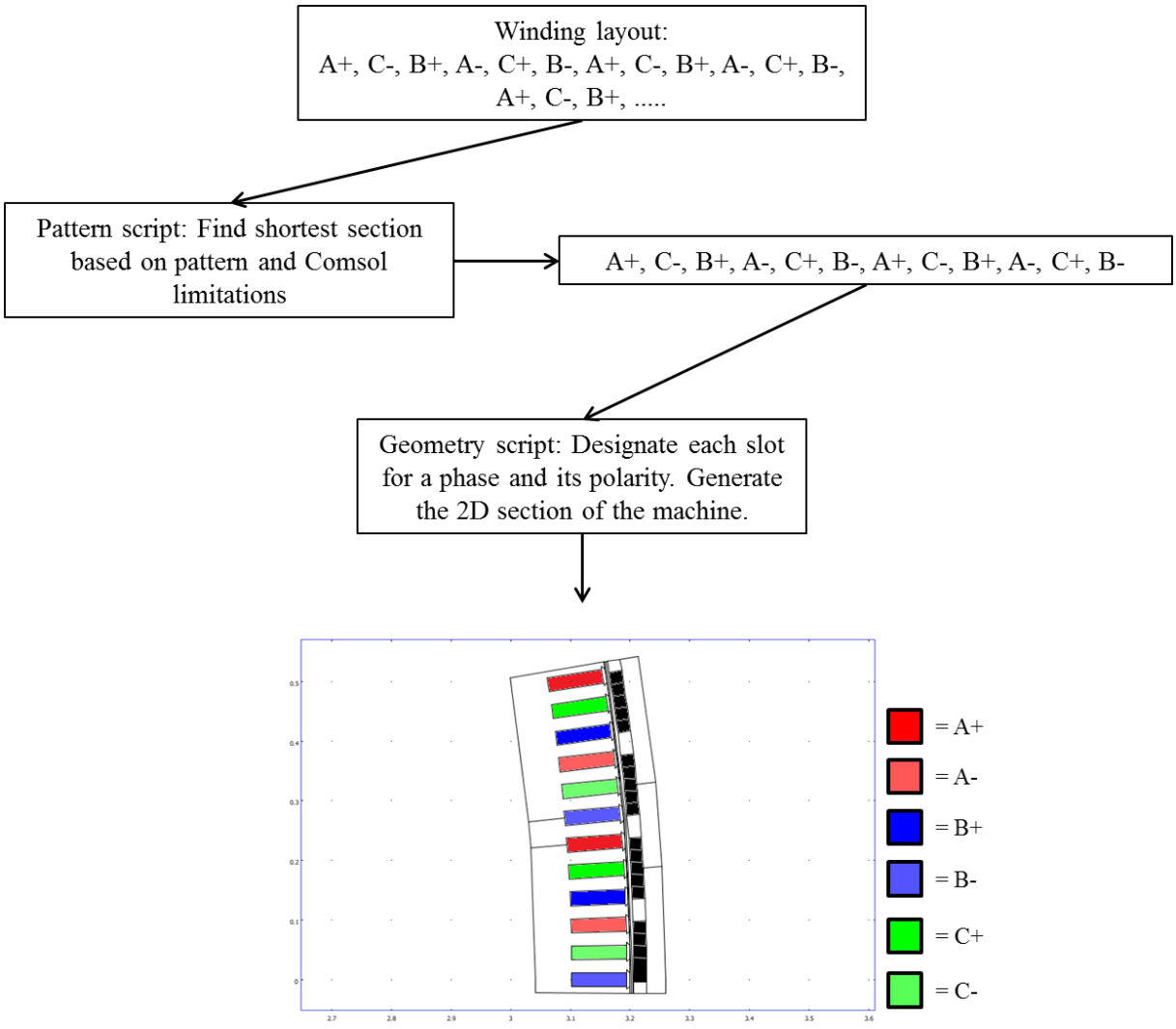

Fig. 4-1 Illustration of the result from the geometry script update.

4.1.1.2 Iron loss calculations

A DW control model was set up by hand in Comsol. Iron losses were calculated based on the old method, that utilizes an area to calculate losses, and the new method, that uses each element. Different areas were used in the old method; this was done in order to investigate differences depending on areas chosen. These areas are numbered 1-6 and can be found in Appendix C.3.1.

The absolute B-field in area 5, is illustrated for each time step in Fig. 4-2, and at time 0 s and 0.01 s in Fig. 4-3.

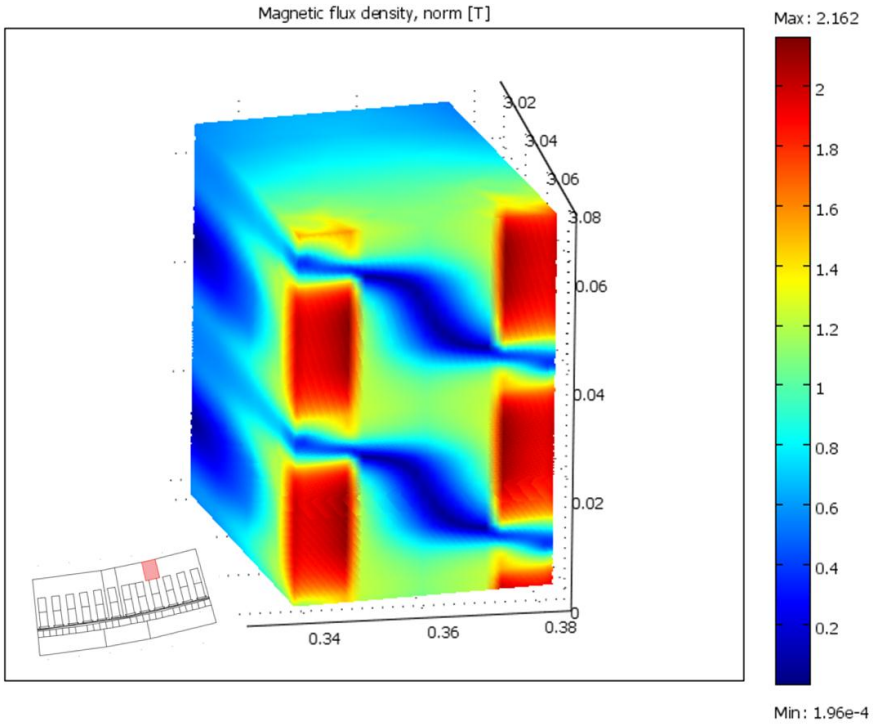

Fig. 4-2 Illustration of B-field in area 5 for each time step. Time is the vertical axis.

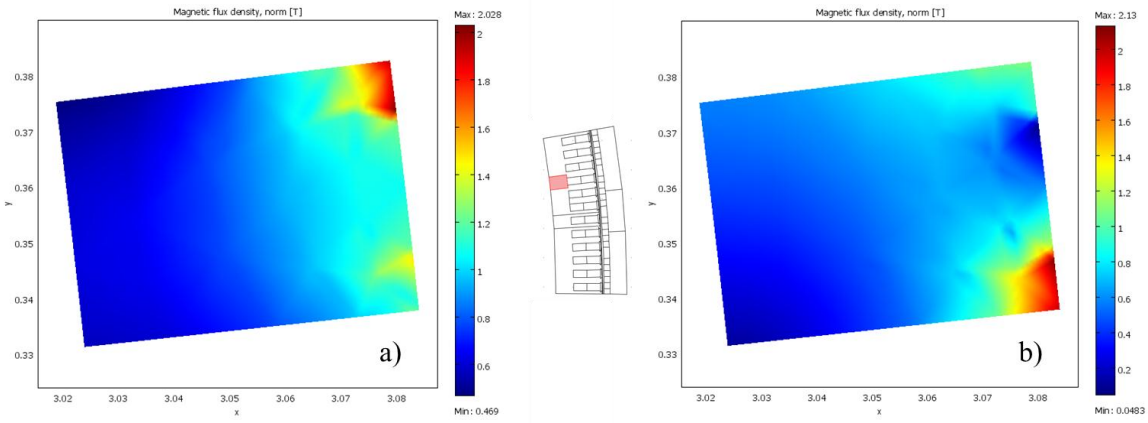

Fig. 4-3 Illustration of the magnetic flux density in area 5 at a) t = 0 s and b) t = 0.01 s.

The results from the new iron loss method are based on a primary and secondary script found in Appendix C.1 and C.2. The result for a random element in the stator, in Fig. 4-4, illustrates how the secondary script creates a B-field signal.

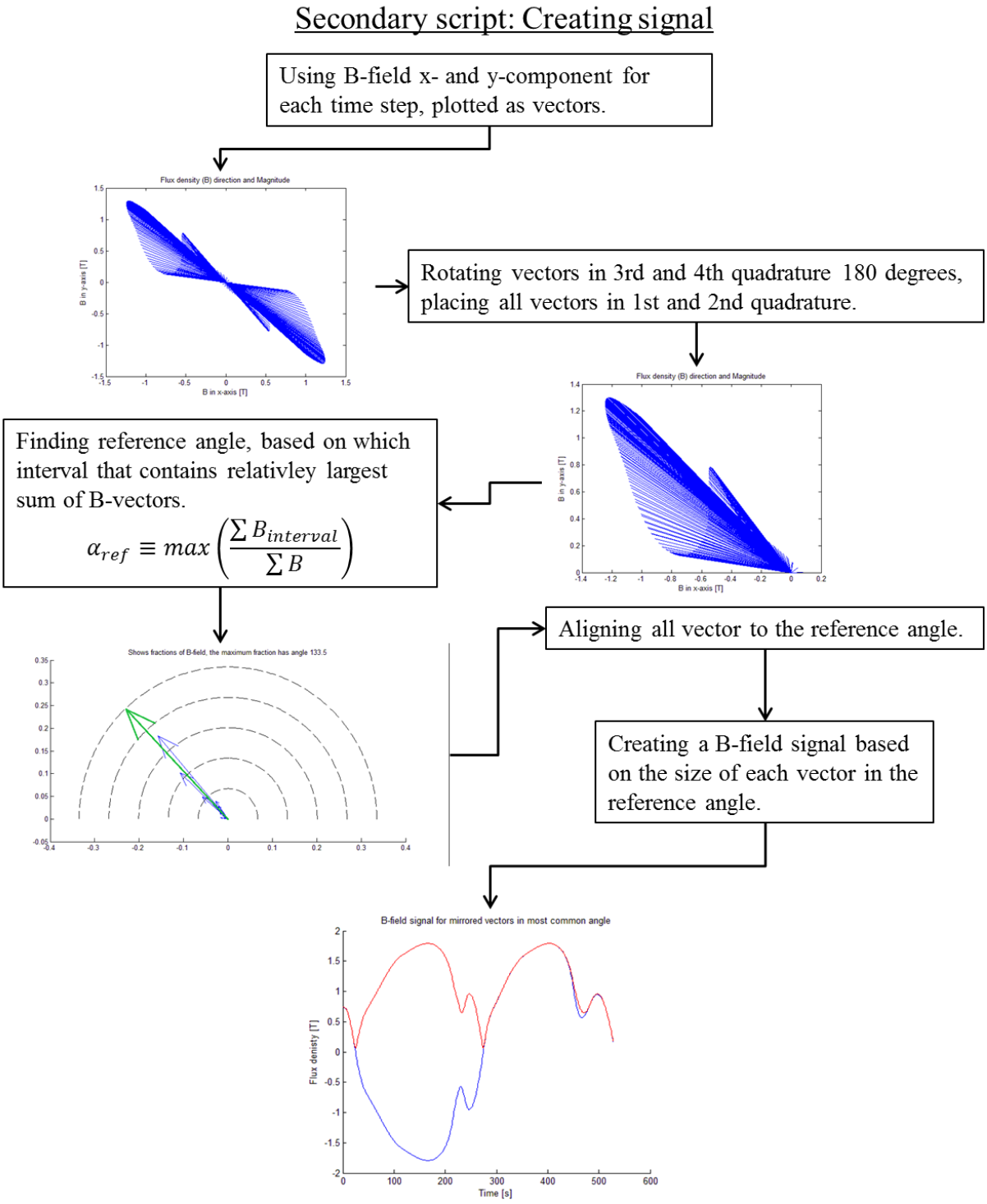

Fig. 4-4 Illustration of the how the secondary script creates a signal from the B-field's x- and y-components. The signal result (blue curve) is plotted together with the absolute value (red curve).

The 1st and 2nd quadrature was divided into intervals of 1 degree. The secondary script used reference angles that were based on which interval that contained:

- The relatively largest sum of the B-vectors, as in Fig. 4-4.
- The relatively largest sum of the B-vectors squared.
- The largest vector, B_{max}.

After the signal was established, it was sent to the primary script. This calculated losses with or without Fourier analysis.

The total stator iron loss results, calculated with both the old method, using different areas, and the new method, using different reference angles, are presented in Table 4-1. Individual iron loss results for area 4 and 5 are presented in Table 4-2. The results from the iron loss calculations can be found in Appendix C.

Table 4-1 Total stator iron loss results for old and new methods.

	Iron loss [W]	**Relative diff. [%]**
Old method		
Area 1	19823	0
Area 2	22134	11.66
Area 3	23810	20.11
New method		
B_{max}	40823	105.93
Rel. most B	41765	110.68
Rel. most B^2	41776	110.74
Rel. most B^2 (no Fourier analysis)	24366	22.91

Table 4-2 Stator loss results of area 4 and 5 individually.

Surface	**Old**	**New, B_{max}**	**New, rel. most B**	**New, rel. most B^2**	**New, B_{max} only 1st harm.**	**New rel. most B^2 (no Fourier analysis)**
Area 4 [W]	41.78	94.21	97.06	97.07	80.66	42.43
Area 5 [W]	13.49	18.39	18.88	18.87	13.61	13.99

4.1.2 Part II

4.1.2.1 No-load EMF-simulations

The electrical properties for the DW- and CW-generators are presented in Table 4-3. The skewing factors are calculated with Equation (9), Equation (10) and from the simulation. Skewing factor from simulation was used in later results.

Table 4-3 Electrical properties of the DW- and CW-generator.

	DW	**CW**
$\mathbf{K_{s\ sinusoidal}}$	0.955	1
$\mathbf{K_{s\ square\ wave}}$	0.83	1
$\mathbf{K_{s\ simulation}}$	0.955	1
$\mathbf{K_w}$	1	0.958
$\mathbf{J_{rms}\ [A/mm^2]}$	3.35	3.0

The phase-emf for the DW-generator is presented in Fig. 4-5 and for the CW-generator in Fig. 4-6. The line-emf for the DW-generator is presented in Fig. 4-7 and for the CW-generator in Fig. 4-8.

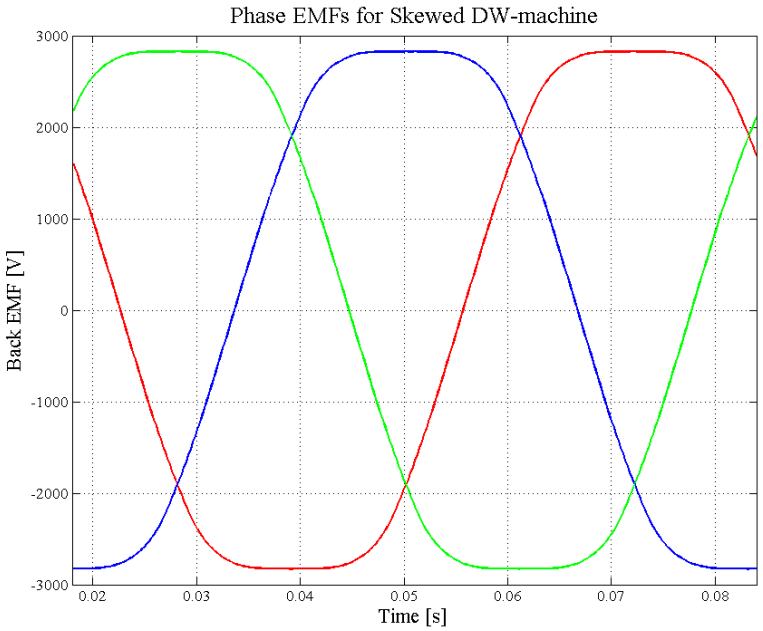

Fig. 4-5 Illustration of DW-generator's phase emf.

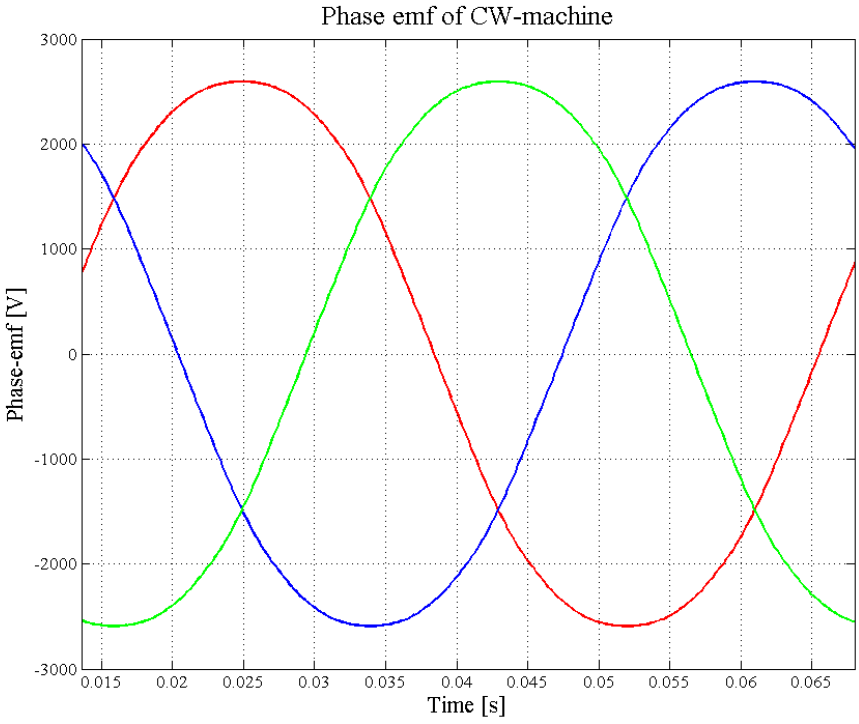

Fig. 4-6 Illustration of CW-generator's phase emf.

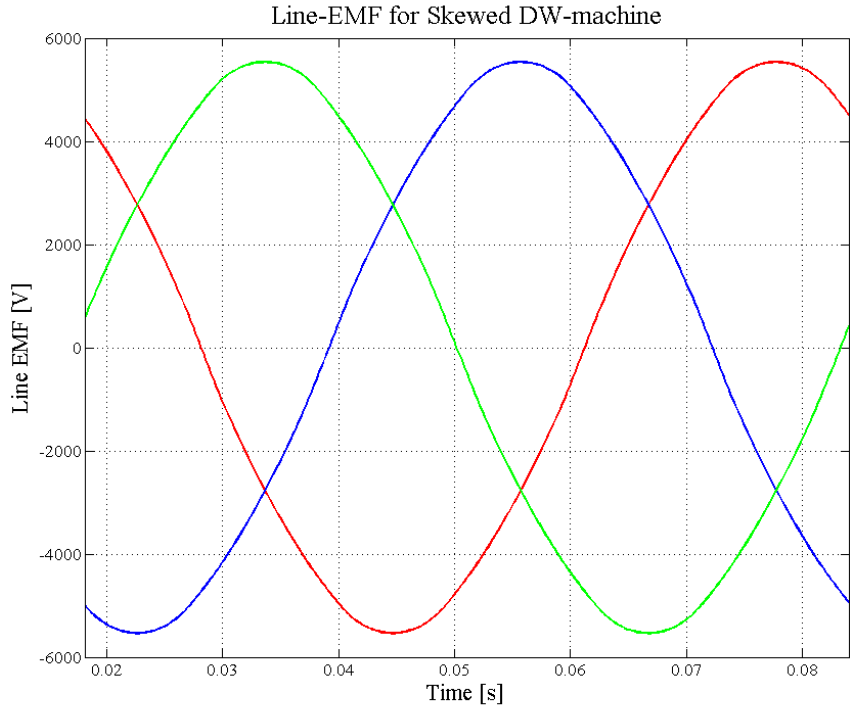

Fig. 4-7 Illustration of DW-generator's line-emf.

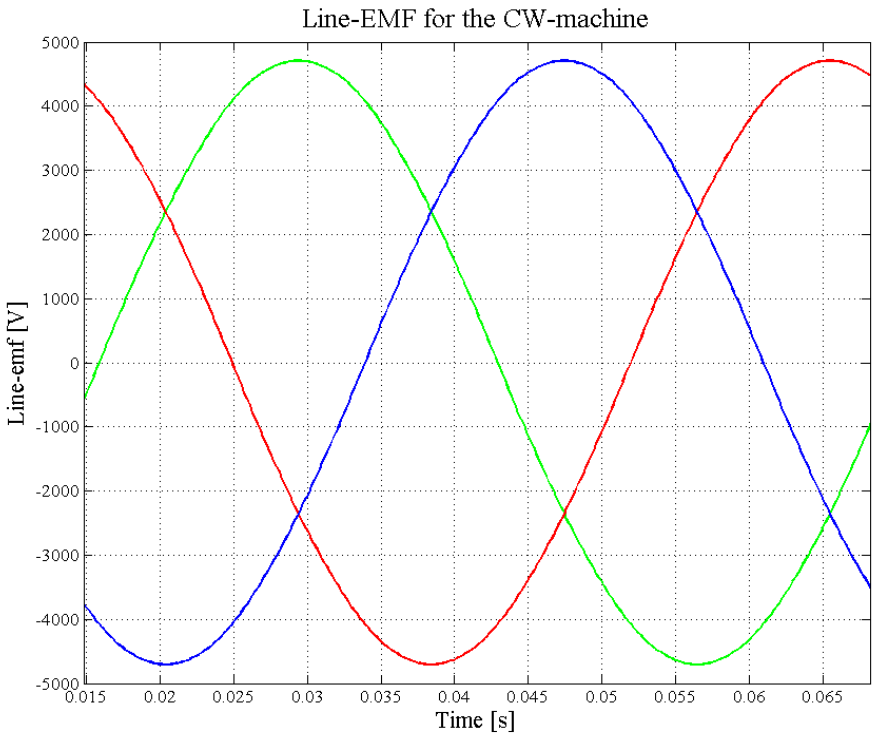

Fig. 4-8 Illustration of CW-generator's line-emf.

The key results from the no-load emf-simulations for the DW- and CW-generators are presented in Table 4-4. More specific plots from emf-simulations can be found in Appendix D.1.1.

Table 4-4 The key results from the EMF-simulation for the DW- and CW-generator.

	DW	CW
Mean Phase peak emf [V]	2827	2593
Mean 1st harm rms emf [V]	2250	1921
Mean Phase THD [%]	10.7	4.5
Mean Line peak emf [V]	5536	4706
Mean Line THD [%]	1.3	0.6

4.1.2.2 Full load-simulations

The magnetic flux distribution at full load is illustrated in for the DW-generator and illustrated in for the CW-generator.

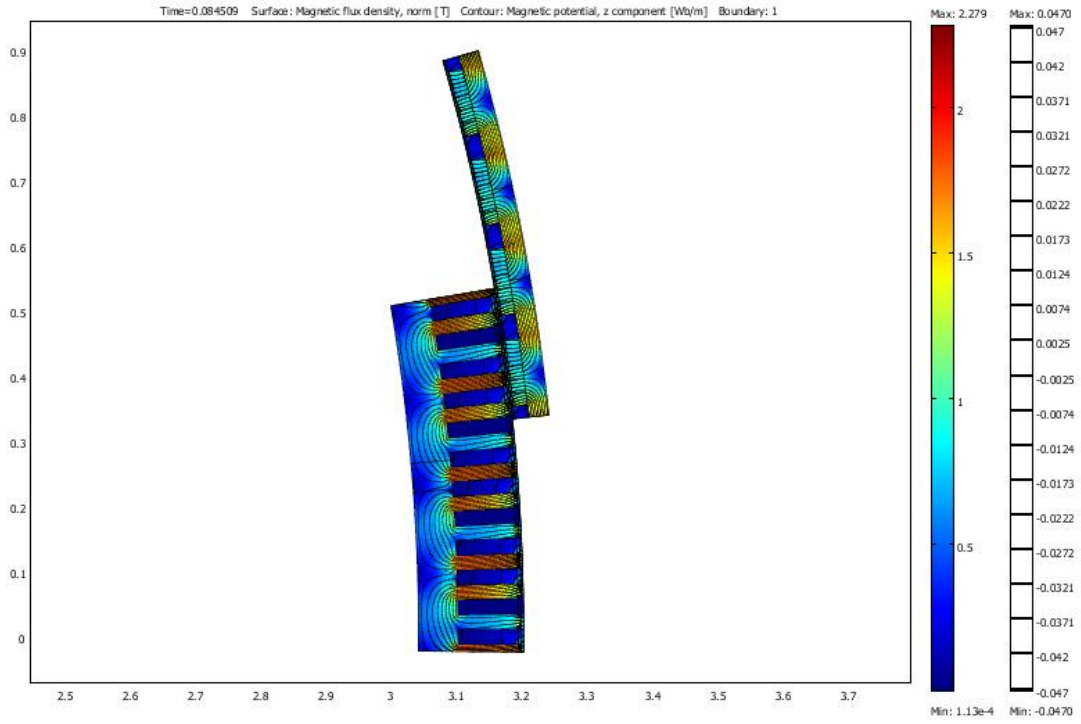

Fig. 4-9 Illustration of B-field in DW-generator at last time step.

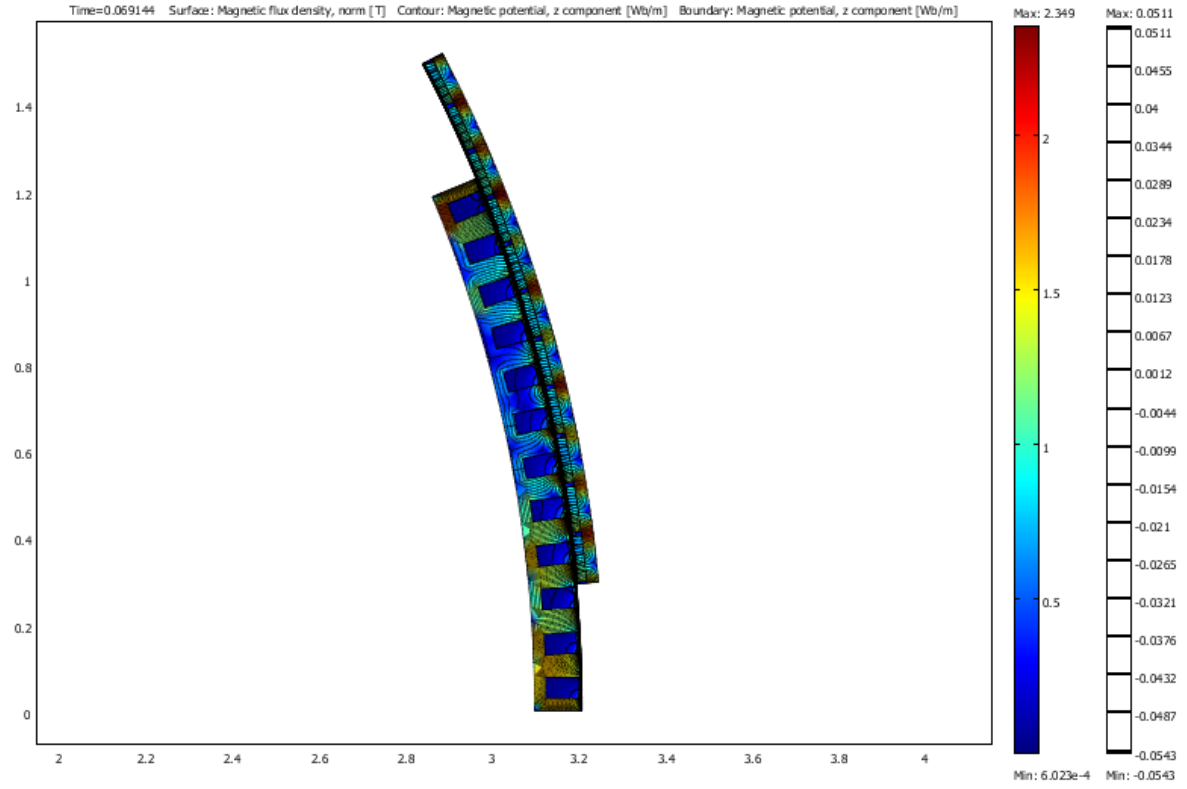

Fig. 4-10 Illustration of B-field in CW-generator at last time step.

The torque ripple p.u. of the DW- and CW-generator is illustrated in Fig. 4-11.

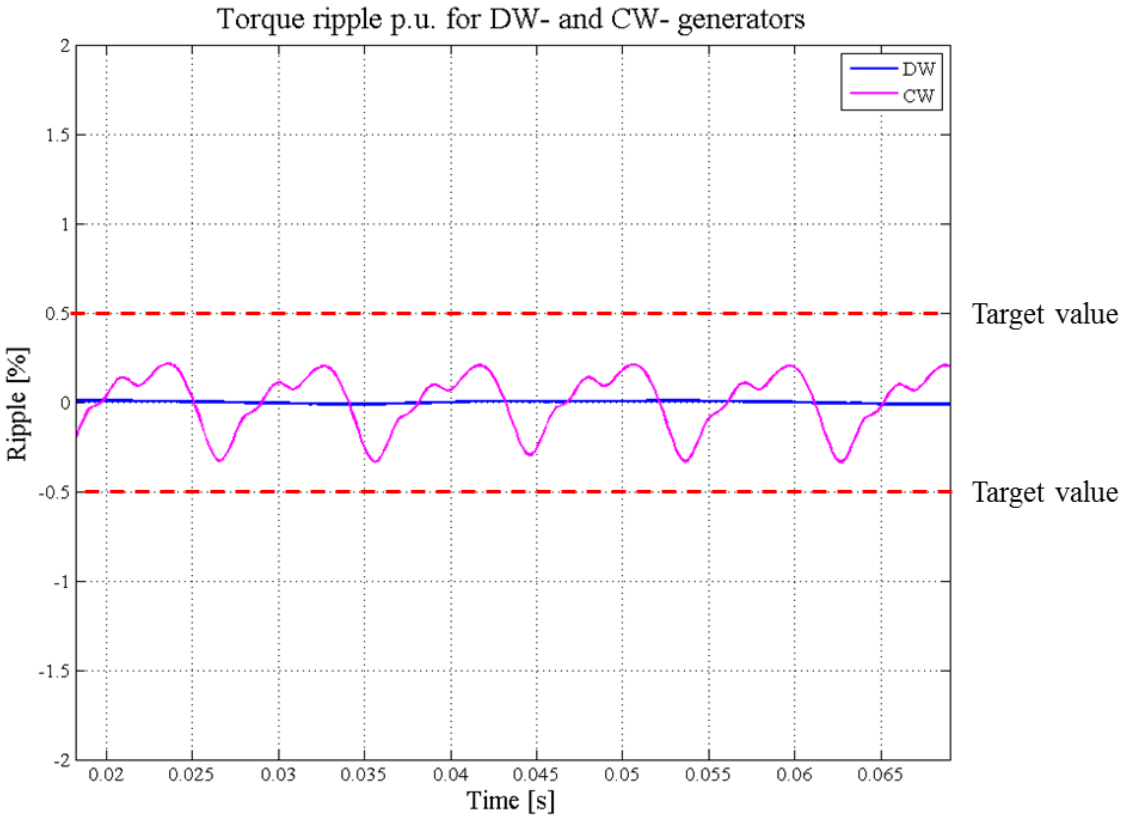

Fig. 4-11 Illustration of torque ripple of DW and CW designs.

The normalized rotor B-field signal for a random chosen element (number 10) in area 6 for the DW and CW is illustrated in Fig. 4-12.

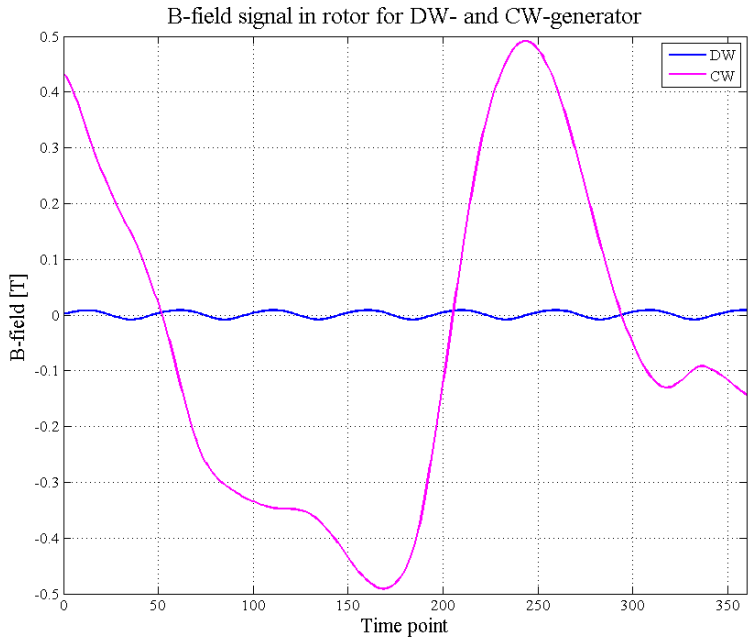

Fig. 4-12 Illustration of B-field signal for element 10 in area 6 in the DW- and CW-generator.

The active weight and apparent power is presented in Table 4-5.

Table 4-5 Active weight and apparent power of the DW- and CW-generator.

	DW	CW
Active weight [ton]	27	23
Apparent power [MVA]	4.3	4.5

The KPIs are presented in Table 4-6. All detailed results are given in Table D- in Appendix D.1.2.

Table 4-6 KPIs from full-load simulations.

	DW	CW
Efficiency [%]	95.37	96.18
Torque per weight [Nm/kg]	111	131
Power per weight [W/kg]	146	173
Power factor	0.89	0.85
Tangential tension [kN/m^2]	48.3	45.5
Torque ripple p.u. [%]	0.02	0.7
Length with end-windings [m]	1.44	1.19
THD line-emf [%]	1.3	0.6

The two generator's KPIs, except the torque ripple and THD, are visualized in a normalized hexane-diagram in Fig. 4-13.

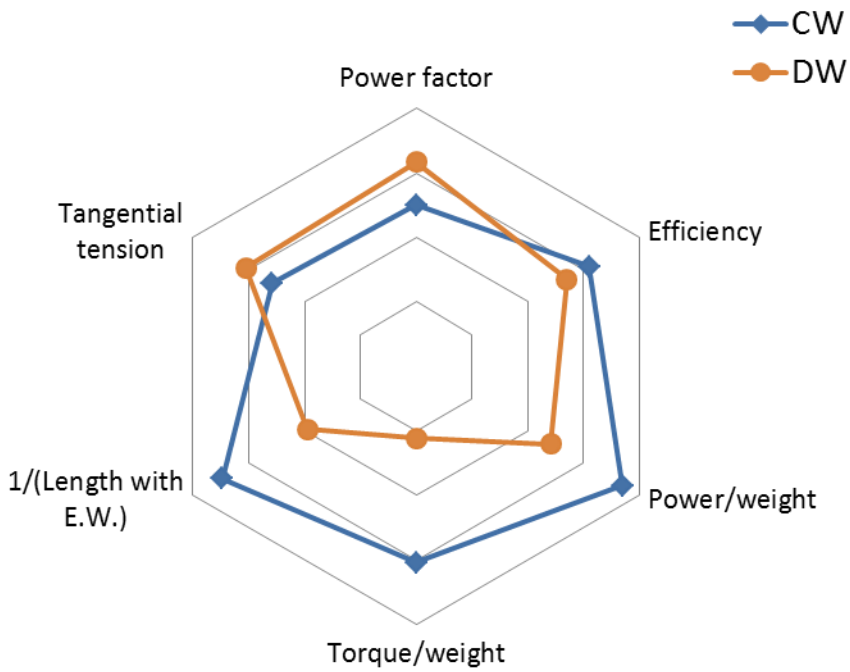

Fig. 4-13 Illustration of the two designs in a normalized hexane-diagram.

4.1.2.3 Thermal analysis

The thermal analysis uses the thermal network model in Appendix E.1. The calculations were performed in a script which can be found in Appendix E.3. The key results from these calculations are presented in Table 4-7, temperatures of all designs can be found in Appendix E.2.

Table 4-7 The key results from the thermal analysis of the DW- and CW-generator.

	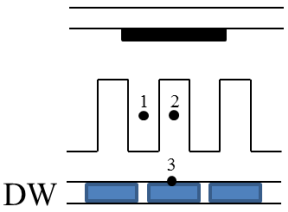	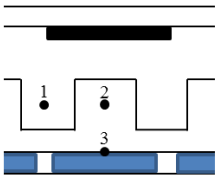
	Losses [kW]	
P_winding	152	120
P_stator	21	20
P_rotor	~0	2
P_magnets	6	11
	Temperatures [°C]	
End-windings	175	173
Slot (1)	140	142
Tooth (2)	108	81
Yoke surface (3)	75	69

4.2 Discussion

4.2.1 Integration and cooling solutions

In Table 2-5 the DD generator is often integrated directly after the hub. This reduces the shaft's length which in turn reduces the weight. It could also be easier to mount the generator, see AWE's solution, compared when placing the generator in the back of the nacelle, as GE's solution. This explains why integrating the DD generator directly after the hub has become a trend in the wind industry.

From Table 2-6 it is clear that Leitwind is not only using passive cooling but also Rolic Invest Sarl's patented solution to cool the generator. The same is true for XEMC Darwind's patented solution where the generator is cooled using the tower as a heat sink. It could therefore be derived that passive cooling might not be sufficient to cool generators of this size, and therefore the wind turbine would need a forced cooling system.

4.2.2 Part I

A discussion about the geometry script and the implementation of the new iron loss method, which mainly discusses matters that are interesting for future reference, is found in Appendix B.3.

4.2.2.1 Geometry script

The new geometry script was successfully implemented. Different winding layouts can now be used and tested, hence a more optimal solution can be found. The designer can save valuable time with this script.

4.2.2.2 Iron Losses

The results in Table 4-1 and Table 4-2 show that the old method has large variations depending on the chosen area. The old method, used on area 3, should however give a good indication on how large the losses are, as it uses an area in the yoke and one tooth that have similar B-field signal. The new iron loss results performed with Fourier analysis returns losses that are almost twice as large, which is not plausible. The main reason is that a Fourier analysis will return the amplitude for each harmonic. This amplitude is likely to be larger than the real amplitude, hence generating a larger loss. It will also add up the losses calculated from the higher harmonics results, which suggest an amplitude and frequency that is not physically there. Therefore this method will be disregarded for accurate loss calculations.

The new method, without Fourier analysis, could however be used to give faster and more accurate loss calculations. The previous way of choosing an area, where suggested B-field maximum occurs, such as area 3 in Appendix C.3.1, is tedious and partly inaccurate. It can be seen in Fig. 4-2 and Fig. 4-3, that this method would miss small differences between each element as the area 5 has maximum values in different locations at different time steps. By calculating the loss for each element one avoids both of these problems. This gives a faster and a more accurate solution. Aligning to the angle with the largest sum B^2 was chosen since the losses will depend roughly on B^2 accordingly to Equation (19).

It is important to note that the script for the new loss method uses zero-crossings to calculate the frequency of the B-field. If the signal contains large harmonics, which can cross zero only to return towards the maximum value instead towards the minimum value, the frequency becomes higher. This frequency is somewhat realistic; however the amplitude for the frequency is lower than for the fundamental frequency, this will in turn lead to miscalculated

iron losses. It is however rare to have large harmonics in the stator yoke, and since the rotor losses are by far the smallest; this problem was neglected in the report.

Another problem with the new iron loss method is negative rotor losses in the DW-generator; this was detected in the iterative design process. The loss function is based on an extrapolated curve which in turn is based on the data given by the manufacturer. The negative values might be a result of the low amplitude of the flux density signal (down to a few mT) in the rotor and that the function cannot extrapolate for these small amplitudes. With these small amplitudes the losses would however be negligible.

4.2.3 Part II

4.2.3.1 Manufacturing

Both machines are in theory easy to segment. The total cost of the coils should however be higher for the DW-generator since it has bent end-windings as in Fig. 2-4 b). The end-windings could either be bent by force or molded into their shape. The DW will also need more coils compared to the CW. These two disadvantages of the DW will favor the CW in the manufacturing process.

4.2.3.2 Losses

The loss results in Table 4-7 suggest that the DW-generator will have lower rotor-core and magnet loss compared to the CW-generator. One explanation could be that in the DW-generator the opposing flux density fields generated by the induced current in each of the copper windings will cancel each other over one pole since the windings are evenly distributed over one pole. For the CW-generator rotor-core and magnet losses are greater due to non-overlapping end-windings. Because of no overlapping end-windings the magnetic flux density field resulting from the induced current will not be canceled over one pole. The field will need to travel further in the rotor yoke. The magnetic field will also be stronger as the field strength is proportional to the number of turns and the current. The rotors normalized B-field result in Fig. 4-12 illustrates this. The B-field in the DW rotor has high frequency due to more teeth, but negligible amplitude. The CW has a lower frequency but significant amplitude.

As the magnets are conductive, this field will cause eddy-current losses in the magnets, hence a higher magnet loss in the CW-generator. Both generators were simulated with laminated magnets to reduce losses. The result could however imply that the laminated magnets in the DW-generator might not be needed. The geometry script was written with the assumption that the machines would need laminated magnets and could not be updated at this stage of the report. The laminated magnets do not however effect on the performance and would thus only be a cost related issue.

The stator losses are smaller for the CW-generator compared to the DW one. The main reasons for this are that the CW has larger slot area which in turn allows higher fill factor. As copper losses are proportional to total winding length, fill factor and current density squared, derived in Appendix F:

$$P_{winding} \propto L_{tot} k_{cu} J^2$$

The higher fill factor allows lower current density for same slot current. As the losses depends on current density squared losses becomes lower with higher fill factor.

The losses are also smaller since the CW-generator has shorter winding length due to lower number of slots and shorter end-windings. The CW has a better utilization of the slots compared to the DW.

4.2.3.3 KPIs

In the iterative design process it was found that the CW-generator needed semi-magnetic slot wedges to lower the torque ripple below the target value of 1 %. If the torque ripple at full load would be above this value, it could cause vibrations in the structure which could lead to failure of the whole turbine. With the semi-magnetic wedges the torque ripple is below the target value and should not cause any difficulties with unwanted vibrations.

Both fractional-slot windings and skewing removes unwanted cogging. The skew and winding factor, in Table 4-5, are kept high in both generators, hence both methods are effective. Notice that the skewing would however not be effective on the CW as it has a lower number of teeth, which would give a low skew factor. This is one example of how the machines have different advantages and must be allowed to be designed in different ways when they are compared.

The torque ripple of the skewed DW-generator is negligible and is expected to be low as it is the purpose of the skewed magnets. It is however unlikely to obtain such a low value which raises questions if the true value of the torque ripple could be found by a 2D-simulation that uses the phase-shift of the skewed magnets to calculate the ripple. The 2D-simulation might not account for everything that happens between the rotor and stator. For a more trustworthy result, a 3D-simulation would be desired but this would however be a very time consuming simulation and too large to be included in the scope of this report.

The phase- and line-emf plots in Fig. 4-5, Fig. 4-6, Fig. 4-7 and Fig. 4-8 gives interesting results.

The DW-generator has a smooth phase-emf but it contains a distinct 3^{rd} harmonic. The 3^{rd} harmonic is however cancelled in the line-emf by a Y-connection. This leaves an almost perfect sinusoidal waveform and a low THD.

The CW-generator's phase emf also has an imperfect phase-emf. This is however removed in the line-emf which returns a nice sinusoidal waveform.

The results in Table 4-4 show that both generators has THD below 2 %, hence the losses due to THD would be negligible.

Both types of generators offer high efficiency. The CW-machine has however higher efficiency, mainly due to lower copper losses explained earlier.

The difference in tangential tension is due to the CW-generator having a longer active length. Both generators offer high tangential tension and are within the target area of 40-50 kN/m^2. The difference between the machines is small and can be considered insignificant.

The CW has slightly longer active length but due to the short end-windings the total length is less compared to the DW-generator. The DW-generator must have longer end-windings because they are bent and overlapping, which can be seen in Fig. 2-4 b). This is an advantage for the CW-generator as the nacelle could be smaller. This allows the CW to have a shorter shaft which in turn reduces weight.

The CW-generator is inside the defined state-of-the-art belt in Fig. 1-2 while the DW-generator is on the borderline. In terms of torque per weight, the CW-generator is superior to the DW. It offers more than 18 % torque per weight of its active material. This is mainly because the CW-machine can have less stator materials. The CW-generator has smaller slot

depth compared to the DW, and as the weight depends on radius squared this cuts significant weight. This is possible because the CW has wide slots which allow it to have a high fill factor and better utilization of the slots.

The result in Fig. 4-9 shows that the DW-generator has a high B-field in the teeth; therefore the number of poles cannot be increased without decreasing the slot area to fit the teeth. This was explained in chapter 2.1.4.5. In a CW-machine this possible since it has a low number of slots. The high pole number gives a shorter magnetic return path which also allows the yoke to be thinner. This is true both for the rotor and the stator yoke. Since the CW-machine does not have equivalent high losses in the teeth, it can have higher losses in the yokes. This decreases the yokes and removes more weight from the machine.

The thinner yokes marginally increase the air-gap diameter which gives slightly more torque at lower current, even though both machines have the same outer diameter.

The DW-generator has a higher power factor than the CW-generator. This is odd as the CW-generator has a more optimal slot depth/width ratio according to Equation (12). The CW has however larger teeth which could lead to larger air gap inductance. It also has semi-magnetic slot wedges that allow more flux, created by the induced current, to travel around the slot, which in turn leads to higher inductance.
The main reason is however suggested to be that the CW has more number of turns in each slot which gives higher inductance.

The power factor difference is however, not of great importance. If the converter rating would lie between both generators apparent power, it could have an impact on the weight and cost of the converter. The rated apparent power, presented in Table 4-5, is larger for the CW-generator as it has lower power factor, but in this report it was assumed that ABB's PCS 6000 Wind converter was used. This converter covers both generator ratings; hence the cost of converter would be the same. The losses in converter for the CW-generator would however be larger but not significantly.

Considering the thermal analysis of both machines, the thermal result in Table 4-7 suggests that the DW-generator has better thermal properties compared to the CW-generator. It has higher losses but gives similar temperatures. In other words the heat is better distributed compared to the CW-generator. The narrow teeth and slots are suggested to be the main reason for this.

As the temperature is more evenly distributed in the DW, it would be easier to cool with an air cooling system, as in Fig. 2-8, compared to the CW. This could explain why the assumed water cooling system does not provide lower temperatures in the generator.

The thermal network in Appendix E.1 assumes a worst case scenario where no heat is transferred from either end-windings or surface towards air-gap, to ambient air. The worst case scenario explains why the temperatures are higher compared to what one would expect in the real case.

From Table 4-7 it can be concluded that the CW has better thermal properties in the axial direction, as the temperature difference between end-windings and slot is smaller compared to the DW. This is because the CW has larger slots with higher fill factor, meaning less thermal resistance in windings.

In reality the DW-machine should however have worse end-winding properties than the model suggests since the end-windings are over-lapping, having less free space between them. To give a better comparison this needs to be looked into more accurately, this is however outside the scope of this report.

5 Conclusion and future work

5.1 Conclusion

5.1.1 Part I

The geometry script was successfully implemented and allowed fast generation of 2-D geometry for DW-machines. This saved valuable time for the designer.

The new method for iron loss calculations could not use the Fourier analysis approach, it could however be used without the Fourier analysis. It offers faster and better loss calculation, especially for DW-machines compared to the old method. The new method is therefore recommended above the old, it could however benefit from further improvements.

5.1.2 Part II

The conclusion from the comparison is presented in bullets in Table 5-1.

Table 5-1 Conclusions of the comparison of DW- and CW-generator.

DW	CW
Electrical	
• Lower rotor losses • Lower magnet loss. • Torque ripple is very low. • Insignificant THD in emf. • Tangential tension in target region. • Higher power factor.	• Lower copper losses which allow higher rotor and magnet loss. • Better utilization of slots. • Easier manufacturing and lower number of coils reduces cost. • Torque ripple below target value. • Insignificant THD in emf. • Higher efficiency. • Tangential tension in target region. • Shorter active length with end-windings, which could reduce weight of the shaft. • Superior torque per weight, due to more poles and less deep slots. • Lower power factor can be handled by same converter.
Thermal	
• Better heat distribution in radial direction, hence better for air cooling systems.	• Better heat distribution in axial direction. • Give similar properties with liquid cooling.

The CW-generator is a state-of-art-machine. Fig. 4-13 illustrates that the CW has better KPIs compared to the DW. Several other advantages are listed in Table 5-1. As the wind turbines grow in size, weight must be reduced. The CW offer great electrical performance and superior

weight efficiency; therefore it is concluded that the PMSG with CW is most suitable choice in wind power applications.

5.2 Future work

During the writing of this report it was found several issues that could be investigated in future work:

- The geometry script should be expanded further. The stator core should be split up in two objects, one for the yoke and one for the teeth. This would allow the designer to extract the losses for the teeth and yoke separately. This is useful in the thermal analysis, where the losses in yoke and teeth are assigned to different nodes.

- The new method for loss calculations should be further investigated. The method using each element could be improved to take the harmonics into account. In an investigation of this method there should be build a segment where the iron losses can be measured. This could then be used to verify the loss function.

- Since skewing results in a force in axial direction in the generator, it would be interesting to investigate its effect on structural stresses and fatigue.

- The thermal analysis should be updated and become a part of the optimization tool. As the geometry changes so does the machine's thermal properties. It is therefore important that the thermal design is a part of optimization at an early stage.

- It is recommended that a more advanced thermal model is developed. A segment should be built where temperatures can be measured to validate the model. The thermal model should also include an analysis that evaluates the pressure head of the cooling system. Calculations could then be done on what kind of pump the system will need.

- For a complete comparison it is recommended that an extensive cost analysis is performed. This should include cost of installation, maintenance, active material, manufacture, structure, efficiency etc. It is important that the analysis include all cost in the generators life-cycle as this is the real cost of the generator.

6 Bibliography

[1] **BTM Consult.** *International wind energy development, World market update 2009.* March 2010.
[2] **Sway AS.** [Online] [Cited: 02 16, 2011.] http://www.sway.no.
[3] **AMSC Windtec.** [Online] [Cited: 02 16, 2011.] http://www.amsc-windtec.com/SeaTitan.html.
[4] **Clipper Windpower.** [Online] [Cited: 02 16, 2011.] htto://www.clipperwind.com.
[5] **Wind Power Ltd.** [Online] [Cited: 02 16, 2011.] http://www.windpower.ltd.uk.
[6] **Krøvel, Østein.** *Design of Large Permanent Magnetized Synchronous Electric Machines.* Trondheim : NTNU, 2010. Phd.
[7] **Americas Wind Energy Inc.** [Online] [Cited: 02 16, 2011.] http://www.awewind.com/.
[8] **Enercon.** [Online] [Cited: 02 16, 2011.] http://www.enercon.de/en-en/.
[9] **Dongfang Electric Corporation.** [Online] [Cited: 02 16, 2011.] http://www.dongfang.com.cn.
[10] **Genaral Electric Energy.** [Online] [Cited: 02 16, 2011.] http://www.gepower.com/.
[11] **Goldwind Science & Technology Co.** [Online] [Cited: 02 16, 2011.] http://www.goldwindglobal.com/.
[12] **Lagerwey Wind.** [Online] [Cited: 02 16, 2011.] http://www.lagerwey.nl/.
[13] **Leitwind AG.** [Online] Leitner technolgies. [Cited: 02 16, 2011.] http://en.leitwind.com.
[14] **Northern Power Systems.** [Online] [Cited: 02 16, 2011.] http://www.northernpower.com/.
[15] **Siemens Energy.** [Online] Siemens AG. [Cited: 02 11, 2011.] http://www.energy.siemens.com/hq/en/power-generation/renewables/wind-power/.
[16] **XEMC Darwind.** [Online] [Cited: 02 16, 2011.] http://xemc-darwind.com/.
[17] *PM Wind Generator Topologies.* **Chen, Y., Pillay, P. and Khan, A.** 6, Seattle : IEEE Transaction on Industry Applications, 2004, Vol. 41.
[18] **Matveev, Alexey.** *Researcher at SmartMotor AS.* Trondheim, Norway.
[19] **Reigstad, T.I.** *Direct Driven Permanent Magnet Synchronous Generator with Diode Rectifiers for Use in Offshore Wind Power.* Trondheim : NTNU, 2007. Master thesis.
[20] *Permanent Magnet 3 MW Low-Speed Generator Development.* **J. Pyrhönen, P. Kurronen, A. Parviainen.** Chania, Crete : ICEM, 2006.
[21] **Smart Motor AS.** *Internal report.*
[22] **Manwell, J.F., McGowan, J.G. and Rogers, A.L.** *Wind Energy Explained.* s.l. : John Wiley & Sons Ltd., 2009. ISBN 978-0-470-01500-1.
[23] **Grauers, A.** *Design of Direct-driven Permanent-magnet Generators for Wind Turbines.* Göteborg : Chalmers University of Technology, 1996. Phd.
[24] **J. Pyrhönen, T. Jokinen, V. Hrabovcoá.** *Design of Rotating Electrical Machines.* s.l. : John Wiley & Sons, Ltd., 2008. ISBN: 978-0-470-69516-6.
[25] **Hanselmann, D.C.** *Brushless Permanent-Magnet Motor Design.* New York : McGraw-Hill, Inc., 1994.
[26] **Say, M.G.** *The Performance and Design of Alternating Current Machines.* London : Sir Isaac Pitman & Sons Ltd., Third ed. 1948.
[27] *Force Density Limits in Low speed PM Machines due to Temperature and Reactance.* **A. Grauers, P. Kasinathan.** 3, s.l. : IEEE Transactions on Energy Conversion, 2004, Vol. 19.
[28] **ABB.** [Online] [Cited: 05 25, 2011.] http://www.abb.com/.
[29] **G. C. Stone, E. A. Boulter, I. Culbert, H. Dhirani.** *Electrical Insulation for Rotating Machines.* s.l. : John Wiley & Sons, Ltd., 2004. ISBN: 0-471-44506-1.
[30] *Cooling and cooling circuits for electric motors.* **Bone, J. C. H.** s.l. : IEE Journal on Electric Power Applications, 2009.

[31] **Stiesdal, Henrik and (SiemensAG).** *Generator with a Stator Comprising Cooling Ducts, and Method for Cooling a Laminated Stator of a Generator . US20090256433A1* 10 15, 2009.
[32] **Klinger, Friedrich.** *Electrical Machine and the Use of Electrical Machine. WO2007128275A1* 11 15, 2007.
[33] **Holman, J. P.** *Heat Transfer.* s.l. : McGraw-Hill, 2002. ISBN: 0-07-112230-6.
[34] **Comsol Group.** [Online] [Cited: 02 03, 2011.] http://www.comsol.com.
[35] *Performance comparison of IPMSM with distributed and concentrated.* **Kwon, S., et al., et al.** Changwon, Korea : IEEE, 2006. 1-4244-0365-0/06.
[36] *A Comparative Study of Winding Factors.* **Zhu, D., et al., et al.** Nanjing, China : IEEE, 2008. 978-7-900714-13-8/08.
[37] *Evaluation of Interior PM and Surface PM Synchronous Machines with Distributed and Concentrated windings.* **Muñoz, A.R., Liang, F. and Degner, M.W.** Dearborn, Michhigan, US : IEEE, 2008. 978-1-4244-1766-7/08.
[38] *Low speed Permanent Magnet synchronous motor comparison.* **Asaf ali, A.B.** 2006.
[39] *Performance Evaluation of Permanent Magnet Synchronous Machines with Concentrated and Distributed windings.* **Magnussen, F., Thelin, P. and Sadarangani, C.** Stockholm, Sweden : KTH (Royal Institute of Technology).
[40] **The Switch.** [Online] [Cited: 02 17, 2011.] http://www.theswitch.com/.
[41] **Longtin, Randy S, Jansen, Patrick L and (GE).** *Wind Turbine Direct Drive Airgap Control Method and System. US2009243301 (A1)* US, 10 01, 2009.
[42] **Klinger, Friedrich, Prof. Dr.-ing.** *Getriebelose Windturbine mit vielpoligem Synchrongenerator. EP1394406A2* Europe, 08 22, 2003.
[43] **Vestas.** [Online] [Cited: 02 18, 2011.] http://www.vestas.com//.
[44] **Aloys, Wobben.** *Wind Energy Facility with Closed Cooling Ciruit. US6676122B1* 01 13, 2004.
[45] **Pasteuning, J. W., Versteegh, C. J. A. and (XEMCDarwind).** *Wind Turbine comprising a Cooling Circuit. WO2010069954A1* 06 24, 2010.
[46] **Pabst, Otto, etc. and (RolicInvestSari).** *Wind Power Plant equipped with Generator Cooling System. EP2136077A2* 12 23, 2009.
[47] **Pluk, K.J.W.** *Offshore Oil & Gas Industry Overview and PM-Machines.* Eindhoven : Eindhoven University of Technology, 2010. EPE.2011.S01.
[48] **Fischer, Torsten, Vilsbøll, Niels and AS), (NEG Micon).** *Offshore Wind Turbine with Liquid-cooling. US6520737B1* 02 18, 2003.

Appendices

A Appendix

A.1 Wind turbine control

During operation it is important that the wind turbine has a good control system which can handle all the different subsystems within the wind turbine. The control system has multiple tasks: measure wind speeds, check health of system components, control runaway speed, control pitching and yawing, control generator torque and grid connection. Without a functional control system, the wind turbine will be unable to produce power successfully and safely.

There are two levels of control systems called supervisory and dynamic control. Supervisory control manages and monitors turbine operations and sequences control actions such as brake release and contactor closing. Dynamic control manages machine operation in which the machine dynamics affect the outcome of the control actions, such as changing blade pitch in response to turbulent winds.

The basic turbine model for variable-speed turbines include the blades inertia which are driven by the aerodynamic torque. A shaft connects the hub and blades to the generator. An electrical torque acts on the generator and a brake is usually placed on the shaft. The turbine is commonly installed with a pitch and yaw control system for controlling the aerodynamic torque.

In variable-speed turbines the aerodynamic and generator torques can be varied independently of each other. Hence the rotational speed can be altered either by changing the generator or aerodynamic torque. [22]

Control system design is a large topic area. In order to limit the scope, this report will focus on control of generator torque, power electronic converters for voltage and frequency control, tripping and over-speed control.

The rotational speed of the turbine is important for a maximum power production. Turbine power curves, such as Fig. A-1, illustrates the optimal rotational speed for maximum power production for different wind speeds. The tip-speed ratio is constant for all maximum power points, while the turbine rotation speed is related to the wind speed. [19]

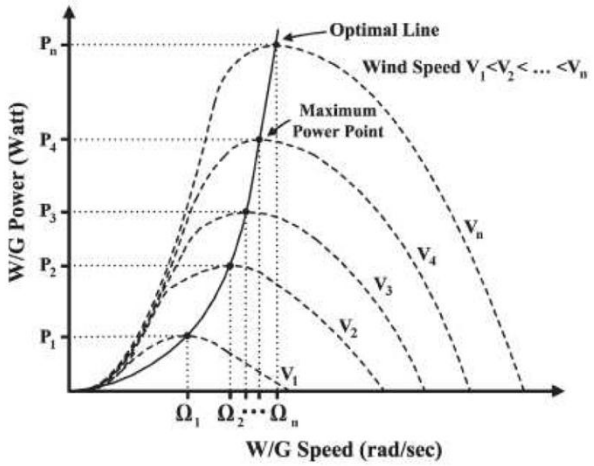

Fig. A-1 Illustration of turbine power curve where optimal rpm for maximum power production is given for certain wind speeds.

A.1.1 Generator torque control

Two types of tracking algorithms (MPPT) are commonly used; one is based on the knowledge on the turbine characteristic (Cp) and the other seek the optimize operation without knowing Cp. [19]

The first has three different tracking algorithms; speed control, torque control and a diode bridge with DC-DC chopper structure. Only torque control will be explained in this report.

The torque control uses the power curve to find the optimal torque reference. Optimal torque control adjusts the generator torque at different wind speed. Control precision depends on the optimal tip-speed ratio and generator's parameters. A PWM with an IGBT is needed for this method. [19]

The last MPPT uses the power and speed linked to the turbines behavior. In general this method is more suitable for small wind turbines with small inertia. For larger turbines the time response is to long because of the turbines high inertia.

The MPPT knowing Cp has higher efficiency and is more suitable for larger wind turbines. [19]

A.1.2 Brakes

Most wind turbines employ a mechanical brake somewhere along the drive-train. Most brakes are capable of stopping the turbine. Brakes incapable of stopping the turbine are used only for parking, which means that they keep the blades and rotor from turning when they are not operating.

In wind turbines there are mainly two types of mechanical brakes that are used: disc brakes and clutch brakes. The disc brake works as follows: A disc is attached on the shaft. During braking brake pads are pushed against the disc by a hydraulically actuated caliper. This much resembles the automobile braking solution.

The clutch brake operates with at least one pressure plate and at least one friction disc. These brakes are normally actuated by springs which mean they are fail-safe by design. The clutch brakes are released by compressed air or hydraulic fluid.

In addition there is an electrical brake called a *dynamic brake.* The basic principle of this brake is to feed power into a resistor bank. This will put a load on the generator hence a torque on the shaft which evidently will decelerate the turbine.

There are three important considerations when deciding upon a brake:

- maximum torque
- length of breaking time
- energy absorption

If the brake is intended to stop the turbine, it must be able to exert a torque above what plausibly could be attained by the blades. It must also start to apply almost immediately and ramp up to full torque in manner of few seconds. The ramp-up time depends on instantaneous and slow deceleration actuation. An instantaneous reaction will exert high transient load to the drive-train while slow deceleration will heat up the brake. Normally when a brake is applied, the time from where the brake start to where the turbine has stopped is less than five seconds.

The energy absorption capability is important since the brake needs to be able to absorb all the kinetic energy in the rotor when turning at its maximum speed, and at the same time be able to absorb additional energy which could be acquired by the blades during the stopping period. [22]

A.2 Literature study on CW and DW

Table A-1 presents five different papers that have compared CW- and DW-machines. These will be the considered for the basis of the comparison.

Table A-1 Present the literature study on different papers comparing CW- and DW-machines.

Source	What is compared	Constant	Discussion
[36]	The winding factors: Inspect the sinusoidal wave form of the back-emf.	-	It only studies different winding factor and how this affects back-emf and harmonics. The paper emphasis the slot width choice for CW which can remove special emf. harmonics.
[37]	Inner-rotor radial-flux machines with interior and surface PMs: are compared with. The rated rotational speed is 1000 rpm.	• Outer diameter • Active length with end-windings • Magnet volume • Air-gap • Peak current	Looking at different speed and due to constant parameters the peak torque is compared. The CW has longer active length which in turn must result in the magnets being thinner or less wide compared to DW if same magnet volume is achieved.
[38]	Low-speed surface mounted PM synchronous motors with same active diameter and length. The winding factors for the DW and CW are 0.9333 and 0.866 respectively.	• Active diameter • Active length	The outer diameter is maybe a better as it says more about the size of each machine. Same goes for the active length compared to active length with end-windings. Poor winding factor for CW.
[35]	Two interior inner-rotor radial-flux high-speed PMSM. Basic parameters and output characteristics, such as inductances, resistances, back-emf., output torque, and efficiency, are compared. Both machines are skewed to reduce torque ripple, THD of back-emf., and cogging torque.	• Rotor dimensions • Air-gap length • Number of turns • Stator outer radius • Axial length • Skew angle	Higher number of poles could be an advantage for the CW which is not accounted for. Number of turns should be allowed as the CW will have lower
[39]	High-speed (2000 rpm) surface PMSM:s with fractional CW is compared to integer DW. Power capability, torque ripple, effects of field-weakening and thermal behavior.	• Exact same dimension except from number of slots.	Thermal behavior analysis is limited to end-windings. Rotor losses are neglected. This is a big advantage for the CW as it should have larger rotor losses. DW is integer and not skewed this will naturally cause larger cogging.
This report	Low-speed surface mounted PMSG. Back-emf's THD, torque per weight, power factor, efficiency, tangential tension, thermal analysis, torque ripple	• Outer diameter • Active length with end-windings • Air-gap • Magnet thickness	Field weakning will not be considered since speed variation is not as large as in the high-speed machines. Magnet volume could differ but must be looked at as a variable parameter as the machines are limited by different designs procedures.

B Appendix

SmartTool Update

B.1 Geometry script

```
function fem = fea_dist_draw(ms)
    % fea_dist_draw generates the geometry 3 phase disitrbuted windings
    % based on parameters  in ms. It returns geometry object for each phase
and
    % direction, slot wedges, stator core, stator air, rotor core, pm's and
    % rotor air. Phases are given in  e.g. rx which is phase 1 in positive
    % direction as:
    %
[rx,ry,sx,sy,tx,ty,slot_wedge,statcore,air_stator,rotcore,pm,air_rotor].
    % These are put in a structure called fem together with boundaries and
    % constants.
    % The code only works for when slot have layer in rotational or radial
    % direction NOT both at the same time.

    % This is an extension to femdraw written by Anders Lagerström


    %% Fetching variables manually
    r_ri    = ms.geom.r_ri;
    r_rii    = ms.geom.r_rii;
    theta_p = ms.geom.theta_p;
    r_rio    = ms.geom.r_rio;
    l_m     = ms.geom.th_pm; %!!!!!!!
    tau_f   = ms.geom.tau_p-ms.geom.w_pm;%!!!!!!!
    Ns     = ms.geom.Ns; %
    Np       = ms.geom.Np; %
    PMseg   = round(ms.geom.w_pm/l_m);%
    g       = ms.geom.g; %
    d_s     = ms.geom.d_s;
    theta_s = ms.geom.theta_s;
    theta_ts = ms.geom.theta_ts;    %Angular pitch of straight tooth.
    alpha_s = ms.geom.s_wp;%!!!!!!!
    r_si    = ms.geom.r_si;
    r_so    = ms.geom.r_so;
    d_sw    = ms.geom.th_sw;%!!!!!!!
    n       = ms.mech.n; %rated speed
    rcth = r_rio-r_rii; % rcth (rotor core thickness)

    % Below need parameters that are needed in Comsol:
    %   Ns,Np,PMseg,g,n,J_cu,F,sym,Br,k_cu,rcth

    %% New Parameters
    %For the machine structure ther should be new variables called
    %ms.el.conc to indicate which drawing code it should use, it should
    %also be ms.el.layers.Nlay_theta and ms.el.layers.Nlay_rad to indicate
    %type of layer.
    Nlay_theta = ms.el.layers.Nlay_theta; %layer in rotational direction
    Nlay_rad = ms.el.layers.Nlay_rad; %layer in radial direction
    Nlay=Nlay_theta*Nlay_rad; %total number of layers
    [wind_tab,p_length]=patternfind(ms.el.wlayout); %get the winding layout
with the shortest pattern
    F = Ns/p_length; %number of sections dependent on winding layout
```

```
    if F/2==round(F/2) %check if the geometry will be symetrical or
asymetrical
        sym = 1;
    else
        sym = 0;
    end
    w_s = ms.geom.w_s; %slot width


    %% Building machine geometry

    %cutting feature
    if F>1
        cut_feat = arc2(0,0,r_so+r_rio,0,theta_s*Ns/F); %creates a cutting
arc at right pos.
        cut_feat = rotate(cut_feat,2*pi-theta_s/2); %when the machine is
sectioned
    else
        cut_feat = circ2(r_rio+r_so,'base','center','pos',[0 0]); %just to
simplify the code
    end

    %% Buildings slots >>>>>>>>>>>>>>
    % Inner rotor >>>>>>>>>>>>>>
    if ms.mech.innerrotor
        if Nlay_rad > 1 %changing winding tab so that the layers are placed
correctly
            [row, column] = size(wind_tab);
            for i=1:row
                wind_tab2(i,:) = wind_tab(row+1-i,:);
            end
            wind_tab = wind_tab2;
            clear wind_tab2 row column
        end
        wedge = r_si+d_sw; %inner length of slot wedge, to reduce number of
operations

        cut_circ = circ2(r_si,'base','center','pos',[0 0]); %circle to
"cut" out slots

        w_sw = w_s*1.375; %width of slotwedge, 1.375 is from relation in
picture
        sw1 = line1([wedge wedge],[w_sw/2 -w_sw/2]); %wedge side 1
        sw2 = line1([r_si r_si],[w_s/2 -w_s/2]); %wedge side 2
        sw3 = line1([r_si wedge],[w_s/2 w_sw/2]); %wedge side 3
        sw4 = line1([r_si wedge],[-w_s/2 -w_sw/2]); %wedge side 4
        sw = geomcoerce('solid',{sw1,sw2,sw3,sw4}); %creates slot wedge

        slot = rect1(d_s,w_s,'base','corner', 'pos', [wedge -w_s/2]); %slot

        if Nlay>1 %to insert the layer in the slot

            extra_theta_line = Nlay_theta-1; %how many lines in slot in
rotational
            extra_rad_line = Nlay_rad-1; %how many lines in radial
direction

            if extra_theta_line>0 && extra_rad_line>0 %splitting slot 1st
in theta then in rad direction
```

```
                all_lines = cell(1,extra_theta_line+extra_rad_line);
%creates a cell for storing lines

                for i=1:extra_theta_line
                    y_coord = -w_s/2+w_s*i/Nlay_theta; %the y-coordinates
                    all_lines(i) = line1([wedge wedge+d_s],[y_coord
y_coord]);
                end
                for i=1:extra_rad_line
                    x_coord = wedge+d_s*i/Nlay_rad; %the x-coordinates
                    all_lines(i+extra_theta_line) = line1([x_coord
x_coord],[w_s/2 -w_s/2]);
                end
            elseif extra_rad_line==0 %when coils are next to each other
                for i=1:extra_theta_line
                    y_coord = -w_s/2+w_s*i/Nlay_theta; %the y-coordinates
                    all_lines(i) = line1([wedge wedge+d_s],[y_coord
y_coord]);
                end
            elseif extra_theta_line==0 %when there is only an upper and
lower coils
                for i=1:extra_rad_line
                    x_coord = wedge+d_s*i/Nlay_rad; %the x-coordinates
                    all_lines(i) = line1([x_coord x_coord],[w_s/2 -w_s/2]);
                end
            end

            windings_pps = geomcoerce('solid', {slot all_lines}); %creates
geometry
            windings = split(windings_pps); %splits the slot into the
layers
            %layers are numbered from lower left

        else %for one layer windings
            windings_pps = geomcoerce('solid', slot); %creates geometry
            windings = windings_pps;
        end

        % periodic boundaries
        pbnd1 = line1([r_ri,r_so],[0,0]);
        pbnd1 = rotate(pbnd1,2*pi-theta_s/2);
        pbnd2 = rotate(pbnd1,2*pi/F);

    % Inner rotor <<<<<<<<<<<<
    %%
    % Outer rotor >>>>>>>>>>>>>>
    else
        wedge=r_so-d_sw; %inner length of slot wedge, to reduce number of
operations

        cut_circ1 = circ2(r_so,'base','center','pos',[0 0]); %circle to
"cut" out slots
        cut_circ2 = circ2(r_so+d_s,'base','center','pos',[0 0]); %circle to
"cut" out slots
        cut_circ = cut_circ2-cut_circ1; %makes a ring solid to evan out
slot wedges

        w_sw = w_s*1.375; %width of slotwedge, 1.375 is from relation in
picture
```

```
        sw1 = line1([wedge wedge],[w_sw/2 -w_sw/2]); %wedge side 1
        sw2 = line1([r_so r_so],[w_s/2 -w_s/2]); %wedge side 2
        sw3 = line1([r_so wedge],[w_s/2 w_sw/2]); %wedge side 3
        sw4 = line1([r_so wedge],[-w_s/2 -w_sw/2]); %wedge side 4
        sw = geomcoerce('solid',{sw1,sw2,sw3,sw4}); %creates slot wedge

        slot = rect1(d_s,w_s,'base','corner', 'pos', [wedge-d_s -w_s/2]);
%slot

        if Nlay>1 %to insert the layer in the slot

            extra_theta_line = Nlay_theta-1; %how many lines in slot in
rotational
            extra_rad_line = Nlay_rad-1; %how many lines in radial
direction

            if extra_theta_line>0 && extra_rad_line>0 %splitting slot 1st
in theta then in rad direction
                all_lines = cell(1,extra_theta_line+extra_rad_line);
%creates a cell for storing lines

                for i=1:extra_theta_line
                    y_coord = -w_s/2+w_s*i/Nlay_theta; %the y-coordinates
                    all_lines(i) = line1([wedge-d_s wedge],[y_coord
y_coord]);
                end
                for i=1:extra_rad_line
                    x_coord = wedge-d_s*i/Nlay_rad; %the x-coordinates
                    all_lines(i+extra_theta_line) = line1([x_coord
x_coord],[w_s/2 -w_s/2]);
                end
            elseif extra_rad_line==0 %when coils are next to each other
                for i=1:extra_theta_line
                    y_coord = -w_s/2+w_s*i/Nlay_theta; %the y-coordinates
                    all_lines(i) = line1([wedge-d_s wedge],[y_coord
y_coord]);
                end
            elseif extra_theta_line==0 %when there is only an upper and
lower coils
                for i=1:extra_rad_line
                    x_coord = wedge-d_s*i/Nlay_rad; %the x-coordinates
                    all_lines(i) = line1([x_coord x_coord],[w_s/2 -w_s/2]);
                end
            end

            windings_pps = geomcoerce('solid', {slot all_lines}); %creates
geometry
            windings = split(windings_pps); %splits the slot into the
layers
            %layers are numbered from lower left

        else %for one layer winding
            windings_pps = geomcoerce('solid', slot); %creates geometry
            windings = windings_pps;
        end

        % periodic boundaries
        pbnd1 = line1([r_si,r_rio],[0,0]);
        pbnd1 = rotate(pbnd1,2*pi-theta_s/2);
```

```
        pbnd2 = rotate(pbnd1,2*pi/F);

        % Outer rotor <<<<<<<<<<<<<<<
    end % Building slots ends <<<<<<<<<<<<<<<

    %% Creating phase objects >>>>>>>>>>>>>>
    slot_parts = cell(length(windings), Ns/F);
    count=1; %counter
    for i = Ns/F:-1:1 %1:Ns/F %rotates and saves all slot in the cell
slot_parts
        for j = 1:length(windings)
            slot_parts(j,count) = rotate(windings{j},theta_s*(i-1));
        end
        count = count+1;
    end
    clear count
    slots = geomcoerce('solid',slot_parts);

    %Below is loop to place objects to phase R+
    %(x = + and y = -)
    [row,column] = find(wind_tab==1);
    phase_rx = cell(1,length(row));
    for i=1:length(row)
        phase_rx(:,i) = slot_parts(row(i),column(i));
    end
    rx = geomcoerce('solid', phase_rx);
    clear row column

    %Below is loop to place objects to phase R-
    [row,column] = find(wind_tab==-1);
    phase_ry = cell(1,length(row));
    for i=1:length(row)
        phase_ry(:,i) = slot_parts(row(i),column(i));
    end
    ry = geomcoerce('solid', phase_ry);
    clear row column

    %Below is loop to place objects to phase S+
    [row,column] = find(wind_tab==2);
    phase_sx = cell(1,length(row));
    for i=1:length(row)
        phase_sx(:,i) = slot_parts(row(i),column(i));
    end
    sx = geomcoerce('solid', phase_sx);
    clear row column

    %Below is loop to place objects to phase S-
    [row,column] = find(wind_tab==-2);
    phase_sy = cell(1,length(row));
    for i=1:length(row)
        phase_sy(:,i) = slot_parts(row(i),column(i));
    end
    sy = geomcoerce('solid', phase_sy);
    clear row column

    %Below is loop to place objects to phase T+
    [row,column] = find(wind_tab==3);
    phase_tx = cell(1,length(row));
    for i=1:length(row)
```

```
    phase_tx(:,i) = slot_parts(row(i),column(i));
end
tx = geomcoerce('solid', phase_tx);
clear row column

%Below is loop to place objects to phase T-
[row,column] = find(wind_tab==-3);
phase_ty = cell(1,length(row));
for i=1:length(row)
    phase_ty(:,i) = slot_parts(row(i),column(i));
end
ty = geomcoerce('solid', phase_ty);
clear row column

% Creating phase objects ends <<<<<<<<<<<<<

%% Rest of stator >>>>>>>>>>>>

% slot wedges
slot_wedge_pps = geomcoerce('solid',{sw});
slot_wedge = cell(1,Ns/F);
for i = 1:Ns/F
    slot_wedge(1,i) = rotate(slot_wedge_pps,theta_s*(i-1));
end
slot_wedge = geomcoerce('solid',slot_wedge);
slot_wedge = slot_wedge-cut_circ;

% Stator core
sec1 = circ2(r_si,'base','center','pos',[0 0]);
sec2 = circ2(r_so,'base','center','pos',[0 0]);
statcore = sec2-sec1;
statcore = cut_feat*statcore;
% adding stator core sector for postprocessing lamination losses
        l4 = line1([r_si,r_so],[0,0]);
        l4 = rotate(l4,theta_s*(Ns/F/2-1));%-theta_s/2);
        l4a = rotate(l4,theta_s);
        statcore = geomcomp({statcore,l4,l4a});
        statcore = geomcoerce('solid',statcore);
% finilize stator core
statcore = statcore-slot_wedge;
statcore = statcore-slots;

% Stator air
if ms.mech.innerrotor
    sec3 = circ2(r_si-g/2,'base','center','pos',[0 0]);
    air_stator = sec1-sec3;
    air_stator = cut_feat*air_stator;
else
    sec3 = circ2(r_so+g/2,'base','center','pos',[0 0]);
    air_stator = sec3-sec2;
    air_stator = cut_feat*air_stator;
end

 % End of rest of stator <<<<<<<<<<<<<<<

%% Building Rotor Geometry

% creating rotor yoke
rec1 = circ2(r_rii,'base','center','pos',[0 0]);
```

```
rec2 = circ2(r_rio,'base','center','pos',[0 0]);
rotcore = rec2-rec1;
rotcore = cut_feat*rotcore;
% adding rotor core sector for postprocessing lamination losses
        l4 = line1([r_rii,r_rio],[0,0]);
        l4 = rotate(l4,theta_p*(Np/F/2-1)+theta_p/2-theta_s/2);
        l4a = rotate(l4,theta_p);
        rotcore = geomcomp({rotcore,l4,l4a});
        rotcore = geomcoerce('solid',rotcore);

% creating PM's

if ms.mech.innerrotor %innerrotor
    s_angle = atan(tau_f/2/r_rio); %starting angle for magnet
    e_angle = theta_p-2*s_angle; %pm pitch angle

    pm1 = arc2(0,0,r_rio,0,e_angle);
    pm2 = arc2(0,0,r_rio+l_m,0,e_angle);
    pm_pps = pm2-pm1;

    if PMseg>1 % for segmenting magnet to calculate magnet losses
        l_pm_pps = line1([r_rio (r_rio+l_m)],[0 0]);
        l_pm = cell(1,PMseg-1);
        for i=1:PMseg-1
            l_pm(i) = rotate(l_pm_pps,e_angle/PMseg*i);
            pm_pps = geomcoerce('solid',{pm_pps l_pm{i}});
        end
        pm_pps = rotate(pm_pps,2*pi-theta_s/2+s_angle);
    else
        pm_pps = rotate(pm_pps,2*pi-theta_s/2+s_angle);
    end
else %outer rotor
    s_angle = atan(tau_f/2/r_ri); %starting angle for magnet
    e_angle = theta_p-2*s_angle; %pm pitch angle

    pm1 = arc2(0,0,r_rii,0,e_angle);
    pm2 = arc2(0,0,r_ri,0,e_angle);
    pm_pps = pm1-pm2;

    if PMseg>1 %for segmenting magnet to calculate magnet losses
        l_pm_pps = line1([r_ri (r_rii)],[0 0]);
        l_pm = cell(1,PMseg-1);
        for i=1:PMseg-1
            l_pm(i) = rotate(l_pm_pps,e_angle/PMseg*(i));
            pm_pps = geomcoerce('solid',{pm_pps l_pm{i}});
        end
        pm_pps = rotate(pm_pps,2*pi-theta_s/2+s_angle);
    else
        pm_pps = rotate(pm_pps,2*pi-theta_s/2+s_angle);
    end

end
     %finilizes PM's
     pm_final = cell(1,Np/F);
for i=1:Np/F %creating all magnets
    pm_final(1,i) = rotate(pm_pps,theta_p*(i-1));
end
%saving all magnets in one object
pm = geomcoerce('solid',pm_final);
```

```
    % creating air_rotor
    if ms.mech.innerrotor
        gap_a1 = circ2(r_rio+l_m+g/2);
        gap_a2 = circ2(r_rio+l_m);
        gap_air = gap_a1+gap_a2; %creates rotor air gap for moving mesh
        gap_b1 = circ2(r_rio);
        air_rotor = gap_air-gap_b1-pm;
    else
        gap_a1 = circ2(r_ri-g/2);
        gap_a2 = circ2(r_ri);
        gap_air = gap_a2-gap_a1; %creates rotor air gap for moving mesh
        gap_b1 = circ2(r_rii)-gap_a2;
        air_rotor = gap_air+gap_b1-pm;
    end
    %the air on rotor side including a subdomain in the middle for moving
mesh
    air_rotor = cut_feat*air_rotor;

    %% Storing in and configuring fem structure

    % solid objects
    s = [];

        s.name = {'rotcore','pm','air_rotor','rx','ry','sx','sy','tx','ty',
...
            'slot_wedge','air_stator','statcore'};
        s.objs = {rotcore,pm,air_rotor,rx,ry,sx,sy,tx,ty,slot_wedge, ...
            air_stator,statcore};

    % curve objects
    c = [];
    c.objs = {pbnd1,pbnd2};

    clear fem
    fem.draw.s = s;
    fem.draw.c = c;

    % Storing necessary constants in fem.const
    function const = femconsts(varargin)
        % 'femconsts' builds the constants field in the fem structure from
        % variables supplied as argument. The name of variables when
        % calling 'femconsts' is the name the constant will have in the fem
        % structure.
        const = cell(1);
        k = 1;
        for i=1:length(varargin)
            const{k} = inputname(i);
            const{k+1} = num2str(varargin{i});
            k = 2*i+1;
        end
    end

    % Constants to be stored in fem.const
    pm_sect = PMseg;
    hmax = (r_so-r_si+d_s+d_sw)/4; % overall max mesh size
    aghmax = g/5;   % airgap max mesh size
    edgehmax = aghmax*2;    % periodic boundary max mesh size
    f = n/60*Np/2;  % electric frequency
```

```
    k_cu_nowedge = ms.el.k_cu_nowedge;  % fill factor below wedge
    t0 = 0; % time of max emf phase 1
    A = 0;  % initialization of winding slot area
    n_pb = ms.el.n_pb;  % number of paralell branches
    n_cs = ms.el.n_cs; % number of coils in series
    L = ms.geom.L;  % active length found by SmartTool
    NN = ms.el.n_s; % number of turns found by SmartTool
    cs = 0; % 'current switch' used for switching stator current on or off
(EMF or full load simulation)
    Aztol = 1e-5;   % Absolute tolerance Az
    lm1tol = 1e2;   % Absolute tolerance lm1
    Vtol = 1e-3;    % Absolute tolerance V*
    rcth = rcth; % Rotor core thickness used for postprocessing rotor core
losses (calculated earlier)
    sym; %if the section is symmetric or not

    % Variable parameters
    Br      = 1.2; % Magnetic remanence [T]
    J_cu    = ms.el.J; % current density

    % Storing constants in fem.const
    fem.const =
femconsts(t0,A,g,F,n_cs,n_pb,Np,Ns,f,J_cu,k_cu_nowedge,NN,L,...
    pm_sect,hmax,aghmax,edgehmax,cs,Aztol,lm1tol,Vtol,rcth,g,sym,Br);

    % Adding constants used in inductance calculation
    fem.const(end+1:end+4) = {'Iac','1[A]','Jac','Iac/A'};

end %end of fea_dist_draw
```

B.2 Pattern script

```
function [wind_sec,p_length]=patternfind(vector)
%patternfind is a function that identifies the shortest number-pattern in
%row vector with then returns the pattern and pattern's length in:
%[wind_sec,p_length].
%
%------------Example------------
%v = [1 2 3 3 6 8 1 2 3 3 6 8 1 2 3 3 6 8];
%[wind_sec,p_length] = patternfind(v)
%wind_sec = 1 2 3 3 6 8
%p_length = 6
%
%Written by Anders Lagerström

wlayout = vector(1,:);
n = size(wlayout,2); %get number of elements
smd = ceil(n/50); % smallest divider due to limitations to comsol which can
%not handle more than 50 sections

m = 1; %counter

for i = smd:n/2 %find all possible dividers because each section can only
    a = n/i; %consist of the dividers
    if round(a) == a
        divider(m) = i;
        m = m+1;
    end
end
```

```
for i = divider
    m = 1;
    for j = 1:n/i-1
        if wlayout(n) == wlayout(n-j*i)
            pat_matrix(m) = 1;
        else
            clear pat_matrix
            break %closes the loop
        end
        m = m+1;
    end
    if exist('pat_matrix')
        break %closes loop because shortest pattern has been found
    end
end

if exist('pat_matrix') %check if there is a pattern and returns result
    p_length = length(pat_matrix)+1;
    wind_sec = vector(:,(1:n/p_length));
    p_length = n/p_length;
else
    disp('No pattern exists')
    p_length = n;
    wind_sec = vector;
end
```

B.3 Discussion regarding geometry script and new iron loss function

B.3.1 Geometry script

While writing the new script it was clear that a lot of computing time could be saved by writing the script in a more efficient way. When the script calculated the whole machine geometry for a generator with many slots, about 400, the computing time was very long. This was discovered when the script was investigated on which loops that took longest time. When creating a new object which consist of an existing object and the same object rotated, such as the stator slots, the operation was very time consuming.

```
for i = 1:Ns/F
        slots = slots + rotate(slot_1, i*theta_s);
end
```

In another loop where the layers in the slots were created, another approach was used. This approach saved all the layers in a cell array so that each layer could be assigned with a phase and a direction. This performed the calculation more than a 100 times faster.

```
for i =1Ns/F
        for j = 1:length(Nlay)
                slot_parts(i,j) = rotate(slot_1, i*theta_s);
        end
end
```

Why this faster is not completely understood, but in discussion with SmartMotor's Comsol expert, Lars-Ottar Kvåle, it is suggested that combining an object with a rotation becomes a union, meaning creating a new object in each loop. While the other method does not need to

create a new object only rotating an existing object each loop. Either of these methods does not affect the final result but it is however important to state the saved time for future reference.

B.3.2 Implementation of new iron loss function

The function that collects the domain number for each of the stator and rotor cores (rotcore_sds) in feabuild-script normally uses the domain numbers for the areas behind the tooth and pole. When this is used with the new function, the function requires the whole areas in stator and rotor core. These domain numbers has been saved as extra objects in the fem-structure so one can separate domains for the old and new loss calculations.

B.3.3 Other results

B.3.3.1 EMF and Torque simulations

The back-emf was simulated. The emf simulation returns the time (t0) where the emf it supposedly has its mid-value and when the current should be turned on in the torque simulation to get best torque output. The results are displayed in Table B-

Table B-1 Results from the emf and torque simulations.

	EMF_3phase.m (Old)	**EMF_3phase_update.m (New)**
t0 [s]	0.00582	0.0111
Mean first harmonic [V]	1082.56	1082.56
Mean Peak emf [V]	1024.09	1024.09
Mean Torque [kNm]	-104.8	4360.9
Peak Torque [kNm]	4240.9	4605.6

The results of t0 are based on phase number 1 and are visualized in Fig. B-2, which indicates the significant phase-shift it would have on the current.

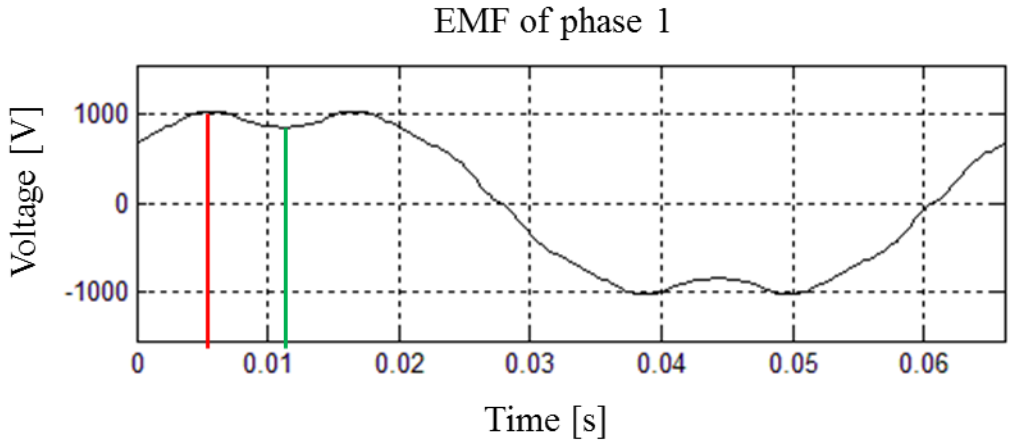

Fig. B-2 Illustrates the output emf for phase 1 where red is t0 = 0.00582 and green is t0 = 0.0111.

Implications in post-processing script of phase-emf:

- The script looks up time for maximum emf-value instead of time for central emf-value in phase one.

- For SmartMotor's own CW-machines the phase voltage will have relatively clean sinusoidal shape, for these the old method works.
- For a sine-wave with third harmonic as the DW-machine the script does not work. This was revealed when the torque was calculated because the current is switch on at the wrong time hence giving no torque.

C Appendix

Loss function update and Control model results

C.1 Finding the B-field direction

C.1.1 Results

Results from four random elements in the stator are presented in Fig. C-, Fig. C-, Fig. C- and Fig. C-.

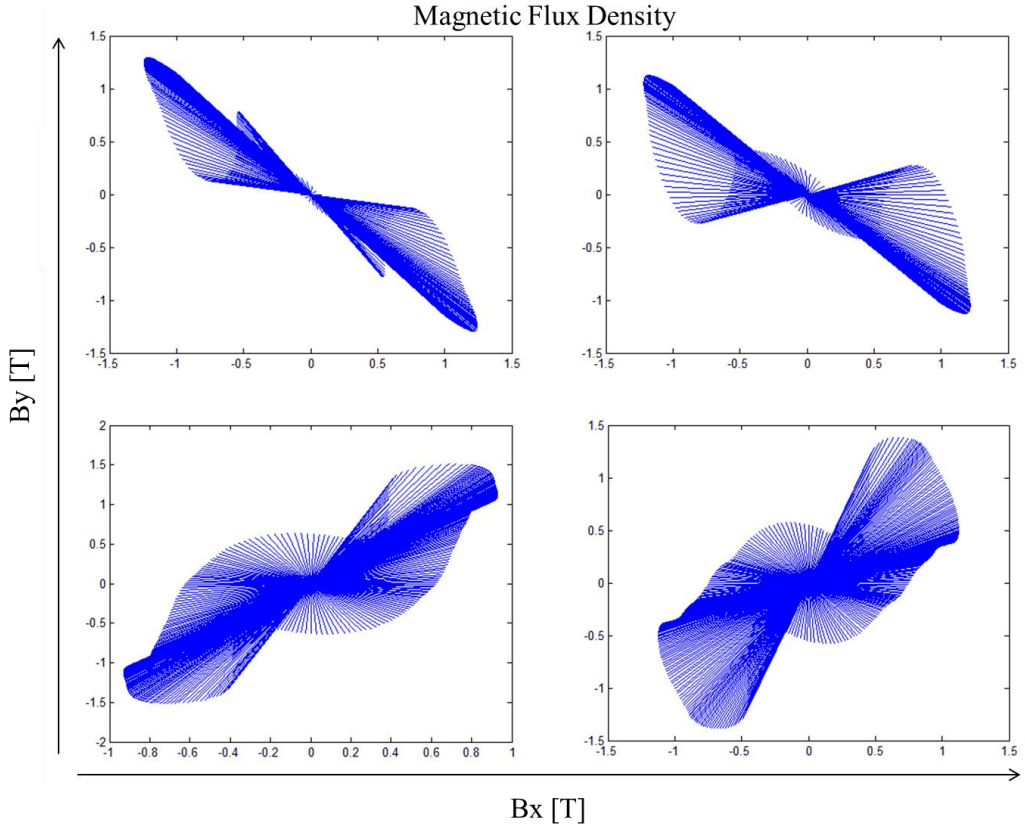

Fig. C-1 Illustration of four random element's (in the stator) B-field magnitude and direction for each time step.

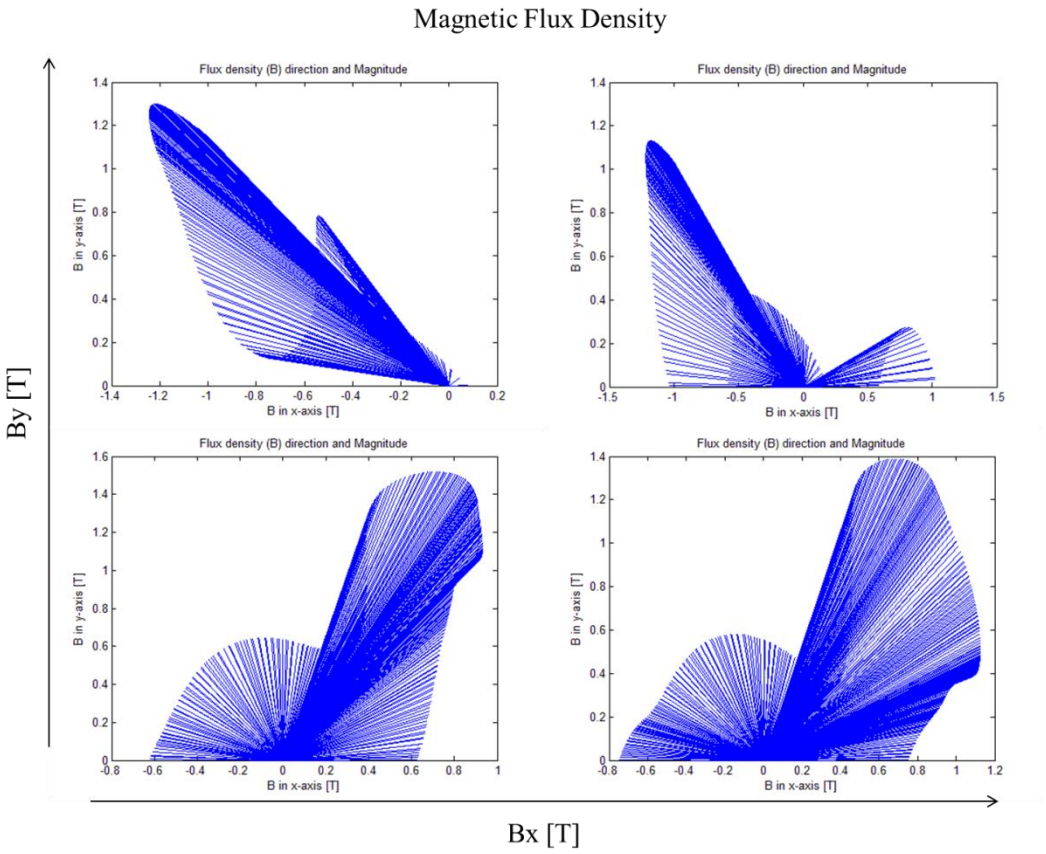

Fig. C-2 Illustration of four random element's B-field magnitude and direction for each time step transferred to the 1st and 2nd quadrant.

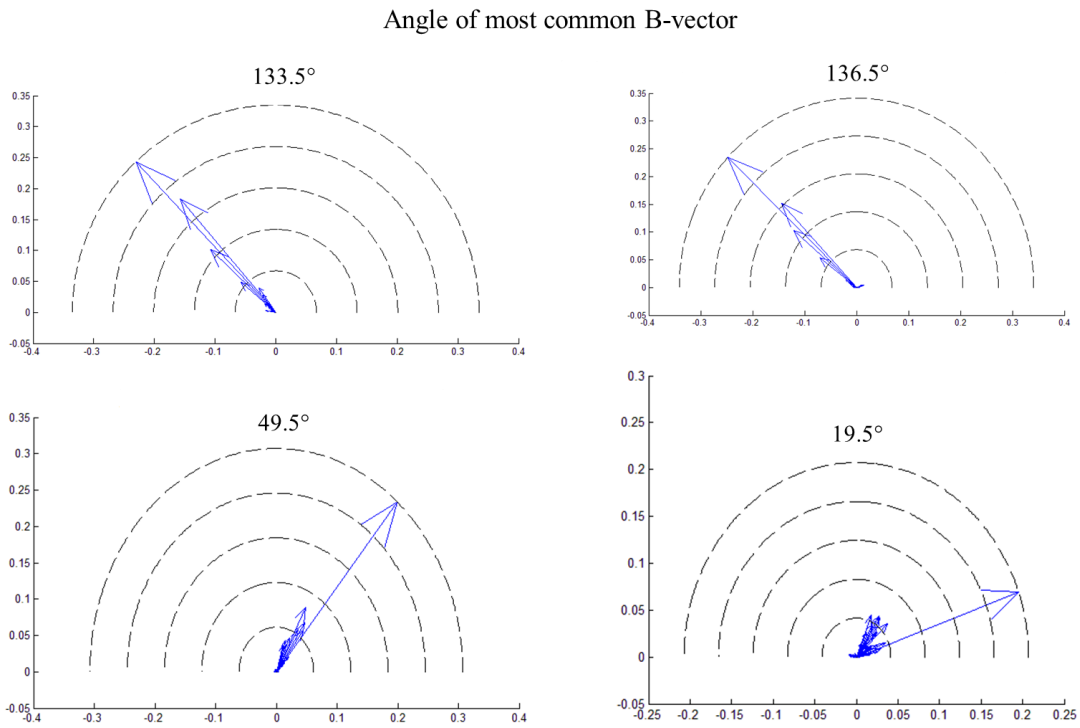

Fig. C-3 Illustration of interval angles with most relative B-field for the four elements.

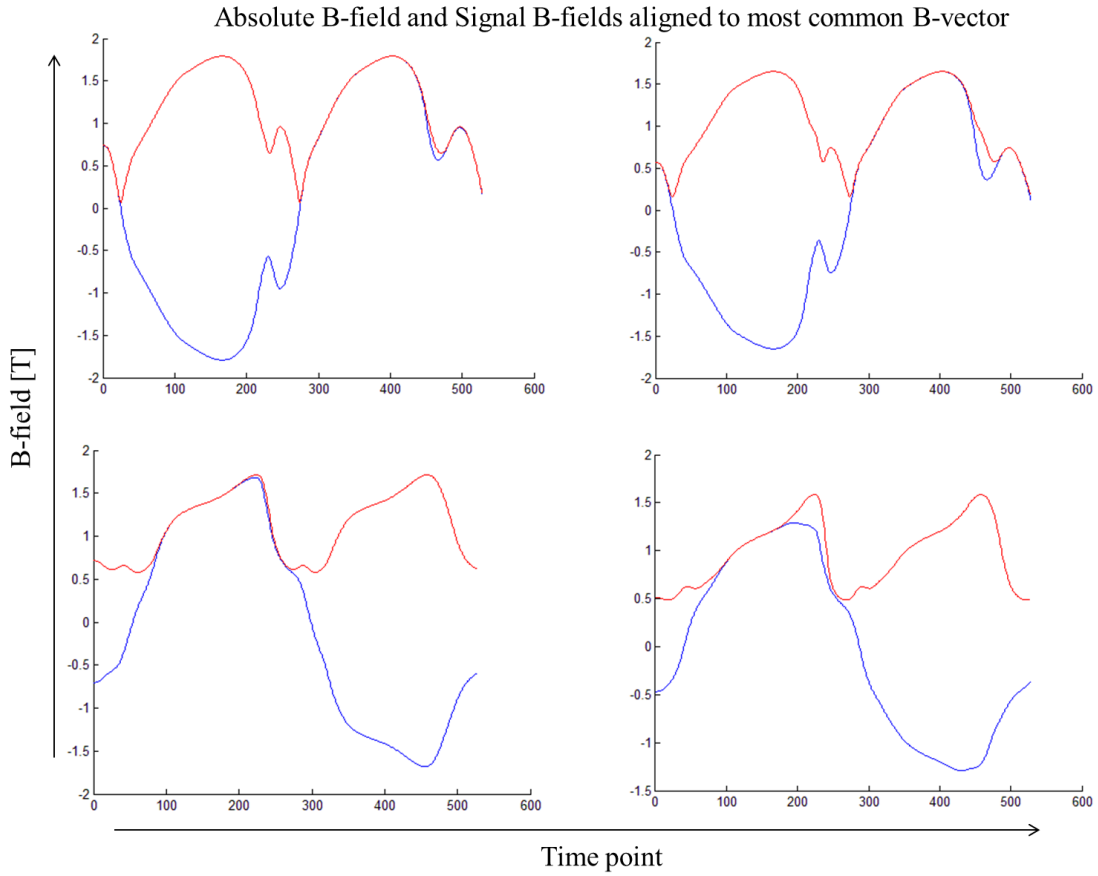

Fig. C-4 Illustration of the absolute B-field (red) and B-field signal aligned to most B (blue) plotted against time points for the four elements.

C.1.2 Script

```
function [B_sig]=find_direction_05(Bx,By)
%function find_direction_v04 has B-field x,y-values for all elements
%as input and will return the angle which contains most B-field.

%Written by Anders Lagerström 2011.03.24

[test_t_e] = size(Bx)~=size(By);

if test_t_e(1)==1 || test_t_e(2)==1
    disp('The number of input arguments are not equally long')
    return
end

Bx = Bx;
By = By;

%get number of time-values and elements
[time, elements] =size(Bx);


for j=1:elements

    %directions do not change for the element
    for u=1:time
```

```
        Bx_n = Bx(u,j);
        By_n = By(u,j);

        %below the angle is given for the polar coordinates
        if Bx_n>0 && By_n>0
            %first quadrant
            angle(u,j) = atan(By_n/Bx_n);
        elseif Bx_n>0 && By_n<0
            %place what should have been in the fourth quadrant in second
            angle(u,j) = atan(By_n/Bx_n)+pi;
        elseif Bx_n<0 && By_n>=0
            %second quadrant
            angle(u,j) = atan(By_n/Bx_n)+pi;
        elseif Bx_n<0 && By_n<0
            %-pi is removed to place the vector in the first quadrant
            %instead in the third.
            angle(u,j) = atan(By_n/Bx_n);
        elseif Bx_n==0 && By_n>0
            angle(u,j) = pi/2;
        elseif Bx_n==0 && By_n<0
            %-pi/2 is replaced with pi/2
            angle(u,j) = pi/2;
        else
            angle(u,j) = 0;
        end

        %absolute value of radial vector
        B_vector(u,j) = sqrt(Bx_n^2+By_n^2);


    end


    %dividing angles into region in order of 3 degrees
    rad_int = pi/60; %radians interval
    k = 1;
    B_values = [0 .5 1 1.5 2 5];
    for u=2:length(B_values)
        B_int(u-1) = B_values(u);
    end
    B_tot = sum(B_vector(:,j)); %total sum of B-field


    for u=0:rad_int:pi-rad_int

        %get index for those vectors within the angle interval
        index = find((angle(:,j)>=u & angle(:,j)<(u+rad_int)));

        %get the B-field fraction for the vectors in angle interval
        B_fraction(j,k) = sum(B_vector(index,j))/B_tot;

        %saves the mean angle for the interval
        %maybe this the B-field should be interpolated so the strength of
        %the B-field decides the angle not just using mean?
        theta(j,k) = u+rad_int/2;

        k=k+1;
    end
```

```
    %get indexnumber for maximum B fraction
    index_max = find(B_fraction(j,:)==max(B_fraction(j,:)));

    %get angle for max B fraction for each element
    f_angle(j) = theta(j,index_max);

    %defining breakage angle for vector
    phi_neg1 = f_angle(j)+pi;
    phi_neg2 = f_angle(j)-pi;

    for u=1:time

        Bx_n = Bx(u,j);
        By_n = By(u,j);

        %below the angle is given for the polar coordinates
        if Bx_n>0
            phi(u,j) = atan(By_n/Bx_n);
        elseif Bx_n<0 && By_n>=0
            phi(u,j) = atan(By_n/Bx_n)+pi;
        elseif Bx_n<0 && By_n<0
            phi(u,j) = atan(By_n/Bx_n)-pi;
        elseif Bx_n==0 && By_n>0
            phi(u,j) = pi/2;
        elseif Bx_n==0 && By_n<0
            phi(u,j) = -pi/2;
        else
            phi(u,j) = 0;
        end

        %get the mirrored size of each flux vector into angle with most B
        if phi(u,j)>phi_neg1
            B_sig(u,j) = (-1)*B_vector(u,j)*cos(phi(u,j)-phi_neg1);
        elseif phi(u,j)<phi_neg2
            B_sig(u,j) = (-1)*B_vector(u,j)*cos(phi(u,j)-phi_neg2);
        elseif phi(u,j)==phi_neg1 || phi(u,j)==phi_neg2
            B_sig(u,j) = 0;
        else
            B_sig(u,j) = B_vector(u,j)*cos(phi(u,j)-f_angle(j));
        end

    end

%     figure
%     hold on
%     plot(1:time,B_sig(:,j));
%     ylabel('Flux denisty [T]')
%     xlabel('Time [s]')
%     title('B-field signal for mirrored vectors in most common angle')
%
%     plot(1:time,B_vector(:,j),'r');


end
```

C.2 Iron losses

C.2.1 Results

Total rotor iron losses for the DW control model and the first CW-machine in the design process are presented in Table C-.

Table C-1 Total rotor iron loss result for three different methods.

	Old, area 6	New, rel. most B^2 (no Fourier analysis)
DW control model [W]	1.19	6.82
First CW-machine [W]	979	1647

C.2.2 Scripts

C.2.2.1 New method with Fourier analysis

```
function loss = lamloss_update(fem,dnr,method)
% lamloss finds lamination loss of domain number 'dnr' in fem structure.
% This is done by analysing the flux density of each element, and finding
% the loss per element based on the flux 'signal'. The sum of loss of 'n'
% harmonics of the flux signal is assumed to be the total loss of each
% element. Sum of all elements in turn is assumed to be total loss for
% domain.
% lamloss_update currently requires auxiliary functions;
% 'oneperiod.m' (post SmartTool 3.3 version)
% 'fourier_by_jump2.m'
% 'jerntapfu_M800_50A.m'
% 'find_direction_v05.m'
% 'find_direction_v06.m'
% method is either 1, 2 or 3 where each number stands for:
% 1 = aligning B-vector to same plane as B_max
% 2 = aligning B-vector to same plane as the plane that contains most B
% 3 = same as 2 but the plane that contains most B^2

wbh = waitbar(0,'Posprocessing data');
% Bexpr =
'Bx_emqa*cos(atan(By_emqa/Bx_emqa))+By_emqa*cos(atan(Bx_emqa/By_emqa))';
area = posteval(fem,'dvol/2','Dl',dnr,'solnum','all','refine','0');
Bx = posteval(fem,'Bx_emqa','Dl',dnr,'solnum','all','refine','0');
By = posteval(fem,'By_emqa','Dl',dnr,'solnum','all','refine','0');
L = 1;%str2double(fem.const{find(strcmp(fem.const,'L'))+1});
F = 36;%str2double(fem.const{find(strcmp(fem.const,'F'))+1});
f = 15.12;%str2double(fem.const{find(strcmp(fem.const,'f'))+1});
rho = 7870;
n = 10; % find losses based on 'n' harmonics of highest amplitude
nrel = length(area.d(1,:)); % number of elements
P = zeros(1,nrel); % Loss vector containing loss per element

waitbar(0,wbh,'Finding loss per element')

if method==1
    for i = 1:100%nrel
        waitbar(i/nrel)
        % assuring only one period of data and equal spacing of data points
        Bxop = oneperiod([fem.sol.tlist',Bx.d(:,i)],f,'noplot');
        Byop = oneperiod([fem.sol.tlist',By.d(:,i)],f,'noplot');
        % finding reference direction based on max B
        absB = sqrt(Bxop(:,2).^2+Byop(:,2).^2); % finding absolute B
```

```
        Bmaxind = find(max(absB));  % finding index of max B
        theta = atan(Byop(Bmaxind,2)/Bxop(Bmaxind,2));  % finding angle of
max B
        Bdata = Bxop(:,2).*cos(theta) + Byop(:,2).*sin(theta); % aligning
all vectors along angle of max B
        % performing harmonic analysis;
        [a_0,a_n,b_n,Ftot_rms,THDu,THDi] = fourier_by_jump2(Bdata',n,1);

        if i==1 | i==10 | i==100
            figure
            plot(Bxop(:,1),Ftot_rms(1)*sqrt(2)*sin(Bxop(:,1)*f*(2*pi)));
            hold on
            plot(Bxop(:,1),Ftot_rms(2)*sqrt(2)*sin(Bxop(:,1)*f*2*(2*pi)));
            plot(Bxop(:,1),Ftot_rms(3)*sqrt(2)*sin(Bxop(:,1)*f*3*(2*pi)));
            plot(Bxop(:,1),Ftot_rms(5)*sqrt(2)*sin(Bxop(:,1)*f*5*(2*pi)));
            plot(Bxop(:,1),Bdata);
        end

        for j = 1:length(Ftot_rms)
            % finding loss of harmonic j of element i
            P(i) = P(i) + jerntapfu_M800_50A(Ftot_rms(j)*sqrt(2),f*j);
        end
        % total loss of element i
        P(i) = P(i)*rho*L*area.d(1,i);
    end
elseif method==2
    for i = 1:nrel
        waitbar(i/nrel)
        %finding B signal based on angle with highest content of B_field
        Bdata = find_direction_v05(Bx.d(:,i),By.d(:,i));
        [a_0,a_n,b_n,Ftot_rms,THDu,THDi] = fourier_by_jump2(Bdata',n,1);
        for j = 1:length(Ftot_rms)
            % finding loss of harmonic j of element i
            P(i) = P(i) + jerntapfu_M800_50A(Ftot_rms(j)*sqrt(2),f*j);
        end
        % total loss of element i
        P(i) = P(i)*rho*L*area.d(1,i);
    end
elseif method==3
    for i = 1:nrel
        waitbar(i/nrel)
        %finding B signal based on angle with highest content of B_field^2
        Bdata = find_direction_v06(Bx.d(:,i),By.d(:,i));
        [a_0,a_n,b_n,Ftot_rms,THDu,THDi] = fourier_by_jump2(Bdata',n,1);
        for j = 1:length(Ftot_rms)
            % finding loss of harmonic j of element i
            P(i) = P(i) + jerntapfu_M800_50A(Ftot_rms(j)*sqrt(2),f*j);
        end
        % total loss of element i
        P(i) = P(i)*rho*L*area.d(1,i);
    end
end

close(wbh)

% total loss of domain 'dnr' multiplied by number of slots
loss = sum(P)*F;

% area = 0;
% for i = 1:length(pd.t)
```

```
%     pts = pd.p(:,pd.t(:,i))';
%     [q,r,e] = qr((pts(2:3,:) - repmat(pts(1,:),2,1))');
%     area = area + abs(prod(diag(r)))/2;
% end

end
```

C.2.2.2 New method without Fourier analysis

```
function loss = lamloss_no_fourier_rev2(fem,dnr)
% lamloss finds lamination loss of domain number 'dnr' in fem structure.
% This is done by analysing the flux density of each element, and finding
% the loss per element based on the flux 'signal'. The sum of loss of 'n'
% harmonics of the flux signal is assumed to be the total loss of each
% element. Sum of all elements in turn is assumed to be total loss for
% domain.

wbh = waitbar(0,'Postprocessing data');

area = posteval(fem,'dvol/2','Dl',dnr,'solnum','all','refine','0');
Bx = posteval(fem,'Bx_emqa','Dl',dnr,'solnum','all','refine','0');
By = posteval(fem,'By_emqa','Dl',dnr,'solnum','all','refine','0');
L = 1;%str2double(fem.const{find(strcmp(fem.const,'L'))+1});
F = 36;%str2double(fem.const{find(strcmp(fem.const,'F'))+1});
%f = 15.12;%str2double(fem.const{find(strcmp(fem.const,'f'))+1});
rho = 7870;
time = fem.sol.tlist;
nrel = length(area.d(1,:)); % number of elements
P = zeros(1,nrel); % Loss vector containing loss per element

waitbar(0,wbh,'Finding loss per element')

for j = 1:nrel
    waitbar(j/nrel)

    Bdata = find_direction_v06(Bx.d(:,j),By.d(:,j));
    %aligning B-values to most common B-direction

    e_max(j) = (max(Bdata)-min(Bdata))/2; %max B-value
    Bdata = Bdata-(max(Bdata)-e_max(j));
    %if there is an offset of the values

    if j==10% | j==10 | j==40 | j==100
        plot(0:length(Bdata)-1,Bdata)
        hold on
    end

    %Below is to collect the frequency
    %!!!! Watch out for large harmonics, if the field contains these so it
    %crosses zero only to return up to maximum value instead of continuing
    %towards minimum the frequency will be wrong.!!!!!!

    index=0;%start value
    k=1;%start value
    while index==0 %extracts the index number for the first zero-crossing
        if (Bdata(k)<0 && Bdata(k+1)>0) ||  (Bdata(k)>0 && Bdata(k+1)<0)
            index=k;
```

```
x_int=abs(Bdata(index))/(abs(Bdata(index))+abs(Bdata(index+1)));
            %for interpolation to get the time for zero emf
        else
            k=k+1;
        end
    end

    index_2=0;
    k=index+1;
    while index_2==0 %extracts the index number for the second zero-
crossing
        if (Bdata(k)<0 && Bdata(k+1)>0) ||  (Bdata(k)>0 && Bdata(k+1)<0)
            index_2=k;

x_int=abs(Bdata(index))/(abs(Bdata(index))+abs(Bdata(index+1)));
            %for interpolation to get the time for zero emf
        else
            k=k+1;
        end
    end

%     %test
%     count=0;
%     for i=1:length(Bdata)-2 %to get the frequency by looking at number of
max-values
%         if (Bdata(i+2)-Bdata(i+1))<0 && (Bdata(i+1)-Bdata(i))>0
%             count=count+1; %number of max values
%         end
%     end
%     f_test(j)=1/(max(time)/count);

    f(j) = 1/(2*(time(index_2)-time(index))); %the frequency

        P(j) = jerntapfu_M800_50A(e_max(j),f(j)); %Loss per kg
        P(j) = P(j)*rho*L*area.d(1,j); %Loss per element
end

close(wbh)

loss =sum(P)*F; %total loss
```

C.3 Control model

C.3.1 Areas

Areas that are used in iron loss calculations are:

- Stator areas:
  - Area 1, illustrated in Fig. C-.
  - Area 2, illustrated in Fig. C-.
  - Area 3, illustrated in Fig. C-.
  - Area 4, the tooth in area 3, illustrated in Fig. C-.
  - Area 5, the yoke in area 3, illustrated in Fig. C-.
- Rotor area:
  - Area 6, illustrated in Fig. C-.

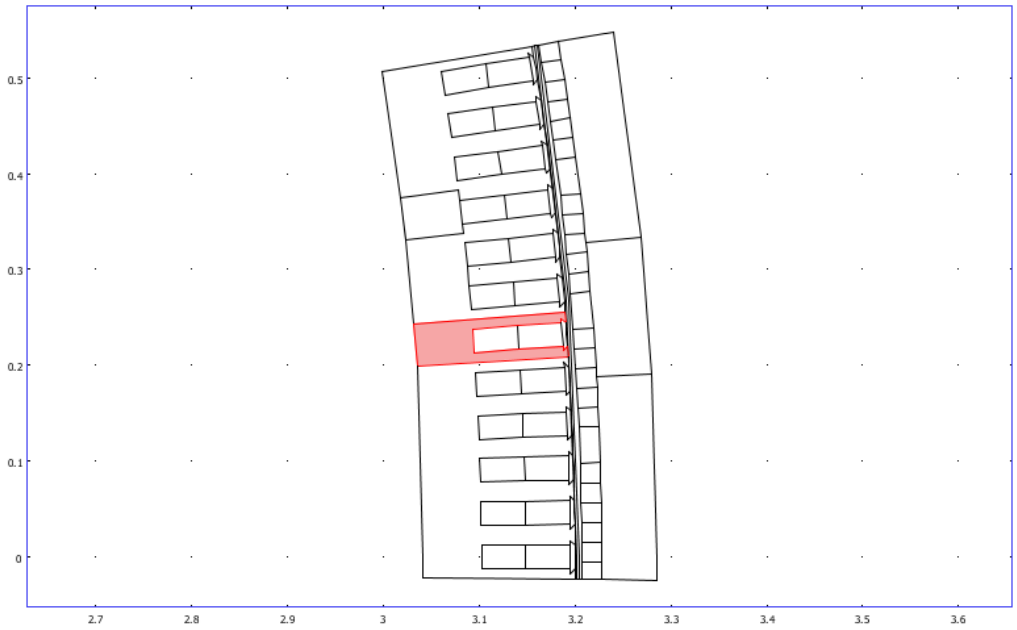

Fig. C-5 Illustration of area 1.

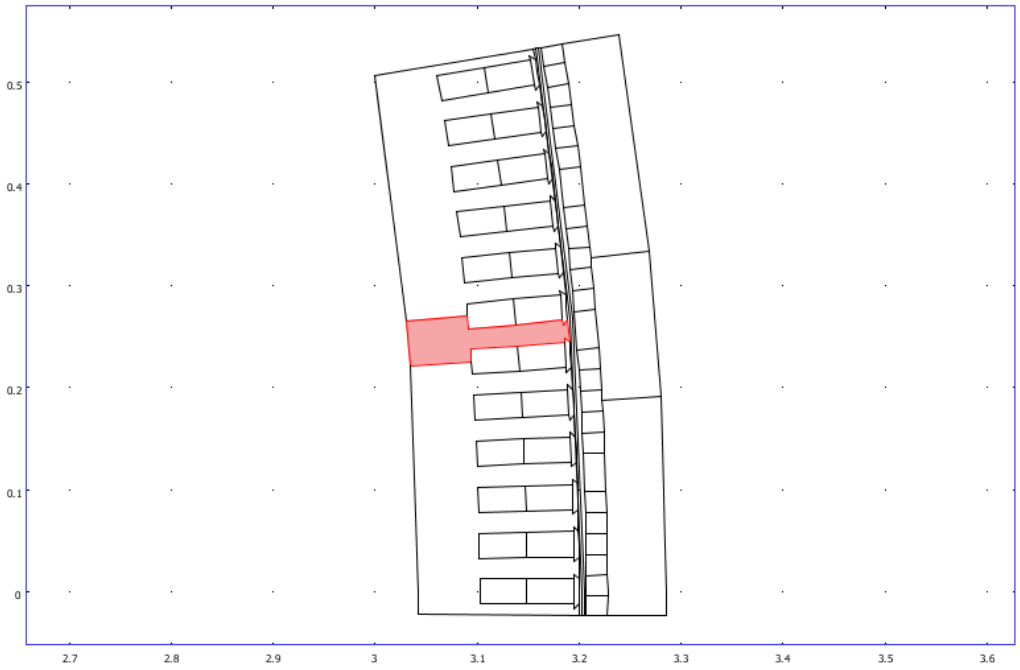

Fig. C-6 Illustration of area 2.

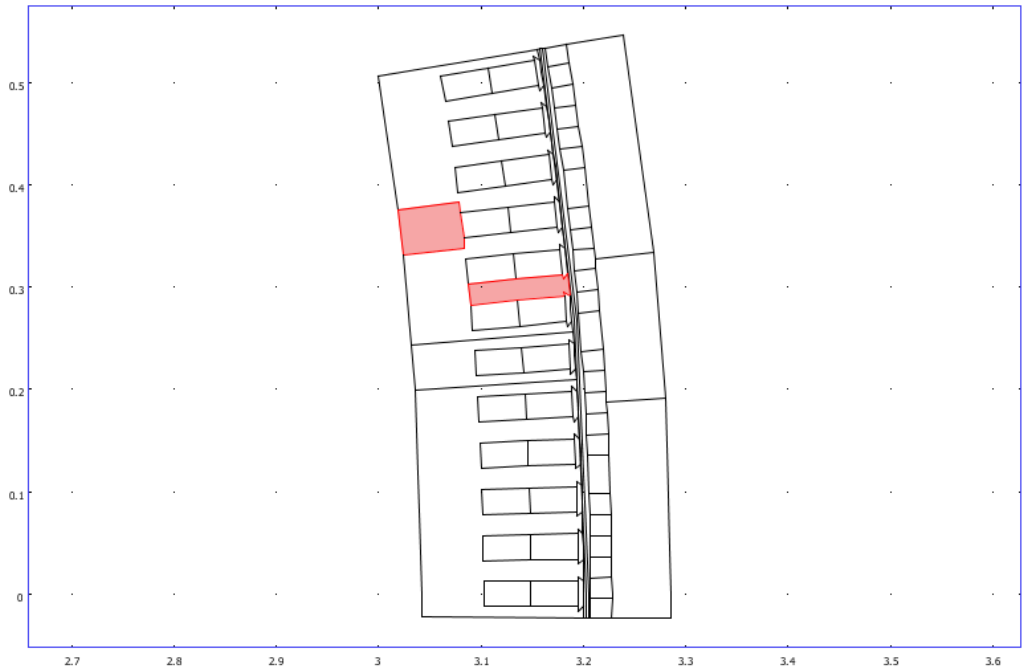

Fig. C-7 Illustration of area 3.

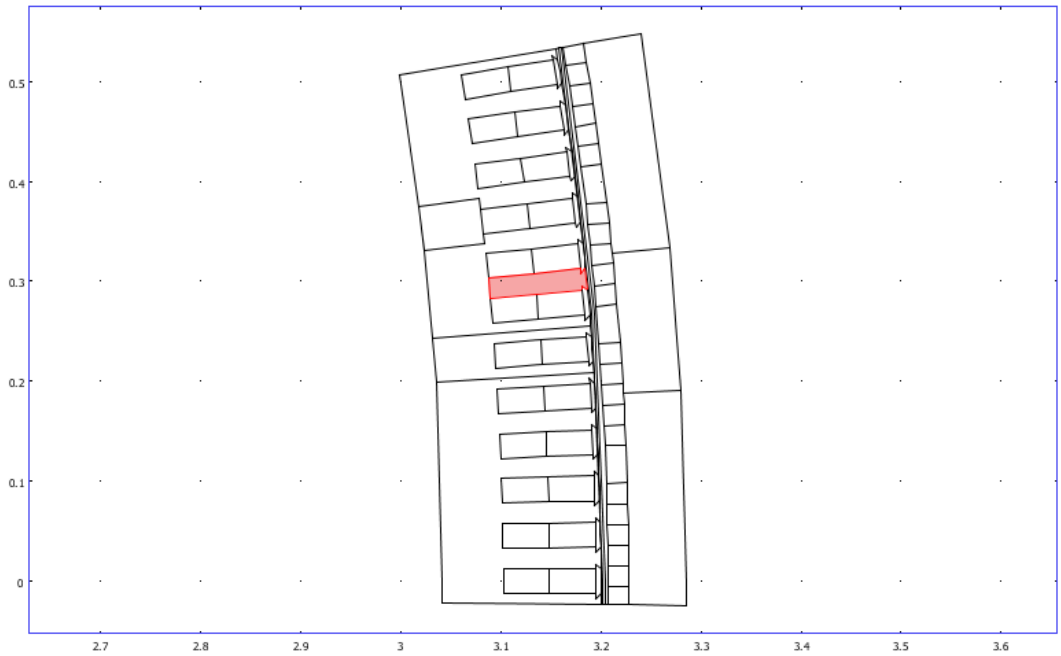

Fig. C-8 Illustration of area 4.

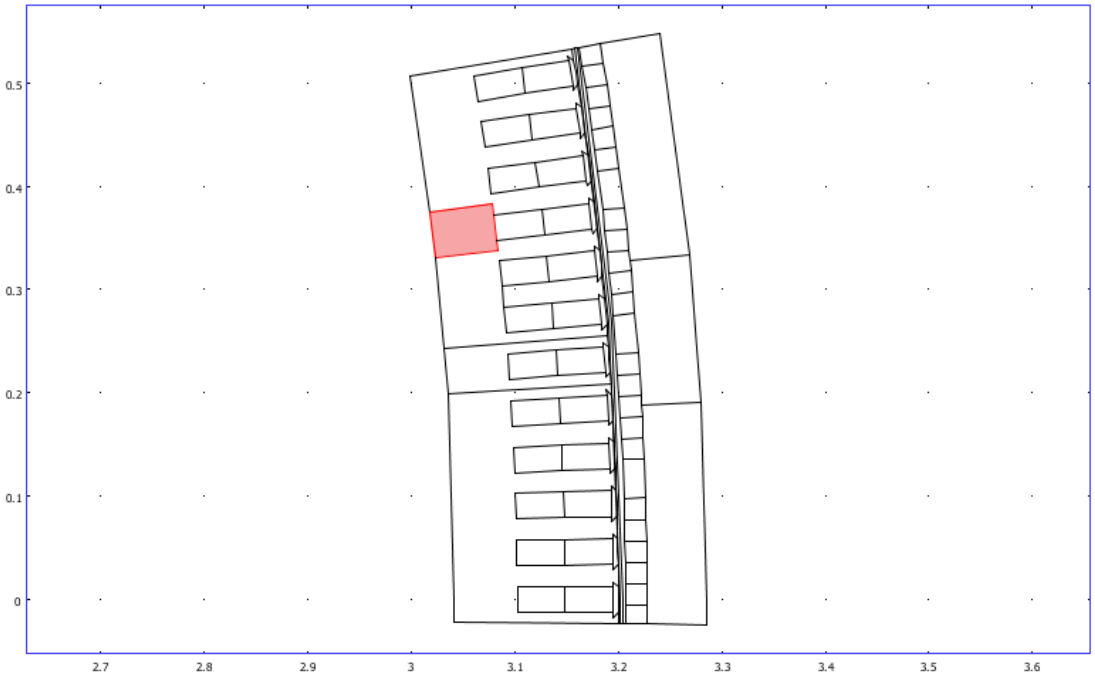

Fig. C-9 Illustration of area 5.

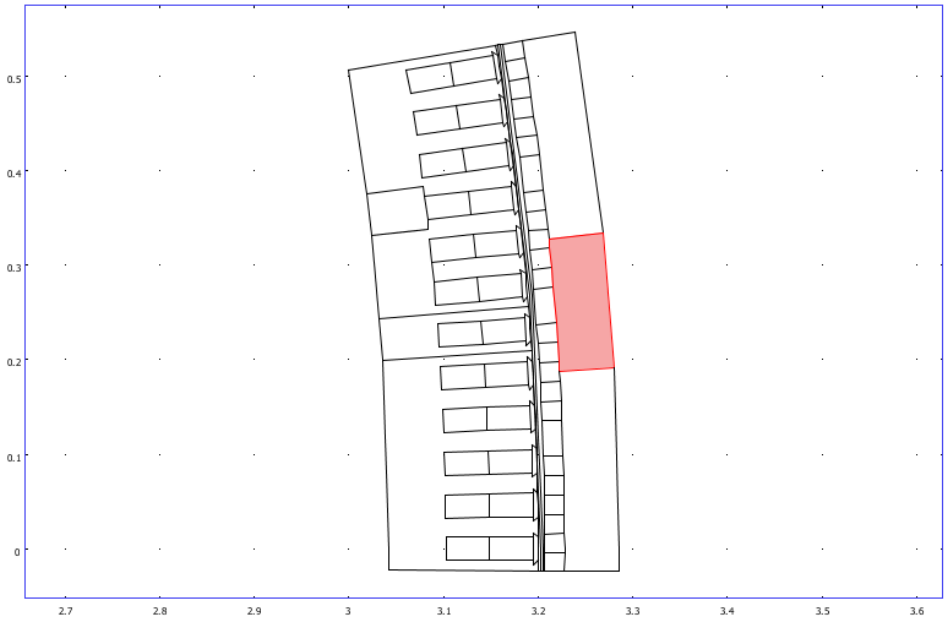

Fig. C-10 Illustration of area 6.

D Appendix

Electrical results from the comparison of DW- and CW-machines

D.1 DW and CW results

D.1.1 EMF

Electrical properties for each design are presented in Table D-.

Table D-1 Presentation of the different skewing and winding factors together with the chosen current density of each design.

	DW(un-skewed)	DW (skewed)	CW no magnetic wedge	CW semi-magnetic wedge	CW-last
$K_{s\ sinusoidal}$	1	0.9549	1	1	1
$K_{s\ square\ wave}$	1	0.8333	1	1	1
$K_{s\ real}$	1	0.9549	1	1	1
K_w	1	1	0.958	0.958	0.958
J_{rms} [A/mm^2]	3.2012	3.3528	3.1190	3.1190	3.0

The effect on the phase-emf for the DW-generator from of skewing the magnets is presented in Fig. D-.

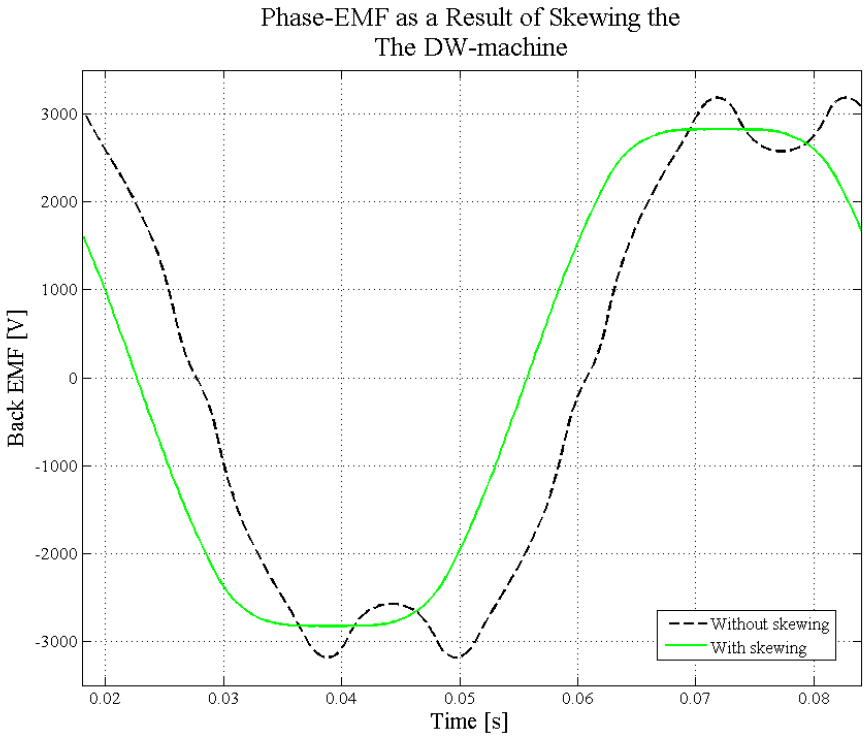

Fig. D-1 Illustration of the phase-emf result of the skewed DW-machine.

The line-emfs for each design are given in Fig. D-. The phase-emfs for each design are given in Fig. D-.

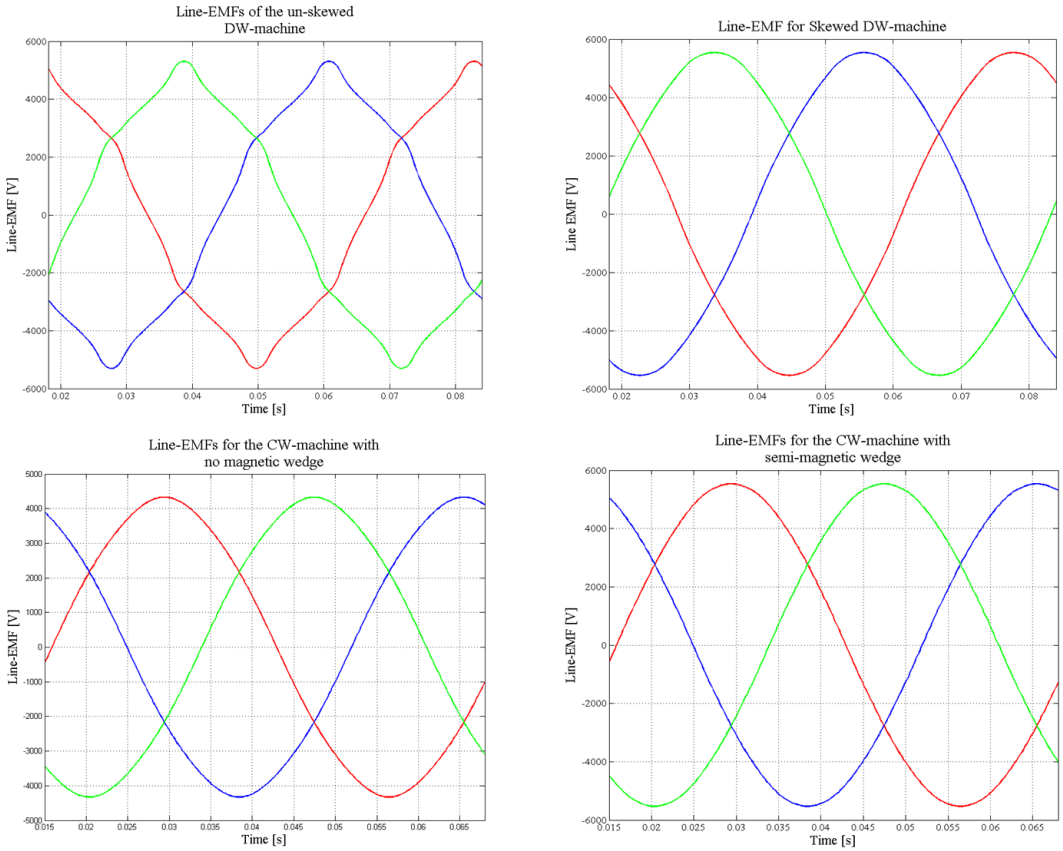

Fig. D-2 Illustration the line emf for each design.

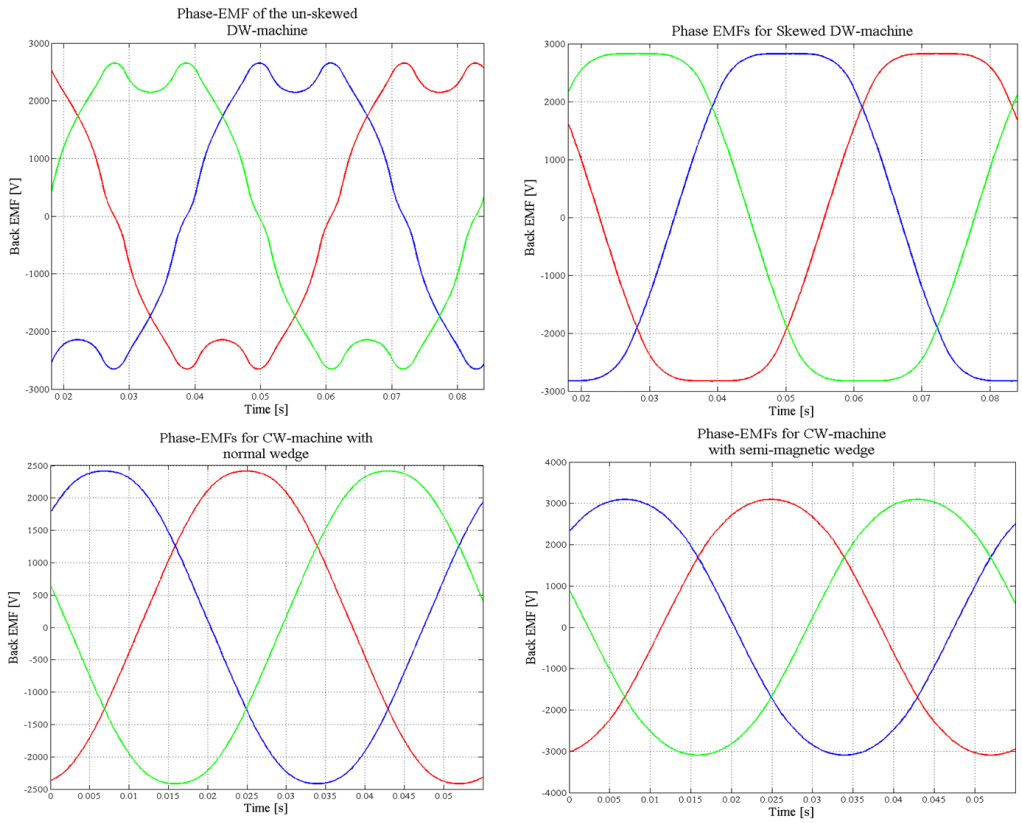

Fig. D-3 Illustration the phase-emf for each design.

The key results from the emf-simulations are given in Table D-.

Table D-2 The result from the EMF simulations for each machine including THD and peak values.

	$DW_{no\ skew}$	**DW_{skewed}**	**CW with no magnetic wedge**	**CW with semi-magnetic wedge**	**CW-last**
Mean Phase peak emf [V]	2654	2827	2416	3093	2593
Mean 1st harm rms emf [V]	1963	2250	1750	2256	1921
Mean Phase THD [%]	17.2	10.69	1.68	3.02	4.49
Mean Line peak emf [V]	5305	5536	4329	5534	4706
Mean Line THD [%]	6.64	1.28	1.07	0.68	0.62

The harmonic content of the phase-emf for each design is presented in Fig. D-. The harmonic content of the line-emf for each design is presented in Fig. D-.

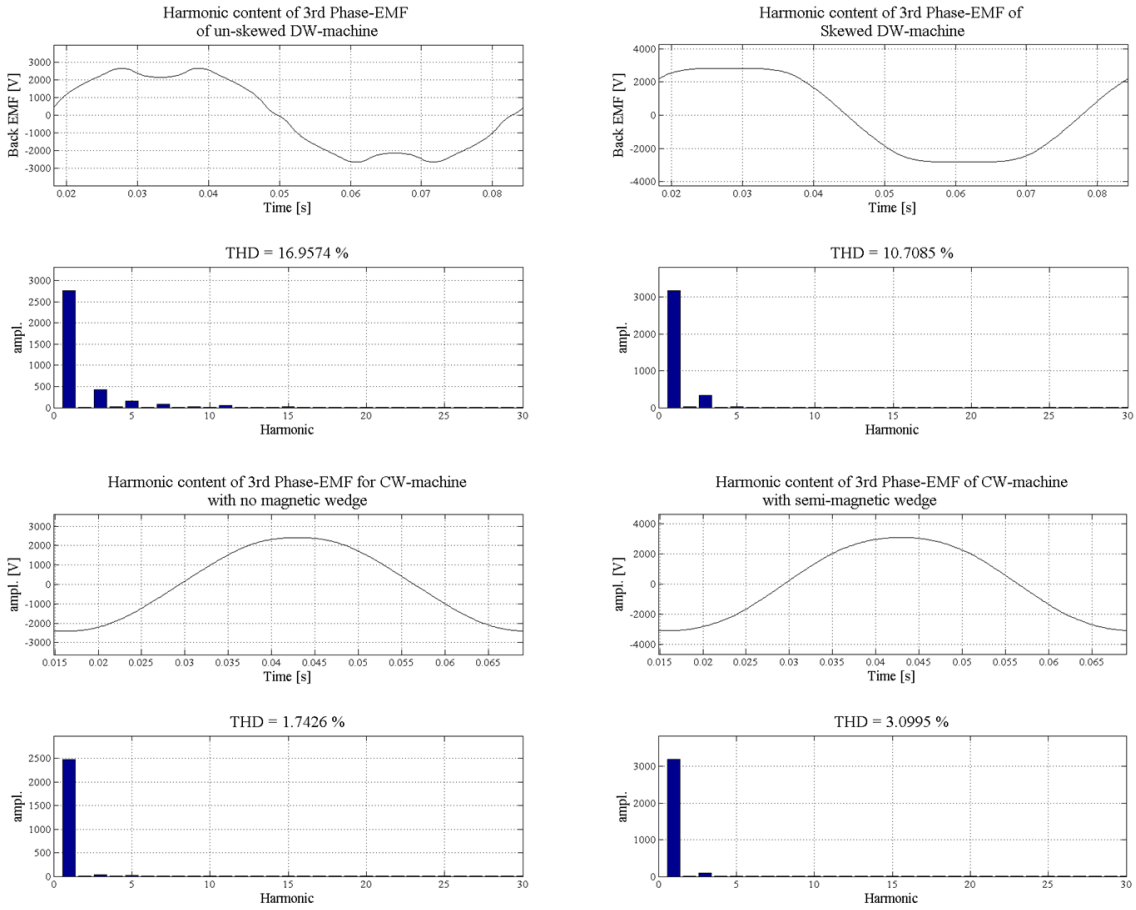

Fig. D-4 Illustration of the THD of each 3rd phase emf for the four different designs.

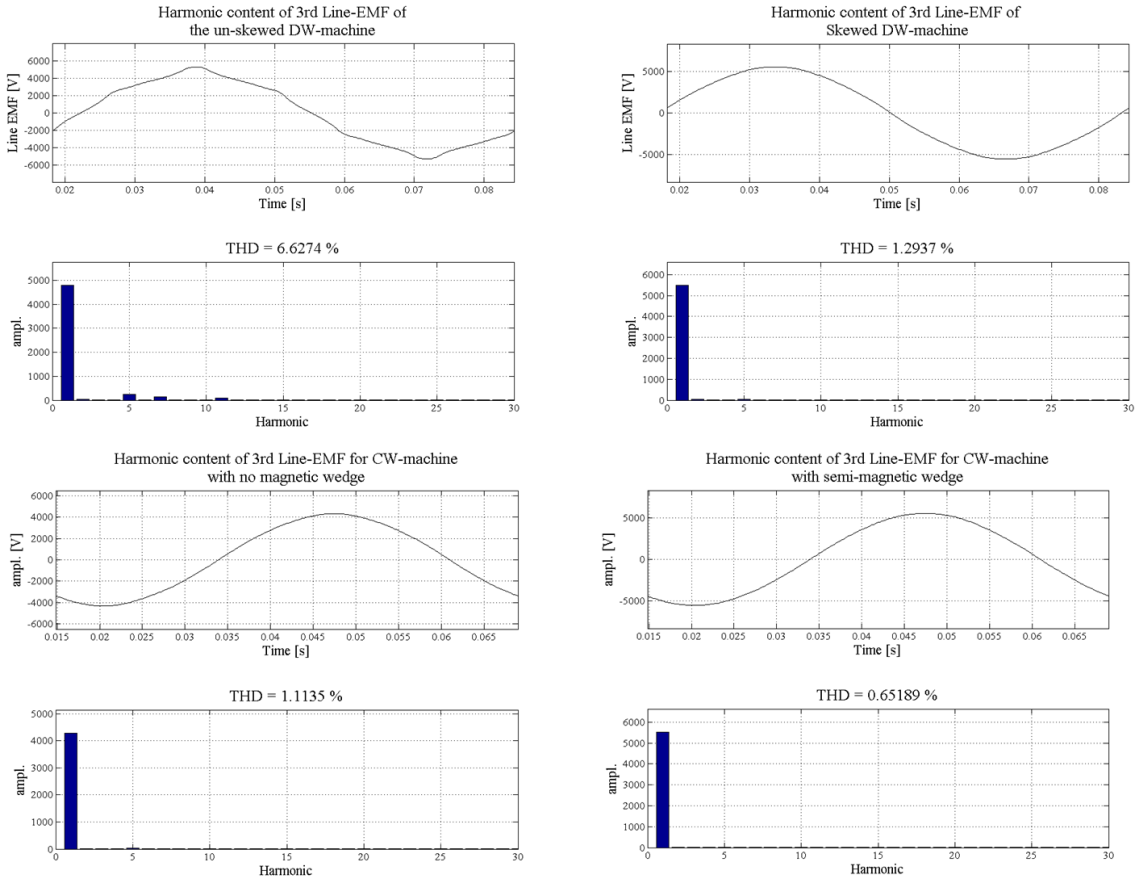

Fig. D-5 Illustration of the THD of each 3rd line emf for the four different designs.

D.1.2 Torque full-load

The results for cogging at no-load and torque ripple at full load for each of the designs are plotted below in Fig. D- and Fig. D-.

All detailed results of from each design during the design process are summed up in Table D-. The skewing result from when DW is skewed compared when it is not is illustrated in Fig. D-8.

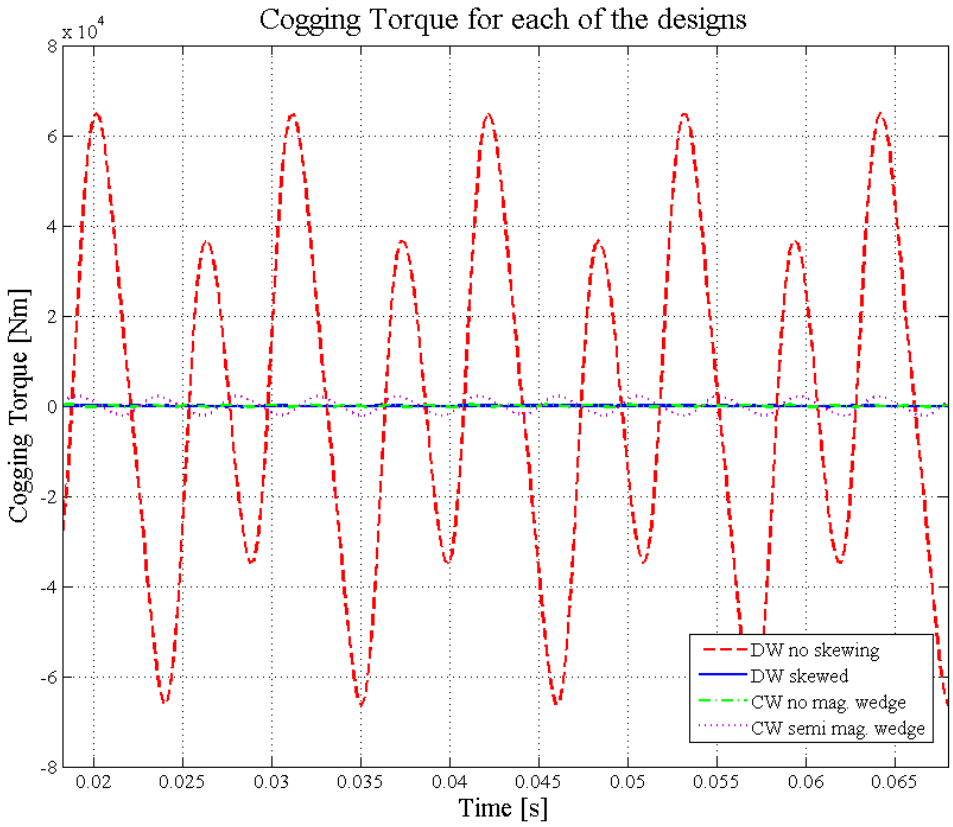

Fig. D-6 Illustration of the cogging torque at no-load for each of designs.

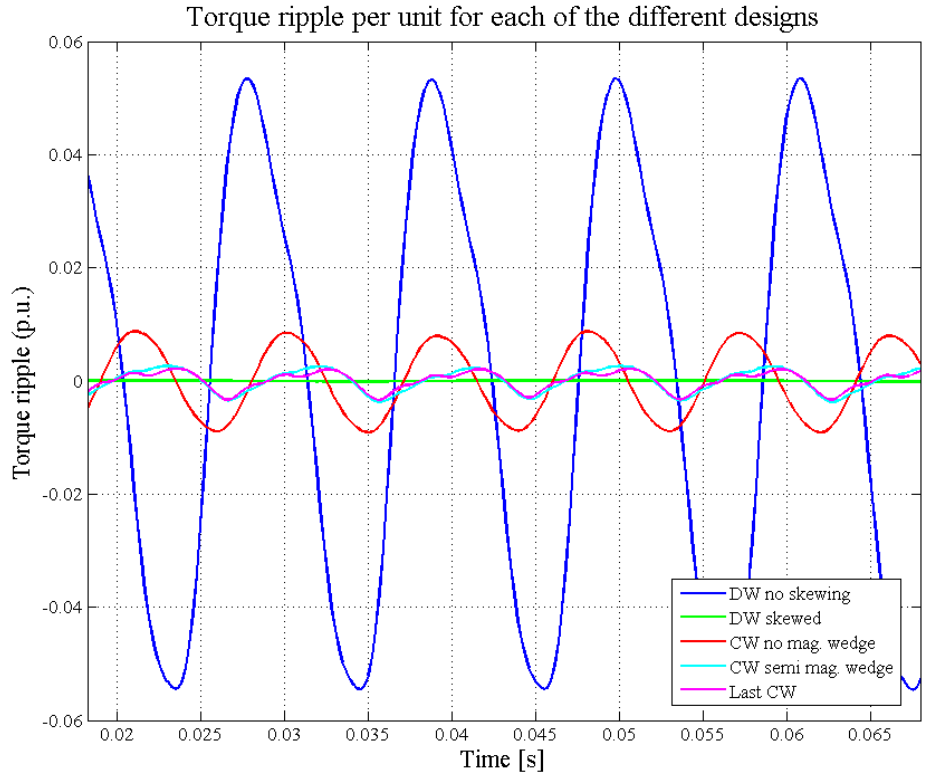

Fig. D-7 Illustration of the torque ripple (p.u.) for each of the design.

Table D-3 Key results for each design.[4]

	DW (un-skewed)	**DW (skewed)**	**CW with no magnetic wedge**	**CW with semi-magnetic wedge**	**CW-final**
Active length [m]	0.9688	0.9688	0.9627	0.9523	1.0325
Length with E.W.	1.44	1.44	-	-	1.1881
Mean Torque [Nm]	3020846	3012286	3047485	3012906	3029653
Torque ripple p.u. [%]	10.81	0.022	1.79	0.79	0.70
d_{ag} Air gap diameter [mm]	6400	6400	6410	6410	6407
Tangential tension [kN/m^2]	48.46	48.33	49.06	49.02	45.51
P_{stator} [kW]	20.865	21.119	18.262	18.693	20.067
P_{rotor} [kW]	0.001	0.001	1.849	1.717	1.653
$P_{magnets}$ [kW]	5.535	5.570	14.754	11.476	10.966
$P_{windings}$ [kW] (at 120 degC)	151.625	157.441	131.854	130.759	120.250
P_{mech}[kW]	3985.9	3974.6	4021.1	3975.4	3997.5
P_{active} [kW]	3807.9	3790.47	3854.3	3812.8	3844.6
Efficiency [%]	95.53	95.37	95.85	95.90	96.18
Mass of rotor core [kg]	3680.97	3680.97	3924.6	3882.2	4268.9
Mass of stator core [kg]	14310.17	14310.17	9657.2	9552.8	10872.4
Mass of magnets [kg]	2276.8	2276.8	2771.2	2741.2	2973.8
Mass of windings [kg]	5213.2	5213.2	5045.4	5003.5	4973.7
Total mass [kg]	27045	27045	21398.3	21179.7	23088.9
Torque/weight [Nm/kg]	111.70	111.38	142.42	142.25	131.22
Power/weight [W/kg]	147.38	145.96	187.92	187.70	173.14
Phase self-inductance [μH]	12066 (12961)	17080 (18841)	13418	23051	15648
Synchronous reactance (p.u.)	0.401 (0.425)	0.428 (0.463)	0.545	0.555	0.527
Power factor [cos(θ)]	0.916 (0.905)	0.904 (0.886)	0.839	0.839	0.845
$U_{line\text{-}line}$ (rms) [V]	3449 (3491)	3987 (4066)	3626	4702	3949
Apparent power [kVA]	4157 (4208)	4194 (4277)	4595	4583	4524
Cogging amplitude [Nm]	65832.52	147.22	321.00	2177.1	4001.4

[4] DW results that is presented in brackets have used analytical inductance calculations in chapter 2.1.6 in order to account for end-winding self-inductance and mutual inductance.

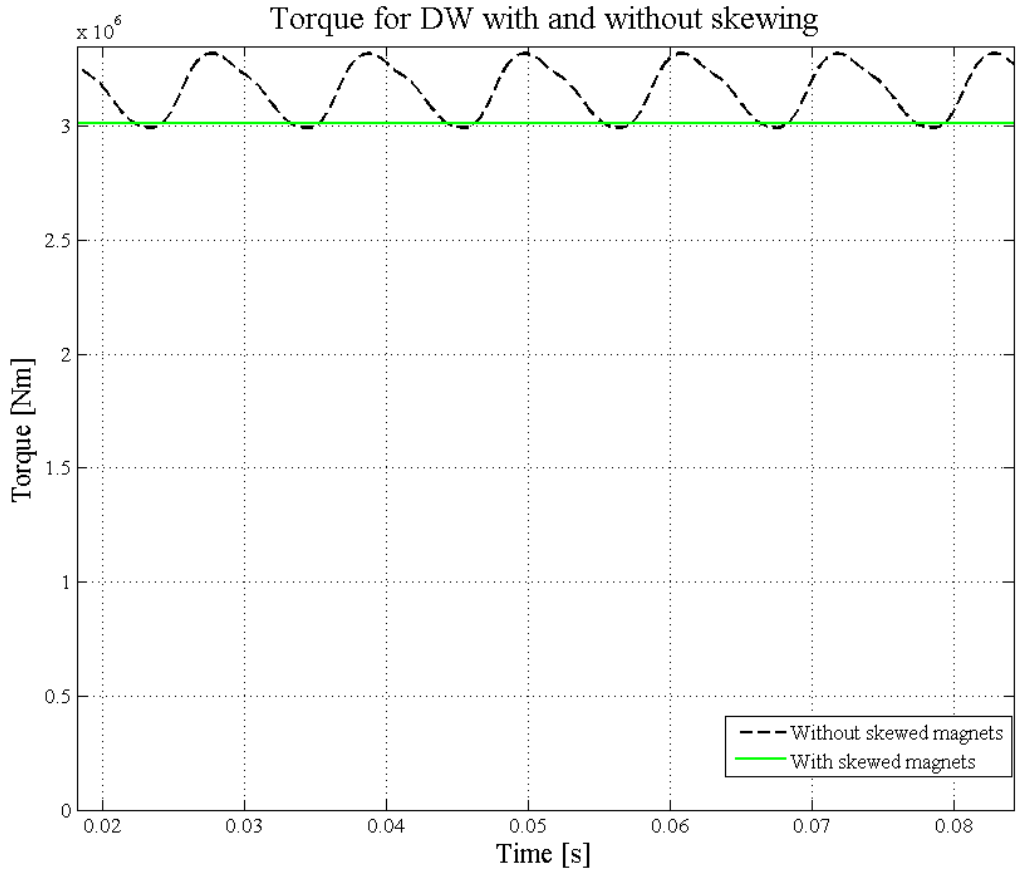

Fig. D-8 Illustration of the torque at full-load when the DW-machine is skewed and if it would not be skewed.

E Appendix

Thermal calculations

E.1 Thermal network

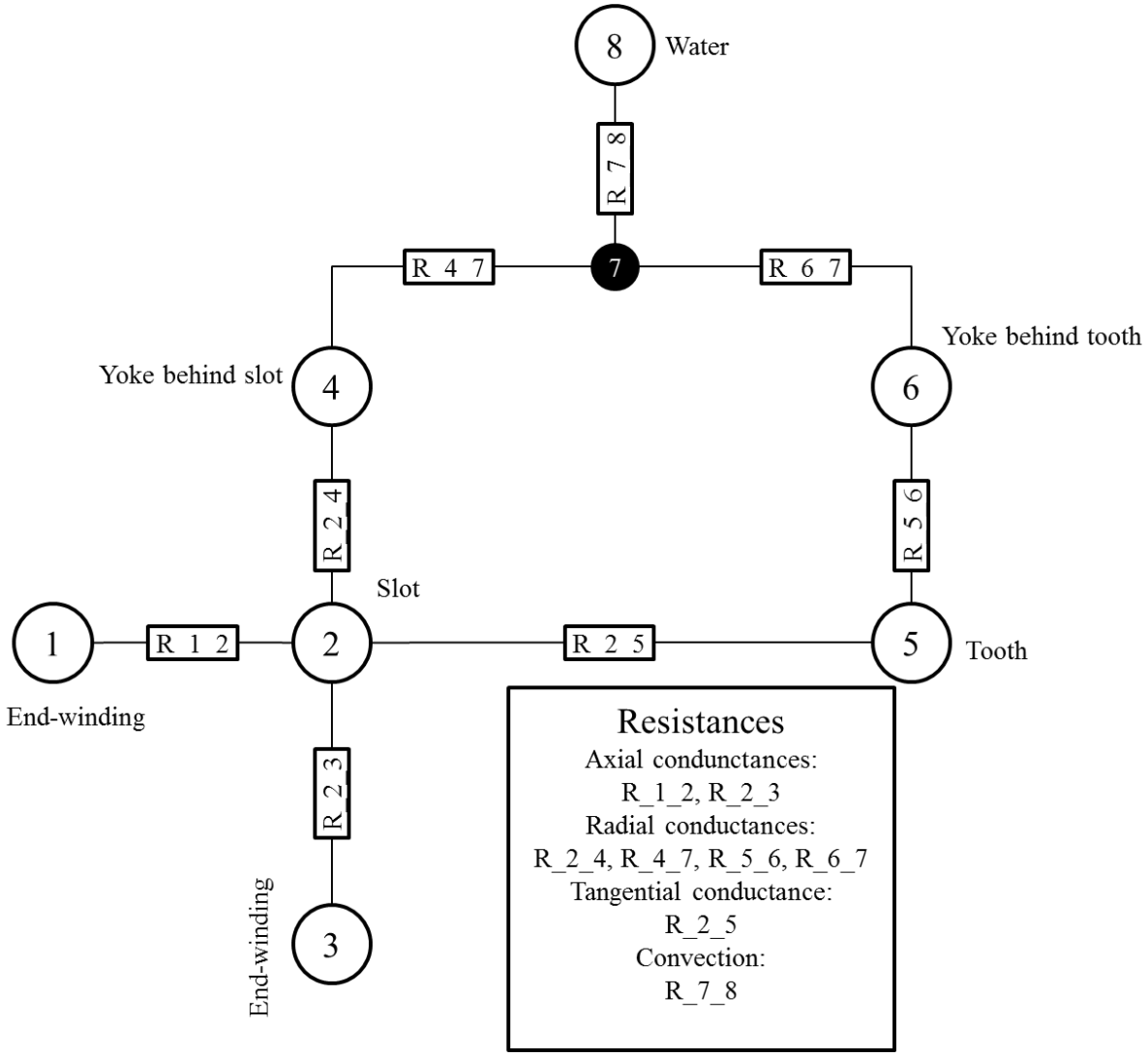

Fig. E-1 Illustration of the thermal network model that was used in the thermal analysis of the machines.

E.2 Temperatures

The key temperatures from the thermal network model for each design are presented in Table E-.

Table E-1 Presenting the key temperatures in °C for each of the designs.

	DW un-skewed	DW-skewed	CW with no mag. wedge	CW with semi-mag. wedge	CW-last
End-windings (node 1 and 3)	173	175	195	195	173
Slot (node 2)	139	140	162	162	142
Tooth (node 5)	108	108	90	90	81
Yoke surface (node 7)	74	75	75	75	69

E.3 Script

```
function [T] = thermal_water(ms,P_yoke,P_teeth,P_magnets,P_rotcore)
%thermal network modell for water cooling on a machine with outer rotor,
%look out for R_so and R_si if applied for inne rotor.
%input is a motor structure (ms) and output is the temperatures in the
%different nodes.

%Simplifications that is made are that it is assumed the copper is in one
%solid piece in the middle of the slot and that the cooling fluid has
%constant temperature.

%All measures are in meter.


%% Geometry
DW=input('Is it DW? (Y=1 and N=0)');

layer=1;%ms.el.layers.Nlay_theta*ms.el.layers.Nlay_rad;
%indicates single or double layer winding

Ns=ms.geom.Ns;
%number of slots

R_so=ms.geom.r_so;
%outer stator radius

R_si=ms.geom.r_si;
%inner stator radius

if DW
    slot_d=ms.geom.d_s+ms.geom.th_sw*2;
    %slot depth including slot wedge at top and bottom
    slot_d_in=ms.geom.d_s;
    %slot depth removing wedges
else
    slot_d=ms.geom.d_s;
    %total slot depth
    slot_d_in=ms.geom.d_s-ms.geom.th_sw;
    %slot depth removing slot wedges
end
```

```
slot_w=ms.geom.w_s;
%slot width

theta_s  =ms.geom.theta_s;
%angular slot pitch

if ms.mech.innerrotor %innerrotor
    tooth_w = ms.geom.theta_s*R_si-slot_w;
    %tooth width
    yoke=R_so-(slot_d+R_si);
    %stator yoke thickness
    R_stat_in = R_si;
    %for winding_length.m
else %outer rotor
    tooth_w=ms.geom.theta_s*R_so-slot_w;
    %tooth width
    yoke=R_so-slot_d-R_si;
    %stator yoke thickness
    R_stat_in = R_so-slot_d;
    %for winding_length.m
end



if DW
    k_cu_in=ms.el.k_cu_nowedge;
    k_cu=k_cu_in*(ms.geom.d_s/slot_d);
    %slot fill factor
else
    k_cu=ms.el.k_cu_slot;
    k_cu_in=ms.el.k_cu_nowedge;
    %slot fill factors
end

L=ms.geom.L;
%active length of machine

Nlay_theta=1;
Nlay_rad=1;
Np       = ms.geom.Np; % number of poles
wlayout  = ms.el.wlayout; %winding layout
J = ms.el.J; %current density

if DW
    [L_tot,L_phase] =
winding_length(Nlay_theta,Nlay_rad,Ns,Np,3,wlayout,'lap',tooth_w,slot_d,slo
t_w,R_stat_in,L);
    %calculates the total length and phase length
    L_ew = (L_tot-Ns*L);
    %total end windings length
    L_ew_s=L_ew/(Ns/2*layer)/2;
    %length of end winding per slot
    %calculating for end windings on both sides of the slot.
else
    L_ew = (3/2*slot_w+ms.geom.tau_s)*pi*Ns/2+0.001*Ns*2;
    L_tot = L_ew + L*Ns;
    L_ew_s=L_ew/(Ns/2*layer)/2;
end

    %area in axial direction
```

```
A_s = slot_w*slot_d;
%slot area
A_cu = k_cu*A_s;
%area copper bar

    %areas in radial and tangetial direction
A_s_rad = L*slot_w;
%slot area in radial direction applied both for (insulation and yoke-
behind-slot).
A_s_tan = L*slot_d;
%slot area in tangential direction (applied for insulation and tooth).
A_t_rad = L*tooth_w;
%tooth area in radial direction (applied for tooth and yoke-behind-tooth).
A_y_rad = A_s_rad+A_t_rad;
%yoke area in radial towards water

    %thicknesses in radial and tangetial direction
if layer==1
    th_ins=(slot_w+slot_d_in)/4-sqrt(((slot_w+slot_d_in)/4)^2-(1-
k_cu_in)*A_s/4);
    %insulation thickness, assuming one bars with equally thick insulation
    %on each side [m]
elseif layer ==2
    th_ins=(3*slot_w+2*slot_d_in)/12-sqrt(((3*slot_w+2*slot_d_in)/12)^2-
A_s/6*(1-k_cu_in));
    %insulation thickness, assuming two bars with equally thick insulation
    %on each side [m]
else
    disp('This code do not apply for more than 2-layers');
end

th_tooth_tan = tooth_w/2;
%tooth thickness (assumed to go in to the middle of the tooth)
th_tooth_rad = slot_d/2;
%thooth thickness (assumed to go from the middle of the tooth)
th_y_rad = yoke/2;
%yoke thickness (assumed to go to the middle of the yoke this will be used
%for both behind slot and behind tooth, heat is assumed not to move in
%tangential direction in the yoke.

%% Losses

    %Water temperature
T_water =50; %[degC]

    %Other parameters
magnet_frac   = ms.geom.w_pm/ms.geom.tau_p;
%magnet fraction
k_st    = 0.95;
%assumed iron stacking factor
r_ri    = ms.geom.r_ri;
%rotor inner radius
r_rii    = ms.geom.r_rii;
%rotor iron inner radius
r_rio    = ms.geom.r_rio;
%rotor outer radius

    %Volumes [m^3]
V_rotcore = pi*(r_rio^2-r_rii^2)*L*k_st;
```

```
%rotor core

if ms.mech.innerrotor
    V_yoke = (pi*(R_so^2-(R_si+slot_d)^2))*L*k_st;
    %yoke
    V_teeth = (pi*((R_si+slot_d)^2-R_si^2)-Ns*slot_d*slot_w)*L*k_st;
    %teeth
else
    V_yoke = (pi*((R_so-slot_d)^2-R_si^2))*L*k_st;
    %yoke
    V_teeth = (pi*((R_so)^2-(R_so-slot_d)^2)-Ns*slot_d*slot_w)*L*k_st;
    %teeth
end

V_magnets = pi*(r_rii^2-r_ri^2)*magnet_frac*L;
%magnets

V_windings = L_tot*slot_d*slot_w*k_cu;
%copper

%Copper losses
To = 120;
%operational temperature, [degC]
sigma_w20 = 58e6;
%electric conductivity of copper at 20 degC
sigma_w = sigma_w20*(234.5+20)/(234.5+To);
%electric conductivity at operational temperature
P_dc = J^2*A_cu*L_tot/sigma_w;
P_windings = P_dc*1;
disp(P_windings)

%k_new=(k_cu_in*J)^2*L_tot*A_s/(P_windings*sigma_w);
%disp(k_new)
    %Loss per volume [W/m^3]

PV_rotcore = P_rotcore/V_rotcore;
%not used in this case

PV_yoke = P_yoke/V_yoke;

PV_teeth = P_teeth/V_teeth;

PV_magnets = P_magnets/V_magnets;
%not used in this case

PV_windings = P_windings/V_windings;

    %Per slot

P_ew = PV_windings*(L_ew_s*A_cu);
%end winding losses

P_s = PV_windings*(L*A_cu);
%slot winding losses

P_y_bs = PV_yoke*(yoke*A_s_rad);
%yoke losses behind slot
```

```
P_t = PV_teeth*(slot_d*A_t_rad);
%tooth losses

P_y_bt = PV_yoke*(yoke*A_t_rad);
%yoke losses behind tooth

%% Material properties
%at room temperature

    % Thermal conductivity

k_copper=394; %from Design of Rotating Electrical Machines
%for copper [W/(m*degC)]

k_iron=40; %from Design of Rotating Electrical Machines
% iron in radial direction [W/(m*degC)]

k_mica=0.5; %from Physics handbook
%for mica insulation [W/(m*degC)]

k_water=0.6;%from Design of Rotating Electrical machines
%for water  [W/(m*degC)]

    % Specific heat at constant pressure

cp_cu=385; %from Design of Rotating Electrical Machines
%[J/(kg*degC)]

cp_iron=460; %from Design of Rotating Electrical Machines
%[J/(kg*degC)]

cp_water=4182;%Engineering Toolbox
%at 50 degC!!!! [J/(kg*degC)] assumed for heat exchanger with air

    % Density

rho_cu=8960; %from Design of Rotating Electrical Machines
%[kg/m3]

rho_iron=7700; %from Design of Rotating Electrical Machines
%[kg/m3]

rho_mica=2800; %from Physics handbook
%[kg/m3]

rho_water=988;%Engineering Toolbox
%at 50 degC!!!! [kg/m3]

    %Prantl, Reynolds and Nusselt numbers

my_water = 0.000547; %Engineering Toolbox
%dynamic viscosity [Pa*s] at 50 degC

Pr_water=cp_water*my_water/k_water;%5.43;%
%Prantl number water at 30 degC.

if ms.mech.innerrotor
```

```
    A_flow_cs = pi*((R_so+0.01^2-(R_so)^2))/Ns;
    %cross section area for water flow assumed 1 cm deep duct on stator
yoke surface.

    Wet_P = theta_s*R_so;
    %wetted perimeter

else
    A_flow_cs = pi*(R_si^2-(R_si-0.01)^2)/Ns;
    %cross section area for water flow assumed 1 cm deep duct on stator
yoke surface.

    Wet_P = theta_s*R_si;
    %wetted perimeter
end

D_H = 4*A_flow_cs/Wet_P;
%Hydraulic diameter

flow_w = (P_windings+P_yoke+P_teeth)/(rho_water*cp_water*10);
%necessary flow of water assuming 10 K increase

flow_water = 500/60/1000/Ns;%2*0.0035/Ns;
%[m^3/s]

Re_D = rho_water*(flow_water/A_flow_cs)*D_H/my_water;
%Reynolds number
if Re_D<2300
    disp('Laminar flow use other equations')
end

Nu_D = 0.023*Re_D^0.8*Pr_water^0.4;
%Nussult number for turbulent flow, Dittus-Boelter correlation

h_water = Nu_D*k_water/D_H;
%heat transfer coefficient for water flow

g=9.81;
%gravity constant [m/s^2]

%% Thermal resistances

    %Conduction

R_ew = (L_ew_s/2+L/4)/(k_copper*A_cu);
%resistance from half a endwinding into a 1/4 a slot, same for upper and
%lower end windings

R_ins_tan = th_ins/(k_mica*A_s_tan);
%resistance for insulation tangential direction

R_ins_rad = th_ins/(k_mica*A_s_rad);
%insulation resistance radial direction

R_t_tan = th_tooth_tan/(k_iron*A_s_tan);
%tooth resistance in tangential direction
```

```
R_t_rad = th_tooth_rad/(k_iron*A_t_rad);
%tooth resistance in radial direction

R_y_bs = th_y_rad/(k_iron*A_s_rad);
%yoke resistance behind slot

R_y_bt = th_y_rad/(k_iron*A_t_rad);
%yoke resitance behind tooth

    %Convection

R_water = 1/(h_water*A_y_rad);
%convection resistance for water coolent

    %Contact resitances

h_c = 1500;
%lowest suggested contact heat coefficient number for cermanic to metal,
%given in post-doc lecture from Robert Nilssen.
R_c_tan = 1/(h_c*A_s_tan);
%contact resitance between insulation and tooth
R_c_rad = 1/(h_c*A_s_rad);
%contact resitanc between insulation and yoke

    %Node conductances

G_1_2 = 1/R_ew;
%from end winding to slot

G_2_3 = G_1_2;
%from other end winding to slot

G_2_4 = 1/(R_ins_rad+R_y_bs+R_c_rad);
%from slot to yoke

G_2_5 = 1/(R_ins_tan+R_t_tan+R_c_tan);
%from slot to tooth

G_4_7 = 1/R_y_bs;
%from yoke behind slot to yoke surface connected with water

G_5_6 = 1/(R_t_rad+R_y_bt);
%from tooth to yoke

G_6_7 = 1/R_y_bt;
%from yoke behind tooth to yoke surface connected with water

G_7_8 = 1/R_water;
%from yoke surface to water

    %Conductance matrix

G(1,:) = [G_1_2 -G_1_2 0 0 0 0 0 0];

G(2,:) = [-G_1_2 G_1_2+G_2_3+G_2_4+G_2_5 -G_2_3 -G_2_4 -G_2_5 0 0 0];

G(3,:) = [0 -G_2_3 G_2_3 0 0 0 0 0];
```

```
G(4,:) = [0 -G_2_4 0 G_2_4+G_4_7 0 0 -G_4_7 0];

G(5,:) = [0 -G_2_5 0 0 G_2_5+G_5_6 -G_5_6 0 0];

G(6,:) = [0 0 0 0 -G_5_6 G_5_6+G_6_7 -G_6_7 0];

G(7,:) = [0 0 0 -G_4_7 0 -G_6_7 G_4_7+G_6_7+G_7_8 -G_7_8];

G(8,:) = [0 0 0 0 0 0 -G_7_8 G_7_8];


    %% Nodal points

I(1) = P_ew/2;
%end winding losses

I(2) = P_s;
%slot winding losses

I(3) = I(1);
%end winding losses

I(4) = P_y_bs;
%yoke losses behind slot

I(5) = P_t;
%tooth losses

I(6) = P_y_bt;
%yoke losses behind tooth

I(7) = 0;
%at yoke surface

I(8) = -sum(I);
%water is assumed to remove all of added losses

%% Temperatures

T_rise = G\I';

T_diff = T_rise(8)-T_water;
%calculates the temperature difference with assumed the constant water
temperature

T = T_rise-T_diff;
%gives the temperatures in each node based on the water temperature
```

F Appendix

F.1 Derivation of copper loss relation.

$$P_{winding} = RI^2$$

Where

$$R = \frac{L_w}{\sigma_w A_{cu}}$$

$$L_w = NL_{tot}$$

Where L_{tot} is total length of all windings both in slots and end-windings.

$$A_{cu} = \frac{k_{cu} A_s}{N}$$

Where A_s is the slot area.

$$I = \frac{I_s}{N}$$

Where I_s is the current in the slot.

$$I_s = Jk_{cu}A_s$$

Where J is the current density and k_{cu} the fill factor.

$$P_{winding} = \frac{NL_{tot}}{\sigma_w \frac{k_{cu}A_s}{N}} \left(\frac{Jk_{cu}A_s}{N}\right)^2$$

$$P_{winding} = \frac{L_{tot}}{\sigma_w} A_s k_{cu} J^2$$

Which leads to:

$$P_{winding} \propto L_{tot} k_{cu} J^2$$